

Dynamics of Electron-Molecule Collisions

Thesis by

Marco Aurelio Pinheiro Lima

In Partial Fulfillment of the Requirements

for the Degree of

Doctor of Philosophy

California Institute of Technology

Pasadena, California

1986

(Submitted March 7, 1986)

ACKNOWLEDGMENTS

I wish to express my appreciation to my research advisor, Professor Vincent McKoy, for his advice, encouragement, and friendship during these last few years. I would like to thank Dr. Winifred Huo and Dr. Barry Schneider for many enlightening and broadening conversations. I would also like to thank all the members of our research group for their warm friendship. Finally, I wish to express my gratitude to Tom Gibson, Zi-ping Luo and Diane Lynch for their assistance and stimulating scientific discussions.

AGRADECIMENTOS

Expresso aqui os meus agradecimentos:

- À Cecília e ao Eduardo pela valiosa paciência, entendimento e apoio que necessitei durante este período.
- Ao Dr. José Roberto Leite pelo apoio logístico e amizade durante todos os momentos necessários.
- Ao Dr. Abel Rosato por ter tido a dolorosa missão de ser o meu procurador no Brasil durante a minha ausência.
- Ao Dr. Lee Mu-tao pelo apoio dado no início da minha estadia no Caltech.
- Aos Drs. Luiz Marco Brescansin, Luiz Eugênio Machado e Kazunori Watari pela amizade e valiosas discussões durante a realização deste trabalho.
- Aos meus cunhados Paulo e Leninha que carinhosamente me mantiveram informado sobre os mais importantes acontecimentos no Brasil durante a minha ausência.
- Às nossas famílias que entenderam a nossa ausência.
- Aos amigos Regina, Luiz, Nestor, Rita, José Nelson, Mayra, Bresca, Ariel, Arnóbio, Albaneide, Hélio e Ivan pelo apoio precioso e amizade que desenvolvemos durante este período.
- Ao Instituto de Estudos Avançados, ao Conselho Nacional de Energia Nuclear e à Fundação de Amparo à Pesquisa do Estado de São Paulo pelo apoio financeiro.

ABSTRACT

We have developed a multichannel formulation for low-energy electron-molecule collisions based on the Schwinger variational method. An important feature of this formulation is that it is capable of dealing with some important aspects of electron-molecule collisions such as electronically inelastic scattering and nonlinear targets. The formulation also allows for the inclusion of a substantial number of closed electronic channels to represent polarization effects, which are very important at low-impact energies.

To assess the accuracy with which polarization is represented in this formulation we have calculated elastic integral and differential cross sections for $e - H_2$ collisions. We have obtained very good agreement between our results and available theoretical and experimental data. We have also examined the shape resonances in $e - CO$ and $e - N_2$ collisions, where polarization plays a very important role in determining the resonance parameters.

Our first application to electron-nonlinear molecule collisions was for $e - CH_4$ scattering. At the static-exchange level of approximation our differential cross sections are in very good agreement with existing measurements at about 7 eV and higher energies. For incident energies below this an interesting feature of the small angle differential cross sections is seen only when polarization effects are included in the calculation. We have also obtained elastic differential and momentum transfer cross sections for $e - H_2O$ scattering. Our calculated differential cross sections agree well with available experimental data, which

extend only to 120° . The differential cross sections, particularly at 15 and 20 eV, show significant backward peaking. This peaking occurs in the experimentally inaccessible region beyond scattering angle of 120° , and, as we will see, it has an important implication in the determination of momentum transfer cross sections.

We also obtained differential and integral cross sections for the electron impact excitation of the $b^3\Sigma_u^+$, $a^3\Sigma_g^+$, $c^3\Pi_u$, and $B^1\Sigma_u^+$ states of H_2 at the two state approximation. In contrast to the triplet excitations, the $B^1\Sigma_u^+$ is a dipole-allowed transition, a feature which introduces several new interesting aspects. Our results for the excitation of the $b^3\Sigma_u^+$ and $B^1\Sigma_u^+$ states are in good agreement with experimental data at all energies.

The results we obtained with the Schwinger multichannel method are very encouraging and illustrate the potential utility of these calculated cross sections. The results of such studies can clearly complement experimental efforts to determine absolute values of these electron-molecule scattering cross sections.

TABLE OF CONTENTS

ACKNOWLEDGEMENTS	ii
AGRADECIMENTOS	iii
ABSTRACT	iv
TABLE OF CONTENTS	vi
I. INTRODUCTION	1
References	4
II. ELECTRON-MOLECULE COLLISIONS	6
References	10
III. THEORY	11
1. Formulation	11
2. Uniqueness of the Scattering Amplitude	15
3. The Choice of a	17
4. (N) and (N+1)-Identical Particle Projectors	19
5. Expansion Techniques	23
References	26
IV. APPLICATIONS TO ELASTIC ELECTRON-MOLECULE COLLISIONS	
1. H ₂	28
References	37
Tables and Figures	40
2. N ₂	50
References	61
Tables and Figures	64
3. CO	70
References	73

Tables and Figures	74
4. CH ₄	79
References	90
Tables and Figures	93
5. H ₂ O	105
References	111
Tables and Figures	112
V. APPLICATIONS TO ELECTRONICALLY INELASTIC ELECTRON- MOLECULE COLLISIONS	
1. Cross sections for electron impact excitation of the a ³ Σ _g ⁺ , b ³ Σ _u ⁺ , and c ³ Π _u states of H ₂	119
References	130
Tables and Figures	133
2. Cross sections for electron impact excitation of the B ¹ Σ _u ⁺ state of H ₂ .	149
References	156
Tables and Figures	158

I. Introduction

Cross sections for the scattering of low-energy electrons by molecules play an important role in the modeling of swarm devices, electrical discharges, plasma etching systems, gas lasers and planetary atmospheres. The need to understand the associated electron collision processes in these devices and media has put enormous demands on our knowledge of the pertinent cross sections. Furthermore, electron energy loss spectroscopy (EELS), in which monoenergetic beams of electrons are inelastically scattered by adsorbate molecules, is one of the most important probes of surface science. Presently, there is at most a very limited and restrictive theory for the interpretation of the angular and energy dependencies in such spectra.

In contrast to the related atomic problem, the progress to date in both theoretical and experimental studies of electron-molecule scattering cross sections has been limited.¹ On the theoretical side, this situation is primarily due to the additional complexities arising from the nonspherical potential fields of molecular targets. Most studies of electronic excitation of molecules by low-energy electrons have hence been carried out using low-order theories. These theories include plane-wave theories such as the Born-Ochkur-Rudge approximation,^{2,3} the impact-parameter method,⁴ and distorted-wave theories.^{5,6} Studies of elastic scattering by molecules have also used local approximations to the nonlocal exchange potentials.⁷ Although such theories and approximations can be computationally easy to apply, they do not contain enough of the collision physics to

yield consistently reliable differential and integral cross sections, particularly at low and intermediate energies.⁸ What is clearly needed are theoretical methods which can provide quantitatively reliable cross sections for elastic and electronically inelastic collisions with both linear and nonlinear molecular targets. Although substantial progress has been made for some systems, no single method has yet been demonstrated for general use.

In what follows we will present the results of our studies⁹⁻¹⁴ of elastic and electronically inelastic electron-molecule collisions which we have obtained using a multichannel extension of the Schwinger variational principle.^{15,16} This multichannel formulation is capable of dealing with several important aspects of electron-molecule collisions such as polarization effects, which are included through closed channels, electronically inelastic scattering with several open and closed channels, and, very importantly, nonlinear targets. Some important features of the method are as follows. As in the original Schwinger principle,¹⁷ the trial scattering functions need not satisfy any specific boundary conditions and hence can be expanded in an L^2 basis. The method avoids the explicit construction of the closed channel Green's function. Furthermore, with the use of an insertion-like quadrature to evaluate the second Born-like terms and with an expansion of the trial function in a Gaussian basis, all matrix elements in the variational expression can be evaluated analytically for an arbitrary molecular target.

In the following section we will discuss some theoretical and phenomenolog-

ical aspects of electron-molecule collisions. This section is intended to be helpful in putting the advantages and limitations of the theory used in our research, in the right perspective. In the third section we present the multichannel extension of the Schwinger variational principle and discuss some essential aspects of its implementation. We will then present results of applications of this formulation to low-energy electron-molecule collisions in the remaining sections. These results will include cross sections for elastic scattering of electrons by H_2 , N_2 , CO , CH_4 and H_2O , and cross sections for excitation of the $X^1\Sigma_g^+ \rightarrow b^3\Sigma_u^+, a^3\Sigma_g^+, c^3\Pi_u$, and $B^1\Sigma_g^+$ transitions in H_2 . Preceding each of these sections we will give a brief summary of the experimental and theoretical data available for the specific process.

References

1. See, for example, S. Trajmar, D. F. Register, and A. Chutjian, *Phys. Repts.* **97**, 219 (1983); *Electron-Molecule Collisions*, edited by I. Shimamura and K. Takayanagi (Plenum, New York, 1984).
2. S. Chung, C. C. Lin, and E. T. P. Lee, *Phys. Rev. A*, **12**, 1340 (1975).
3. D. C. Cartwright, and A. Kuppermann, *Phys. Rev.* **163**, 86 (1967).
4. A. V. Hazi, *Phys. Rev. A*, **23**, 2232 (1981).
5. T. N. Rescigno, C. W. McCurdy, Jr., and V. McKoy, *J. Phys. B.* **7**, 2396 (1974).
6. A. W. Fliflet and V. McKoy, *Phys. Rev. A* **21**, 1863 (1980).
7. See, for example, L. A. Collins, W. D. Robb, and D. W. Norcross, *Phys. Rev. A* **20**, 1838 (1979).
8. D. C. Cartwright, A. Chutjian, S. Trajmar, and W. Williams, *Phys. Rev. A* **16**, 1013 (1977).
9. M. A. P. Lima, T. L. Gibson, K. Takatsuka, and V. McKoy, *Phys Rev. A* **30**, 1741 (1984).
10. T. L. Gibson, M. A. P. Lima, K. Takatsuka, and V. McKoy, *Phys Rev. A* **30**, 3005 (1984).
11. M. A. P. Lima, T. L. Gibson, W. M. Huo, and V. McKoy, *Phys. Rev. A* **32**, 2696 (1985).
12. M. A. P. Lima, T. L. Gibson, W. M. Huo, and V. McKoy, *J Phys B: At. Mol. Phys.* **18**, L865 (1985).

- 13 M. A. P. Lima, T. L. Gibson, W. M. Huo, L. M. Brescansin, and V. McKoy, "Swarm Studies and Inelastic Electron-Molecule Collisions," edited by L. Pitchford, V. Mckoy, A. Chutjian, and S. Trajmar, Springer Ser. Atom. Plasm (Springer, Berlin, Heidelberg, 1986).
14. W. M. Huo, V. McKoy, M. A. P. Lima and T. L. Gibson, *Thermophysical Aspects of Reentry Flow*, edited by J. Moss and C. Scott (AAILA, New York, 1986).
15. K. Takatsuka and V. McKoy, *Phys Rev. A* **24**, 2473 (1981).
16. K. Takatsuka and V. McKoy, *Phy. Rev. A* **30**, 1734 (1984).
17. B. A Lippmann and J. Schwinger, *Phys Rev.* **79**, 469 (1950).

II. Electron-molecule Collisions

A variety of processes may occur in the collision of an electron with a molecule. Which processes occur depend on the incident energy of the electron and on the specific target molecule. Two classes of collisions may be distinguished. The first involves rearrangement collisions¹ such as ionization, dissociation, dissociative attachment, etc., while the second takes place in a single arrangement channel, *e.g.*, rotational, vibrational and electronic excitation. We confine our attention to collisions without rearrangement processes. This is achieved either by means of threshold laws or by assuming, when possible, that the rearrangement collisions are very improbable. Cross sections represent the time-independent probability for the occurrence of a particular collision process and are well defined for most electron scattering experiments. The total integrated cross section provides useful information about the electron molecule interactions. However, more detailed insight into the nature of these interactions may be gained from the differential cross sections. For electron impact excitation we can define a doubly differential cross section as: the ratio of the number of electrons detected in a differential solid angle $d\Omega_{\vec{k}_f}$ with energy range between E_f and $E_f + dE_f$ per unit time and per unit scatterer, to the relative flux of the incident electrons with respect to the molecule. This cross section can be written as

$$\frac{d^2\sigma}{d\Omega_{\vec{k}_f} dE_f}(E_i, E_f, \Omega), \quad (1)$$

where $E_f - E_i$ refers to the excitation energy of the target. If the excitation is

to a discrete state, this equation can be integrated to yield

$$\frac{d\sigma}{d\Omega_{\vec{k}_f}}(E_i, E_f, \Omega). \quad (2)$$

The target molecules are freely rotating and hence, the physical cross sections must be averaged over molecular orientation. For this reason, the differential cross section becomes independent of the azimuthal angle, ϕ ; *i.e.*,

$$\sigma_{exp}(E_i, E_f, \theta) = \frac{1}{2\pi} \int_0^{2\pi} \left[\frac{d\sigma(\Omega)}{d\Omega} \right] d\phi. \quad (3)$$

Many of the difficulties arising in studies of electron-molecule collision can be traced to the computational problems associated with accurately representing the many-electron system and the nonspherical electronic and nuclear force fields experienced by the incident and scattered electrons. Further difficulties are due to the rotational and vibrational degrees of freedom of the target. The Born-Oppenheimer approximation permits a separation of nuclear and electronic variables so that one can first solve the electronic problem with the nuclei fixed, obtaining electronic wavefunctions and energies that depend parametrically on the nuclear coordinates. The nuclei are then assumed to move in response to the adiabatic potential energy associated with a stationary electronic state. Within the Born-Oppenheimer fixed nuclei approximation the total wavefunction (molecule and incoming electron) can be written as a product; *i.e.*,

$$\Psi(\vec{r}_1, \dots, \vec{r}_{N+1}, \vec{R}_\alpha) = \Psi_e^{FN}(\vec{r}_1, \dots, \vec{r}_{N+1}, \vec{R}_\alpha) \chi(\vec{R}_\alpha), \quad (4)$$

where χ is the nuclear wave function and the fixed nuclei (FN) electronic function Ψ_e^{FN} depends only parametrically on the nuclear coordinates \vec{R}_α . In the above

expression, $\vec{r}_1, \dots, \vec{r}_N$ are coordinates for the target electrons and \vec{r}_{N+1} is the incoming electron coordinate. The most convenient electronic coordinates here are those referred to the *body* frame. This is a frame directed along the symmetry axis of the molecule and having a common origin with the laboratory frame at the center of mass of the molecule. The *lab* frame has a space fixed z-axis often chosen along the initial momentum \vec{k}_o of the incident electron. The validity of the fixed-nuclei (or Born Oppenheimer) approximation is very well established in the literature² and will not be discussed here.

We discuss only the "impulse limit" appropriate for non-resonant (or short-lived resonant) scattering which is used throughout this work. This limit is applied at energies sufficiently high such that the velocities of the incident and outgoing electrons are considerably larger than those of the nuclei. From a classical point of view, a "fast collision" is the one in which the collision time τ_C is much less than the period of nuclear rotation $\tau_R \sim 10^{-12} \text{sec}$ or vibrational $\tau_V \sim 10^{-14} \text{sec}$. Therefore, even for collision process corresponding to an incident energy of 1 eV ($\tau_C \sim 10^{-16} \text{sec}$), the impulse limit remains a good approximation.

In the impulse limit the nuclear wave function $\chi(R)$ of Eq. (4) are simply the unperturbed nuclear wavefunctions for the molecule. The scattering amplitude for the process $(\vec{k}_o, \eta_o, \nu_o) \rightarrow (\vec{k}, \eta, \nu)$ is then given by

$$f_{\eta\nu, \eta_o, \nu_o}(\vec{k}, \vec{k}_o) = \langle \chi_{\eta\nu}(R) | f_{\eta, \eta_o}^{FN}(\vec{k}, \vec{k}_o) | \chi_{\eta_o, \nu_o}(R) \rangle, \quad (5)$$

where \vec{k}_o (\vec{k}), η_o (η) and ν_o (ν) are, respectively, the momentum of the electron, the target electronic quantum numbers, and the rotational plus vibrational quan-

tum numbers before (after) the collision, and f_{η,η_0}^{FN} is the fixed-nuclei scattering amplitude corresponding to an electronic transition $\eta_0 \rightarrow \eta$ of the molecule.

In the next section we present a multichannel theory for calculating the scattering amplitude F_{η,η_0}^{FN} . Details involved in obtaining the cross sections from the fixed-nuclear scattering amplitude F_{ν,ν_0}^{FN} are given, when necessary, in the discussion of the applications.

References

1. C. J. Joachain, *Quantum Collision Theory* (North Holland, New York, 1975).
2. See for example, N. F. Lane, *Rev. Mod. Phys.* **52**, 29 (1980).

III. Theory

In recent years many theories¹ have been proposed for dealing with the problem of the scattering of low-energy electrons by molecules within the framework of the fixed-nuclei approximation. Some of them have been successfully applied² to both elastic and inelastic collisions for small linear molecules. However, none of the existing methods can readily address simultaneously several important problems which arise in a realistic treatment of low-energy electron-molecule collisions. These problems include polarization effects, electronic inelastic scattering and collisions with non-linear targets. In the following we outline the theory³ of electron-molecule collisions which we have recently developed and which, as we will see, is applicable⁴⁻¹⁰ to a wide range of such collisions.

1. Formulation

The Hamiltonian for the collision system can be written as

$$H = (H_N + T_{N+1}) + V = H_0 + V, \quad (1.1)$$

where H_N is the target Hamiltonian, T_{N+1} is the kinetic energy operator for the incident electron, and V is the interaction potential between the incident electron and the target; i.e.,

$$V = \sum_{i=1}^N \frac{1}{r_{i,N+1}} - \sum_{\alpha} \frac{Z_{\alpha}}{R_{\alpha,N+1}}. \quad (1.2)$$

In Eq. (1.2) the first and second terms are the electron repulsion and electron-nuclei attraction, respectively. Our goal is to obtain a multichannel Schwinger variational principle for the scattering matrix associated with the Hamiltonian

of Eq. (1.1). One could begin by writing the Lippmann-Schwinger equation for the Hamiltonian $H = H_0 + V$; i.e.,

$$\Psi_m^{(+)} = S_m + G_0^{(+)} V \Psi_m^{(+)}, \quad (1.3)$$

where $G_0^{(+)}$ is the Green's function associated with $E - H_0$ and S_m is the regular solution of $E - H_0$. Based on this equation it is straightforward to construct the Schwinger variational functional for the scattering amplitude; i.e.,

$$f_{m,n} = -\frac{1}{2\pi} \frac{\langle S_m | V | \Psi_n^{(+)} \rangle \langle \Psi_m^{(-)} | V | S_n \rangle}{\langle \Psi_m^{(-)} | V - V G_0^{(+)} V | \Psi_n^{(+)} \rangle}. \quad (1.4)$$

Formally, this variational principle is complete and has no major drawbacks at least for the collisions of nonidentical particles. However, as pointed out by Geltman,¹¹ the continuum states of the target molecule must be included in the total Green's function $G_0^{(+)}$ in order to make the wave function on the left-hand side of Eq. (1.3) antisymmetric. This certainly suggests that it would be difficult to construct and treat this Green's function exactly in the collision of identical particles. For this reason Eq. (1.3) is usually avoided and instead the Schwinger principle is normally applied to the coupled equations which are more manageable.¹²

To obtain a multichannel Schwinger variational principle based on the total $(N+1)$ -particle wave function, we proceed as follows. We begin by introducing a projection operator P which defines the open-channel space in terms of the eigen-functions of H_N :

$$P = \sum_{\ell=1}^{open} | \Phi_{\ell}(1, 2, \dots, N) \rangle \langle \Phi_{\ell}(1, 2, \dots, N) | \quad (1.5a)$$

and

$$H_N \Phi_\ell = E_\ell \Phi_\ell, \quad E - E_\ell > 0, \quad (1.5b)$$

where E is the total energy of the $(N+1)$ particle system. Note that the projector of Eq. (1.5a) is different from the P operator of Feshbach formalism.¹³ With this operator we obtain a projected Lippmann-Schwinger equation for the m th scattering state.

$$P\Psi_m^{(+)} = S_m + G_P^{(+)}V\Psi_m^{(+)}, \quad (1.6)$$

where $\Psi_m^{(+)}$ is the total scattering wave function with plane-wave plus outgoing-wave boundary conditions. S_m is hence the product of the target wave function Φ_m and an incident plane wave; i.e.,

$$S_m = \Phi_m(1, 2, \dots, N) e^{i\vec{k}_m \cdot \vec{r}_{N+1}}. \quad (1.7)$$

The outgoing-wave Green's function $G_P^{(+)}$, which is defined only in the open-channel space, is given by

$$G_P^{(+)} = \sum_{\ell=1}^{\text{open}} |\Phi_\ell\rangle g_\ell^{(+)}(\vec{r}_{N+1}, \vec{r}'_{N+1}) \langle \Phi_\ell| \quad (1.8a)$$

with

$$g_\ell^{(+)}(\vec{r}, \vec{r}') = -\frac{1}{2\pi} \frac{e^{ik_\ell|\vec{r}-\vec{r}'|}}{|\vec{r}-\vec{r}'|}. \quad (1.8b)$$

To recover the closed channel content of $\Psi_m^{(+)}$, we must require the $\Psi_m^{(+)}$ to be indeed an eigenstate of the Schrodinger equation,

$$\hat{H}\Psi_m^{(+)} = 0, \quad (1.9a)$$

and not only a solution of Eq. (1.6). This can be achieved by requiring that

$$\hat{H}\Psi_m^{(+)} = \hat{H}(aP\Psi_m^{(+)} + (1 - aP)\Psi_m^{(+)}) = 0, \quad (1.9b)$$

where a is an arbitrary constant to be determined later. Inserting Eq. (1.6) into Eq. (1.9b), we obtain

$$\hat{H}(a(S_m + G_P^{(+)}V)\Psi_m^{(+)} + (1 - aP)\Psi_m^{(+)}) = 0. \quad (1.10)$$

With some manipulations this equation can be put in the form

$$A^{(+)}\Psi_m^{(+)} = VS_m, \quad (1.11a)$$

where

$$A^{(+)} = \frac{1}{a}\hat{H} - \frac{1}{2}(P\hat{H} + \hat{H}P) + \frac{1}{2}(PV + VP) - VG_P^{(+)}V. \quad (1.11b)$$

In obtaining Eq. (1.11) we used the equation

$$[H_0, P] = 0 \quad (1.12a)$$

and

$$\begin{aligned} \hat{H}P\Psi_m^{(+)} &= \hat{H}_0P\Psi_m^{(+)} - VP\Psi_m^{(+)} \\ &= \frac{1}{2}[\hat{H}_0P + P\hat{H}_0]\Psi_m^{(+)} - VP\Psi_m^{(+)}. \end{aligned} \quad (1.12b)$$

In what follows we discuss the apparent arbitrariness in the definition of $A^{(+)}$ due to the parameter a in Eq. (1.11b). We will see that the choice of a is very important in obtaining a variational method for the scattering amplitude and

also to ensure that the scattering amplitude is uniquely and correctly defined by the solutions of Eqs. (1.11).

2. Uniqueness of the Scattering Amplitude

The motivation for the present discussion can best be seen through the following conjecture. Imagine a solution, say $F_m^{(+)}$, which simultaneously satisfies the following two equations,

$$-\frac{1}{a}\hat{H}F_m^{(\pm)} = \beta \quad (2.1a)$$

and

$$\left[\frac{1}{2}(PV + VP) - VG_P^{(\pm)}V - \frac{1}{2}(P\hat{H} + \hat{H}P)\right]F_m^{(\pm)} - VS_m = \beta, \quad (2.1b)$$

where β is a number or a function. Then the family of solutions of Eqs. (1.11) must include $F_m^{(+)}$ since, by substituting Eq. (2.1a) into Eq. (2.1b), we recover Eqs. (1.11). Now, if β is different from zero, $F_m^{(\pm)}$ is not a solution to the Schrodinger equation. However, as we shall see, this problem is closely related to the nonuniqueness of solutions of inhomogeneous equations, and therefore, under certain conditions, $F_m^{(\pm)}$ can uniquely give the correct scattering amplitude. To see this let us write $F_m^{(\pm)}$ as

$$F_m^{(\pm)} = \bar{\Psi}_m^{(\pm)} + \gamma_m^{(\pm)}, \quad (2.2)$$

where $\bar{\Psi}_m^{(\pm)}$ are exact solutions of the Schrodinger equation with appropriate boundary condition. Obviously, $\bar{\Psi}_m^{(\pm)}$ are also solutions of Eq. (1.11); i.e.,

$$A^{(\pm)}\bar{\Psi}_m^{(\pm)} = VS_m. \quad (2.3)$$

Insertion of Eq. (2.2) into Eqs. (1.11) gives

$$A^{(\pm)}\gamma_m^{(\pm)} = 0. \quad (2.4)$$

Therefore, $\gamma_m^{(\pm)}$ must at most be a solution of the homogeneous counterpart of Eq. (1.11a). It is well known in elementary theory¹⁴ of linear operators that, if

$$A^{(+)\dagger} = A^{(-)}, \quad (2.5)$$

the homogeneous solutions $\gamma_m^{(\pm)}$ will have the following properties:

$$\langle \gamma_m^{(-)} | V | S_n \rangle = 0 \quad (2.6a)$$

and

$$\langle S_m | V | \gamma_n^{(+)} \rangle = 0. \quad (2.6b)$$

Considering these properties of $\gamma_m^{(\pm)}$, we now address the question of uniqueness of the scattering amplitude. The scattering amplitude can be defined from Eqs. (1.11) as

$$\begin{aligned} f_{m,n} &= \langle S_m | V | F_n^{(+)} \rangle = \langle F_m^{(-)} | V | S_n \rangle \\ &= \langle F_m^{(-)} | A^{(+)} | F_n^{(+)} \rangle. \end{aligned} \quad (2.7)$$

Insertion of Eq. (2.2) into Eq. (2.7), together with Eqs. (2.4) and (2.6), gives

$$\begin{aligned} f_{m,n} &= \langle S_m | V | \Psi_n^{(+)} \rangle = \langle \Psi_m^{(-)} | V | S_n \rangle \\ &= \langle \Psi_m^{(-)} | A^{(+)} | \Psi_n^{(+)} \rangle, \end{aligned} \quad (2.8)$$

which is the correct value for the scattering amplitude. Therefore, if we choose a in Eq. (1.11b) such that $A^{(+)\dagger} = A^{(-)}$, the homogeneous solutions $\gamma_m^{(\pm)}$ will not contaminate the correct solutions $\Psi_m^{(\pm)}$. Consequently, $F_m^{(\pm)}$ will define uniquely and correctly the scattering amplitude.

3. The Choice of a

Based on the inhomogeneous Equation (1.11), one can construct a fractional form for the scattering amplitude,

$$f(\vec{k}_m, \vec{k}_n) = -\frac{1}{2\pi} \frac{\langle S_m | V | \Psi_n^{(+)} \rangle \langle \Psi_m^{(-)} | V | S_n \rangle}{\langle \Psi_m^{(-)} | A^{(+)} | \Psi_n^{(+)} \rangle}. \quad (3.1)$$

This form for the scattering amplitude is known¹⁵ to produce variational stable results for approximative solutions of equations such as Eqs. (1.11), if $A^{(+)\dagger} = A^{(-)}$. We note that, since the operator $A^{(+)}$ in the denominator of Eq. (3.1) is totally symmetric, the condition $A^{(+)\dagger} = A^{(-)}$ holds for any value of a for functions of the L^2 -space. However, due to the presence of the full Hamiltonian in $A^{(+)}$, namely,

$$\frac{1}{a} \hat{H} - \frac{1}{2} (P \hat{H} + \hat{H} P), \quad (3.2)$$

this is not true for the continuum functions. The functions $\Psi_m^{(\pm)}$ may be written in a somewhat general form

$$\Psi_m^{(\pm)} = \sum_n^{\text{open}} A[\Phi_n(1\dots N)\phi_n^e] + \sum_q C_q \Psi_q(1\dots N+1), \quad (3.3)$$

where Φ_n is the open channel wave function, ϕ_n^e is the scattered electron wave function, and A is the antisymmetrizer defined by

$$PA\Phi_n\phi_n^e = \Phi_n\phi_n^e \quad (3.4a)$$

and hence,

$$A^2 = (N + 1)A. \quad (3.4b)$$

In Eq. (3.3) Ψ_q is any L^2 antisymmetric $(N+1)$ -particle wave function. Orthogonality conditions can be imposed on ϕ_n^e without loss of generality. These conditions are

$$\int \Phi_n^*(1\dots N)\phi_n^e(1) = 0 \quad (3.5a)$$

$$\int \Psi_q^*(1\dots N + 1)\phi_m^e(1) = 0 \quad (3.5b)$$

which are not restrictive because Ψ_q contains terms such as $A\Phi_n\phi_n^b$, where ϕ_n^b is a bound state function. The key condition for a is on the continuum functions; *i.e.*,

$$\begin{aligned} & \langle A\Phi_m\phi_m^e \mid \frac{1}{a}\hat{H} - \frac{1}{2}(P\hat{H} - \hat{H}P) \mid A\Phi_n\phi_n^{e'} \rangle \\ & = \langle A\Phi_n\phi_n^{e'} \mid \frac{1}{a}\hat{H} - \frac{1}{2}(P\hat{H} - \hat{H}P) \mid A\Phi_m\phi_m^e \rangle. \end{aligned} \quad (3.6)$$

By selecting

$$a = N + 1 \quad (3.7)$$

we see that both terms in Eq. (3.6) vanish; *i.e.*,

$$\langle A\Phi_\ell\phi_\ell^t \mid \frac{\hat{H}}{N+1} - \frac{1}{2}(P\hat{H} + \hat{H}P) \mid A\Phi_{\ell'}\phi_{\ell'}^r \rangle = 0 \quad (3.8)$$

for $t, r, = s, s'$ and $\ell, \ell' = m, n$. Thus, the choice of a ensures that the operator (3.2) is Hermitian. Consequently, $A^{(+)\dagger} = A^{(-)}$, and Eq. (3.1) gives variational stable scattering amplitudes which are uniquely and correctly defined by Eqs. (1.11).

4. (N) and (N+1)-Identical Particle Projectors

We shall now examine a preliminary study on the relationship of our theory with the Feshbach formalism.¹³ First we define a projection operator P_F which, acting on the full scattering wave function $\Psi_m^{(\pm)}$, is such that

$$P_F \Psi_m^{(\pm)} \rightarrow \Psi_m^{(\pm)} \quad (4.1)$$

$$r_1 \rightarrow \infty$$

$$r_2 \rightarrow \infty$$

...

$$r_{N+1} \rightarrow \infty,$$

where r_1, \dots, r_N are the coordinates of the target electrons and r_{N+1} is the incident particle coordinate. The projected wave function $P_F \Psi_m^{(\pm)}$ yields asymptotically the scattering amplitude. A second operator, Q_F , containing only L^2 -function is then defined as

$$Q_F = 1 - P_F. \quad (4.2)$$

Since P_F is a projector, it follows that

$$P_F^2 = P_F \quad (4.3a)$$

$$Q_F^2 = Q_F \quad (4.3b)$$

$$P_F Q_F = Q_F P_F = 0. \quad (4.3c)$$

For the expansion of $\Psi_m^{(\pm)}$ given by Eq. (3.3), we have

$$P_F \Psi_m^{(\pm)} = \sum_n^{\text{open}} A[\Phi_n(1\dots N)\phi_n^e] \quad (4.4a)$$

and

$$Q_F \Psi_m^{(\pm)} = \sum_q \Psi_q(1\dots N+1). \quad (4.4b)$$

In our theory the P projector is defined in the N -body space. Therefore, the action of P on the scattering function $\Psi_m^{(\pm)}$ distinguishes the incident electron from the target electrons; i.e.,

$$P \Psi_m^{(\pm)} = \sum_n^{\text{open}} \Phi_n(1\dots N)\phi_n^e + \sum_n^{\text{open}} \Phi_n\phi_n^b, \quad (4.5)$$

where ϕ_n^e and ϕ_n^b are the one-particle functions defined below Eq. (3.3). Equation (4.5) yields asymptotically the scattering amplitude only for the $(N+1)$ th electron coordinate; i.e.,

$$P \Psi_m^{(\pm)} \rightarrow \Psi_m^{(\pm)} \quad (4.6a)$$

$$r_{N+1} \rightarrow \infty$$

$$P \Psi_m^{(\pm)} \rightarrow 0 \quad (4.6b)$$

$$r_1 \rightarrow \infty$$

...

$$r_N \rightarrow \infty.$$

The equivalence between incident electron and target electrons is obtained through the operator

$$Q = 1 - P, \quad (4.7)$$

which, when applied to $\Psi_m^{(\pm)}$, gives

$$Q\Psi_m^{(\pm)} \rightarrow 0 \quad (4.8a)$$

$$r_{N+1} \rightarrow \infty$$

$$Q\Psi_m^{(\pm)} \rightarrow \Psi_m^{(\pm)} \quad (4.8b)$$

$$r_1 \rightarrow \infty$$

...

$$r_N \rightarrow \infty.$$

We can relate the actions of P_F and P on $\Psi_m^{(\pm)}$ by comparison of Eqs. (4.4a) and (4.5). They differ in two aspects: the absence of the antisymmetrizer and the presence of the second term in the left-hand side of Eq. (4.5). If we apply the antisymmetrizer on Eq. (4.5), we obtain

$$AP\Psi_m^{(\pm)} = \sum_n^{\text{open}} A\Phi_n(1\dots N)\phi_n^a + \sum_n^{\text{open}} A\Phi_n(1\dots N)\phi_n^b \quad (4.9a)$$

that together with Eqs. (4.4), gives

$$AP\Psi_m^{(\pm)} = P_F\Psi_m^{(\pm)} + Q'_F\Psi_m^{(\pm)}, \quad (4.9b)$$

where Q'_F is a part of Q_F that can be written as

$$Q'_F = \sum_q \lambda_q |\Psi_q\rangle \langle \Psi_q|. \quad (4.10)$$

In the above definition, λ_q are real numbers and Ψ_q are functions in the Q_F -space. Since λ_q are not just normalization factors, Q' is not, in general, a projector. However, due to orthogonality conditions between ϕ_n^g and ϕ_n^b , the products $P_F Q'_F$ and $Q'_F P_F$ vanish; i.e.,

$$P_F Q'_F = Q'_F P_F = 0. \quad (4.11)$$

Equation (4.5) can now be used to obtain the value of a in Eq. (1.11) in a more elegant manner. We have seen in Sec. 3 that the condition on a is in the term

$$R_1 = \langle \Psi_m^{(-)} | \frac{1}{a} \hat{H} - \frac{1}{2} (P \hat{H} + \hat{H} P) | \Psi_n^{(+)} \rangle. \quad (4.12)$$

If we consider the Eq. (3.4b) and

$$[\hat{H}, A] = 0, \quad (4.13)$$

Eq. (4.12) can be written as

$$R_1 = \langle \Psi_m^{(-)} | \frac{1}{a} \hat{H} - \frac{1}{2(N+1)} (P A \hat{H} + \hat{H} A P) | \Psi_n^{(+)} \rangle. \quad (4.14)$$

Insertion of Eq. (4.9b) into Eq. (4.14) gives

$$R_1 = \langle \Psi_m^{(-)} | \frac{1}{a} \hat{H} - \frac{1}{2(N+1)} (P_F \hat{H} + \hat{H} P_F) | \Psi_n^{(+)} \rangle \\ + (\text{terms containing } Q'_F). \quad (4.15)$$

If now we apply the unit operator of the Feshbach's space on the right side of $\Psi_m^{(-)}$ and on left side of $\Psi_n^{(+)}$, we obtain

$$R_1 = \langle \Psi_m^{(-)} | P_F \hat{H} P_F | \Psi_n^{(+)} \rangle \left(\frac{1}{a} - \frac{1}{N+1} \right) + (\text{ terms containing } Q_F). \quad (4.16)$$

Since $A^{(+)+} = A^{(-)}$ for any value of a in the L^2 -space, we do not need to consider the terms in Eq. (4.16) containing Q_F . Therefore, we can focus our attention only on the first term on the right hand side of Eq. (4.16); i.e.,

$$R_2 = \langle \Psi_m^{(-)} | P_F \hat{H} P_F | \Psi_n^{(+)} \rangle \left(\frac{1}{a} - \frac{1}{N+1} \right). \quad (4.17)$$

Since $P_F H P_F$ is not Hermitian, the Hamiltonian terms $\frac{1}{a} \hat{H} - \frac{1}{2}(P \hat{H} + \hat{H} P)$ will be Hermitian only if $R_2 = 0$. This, obviously, leads to $a = N + 1$.

5. Expansion Techniques

In our procedure $\Psi_n^{(+)}$ is expanded in a basis of Slater determinants which are constructed from an orthogonal set of molecular orbitals, additional basis functions, and plane-wave functions, if necessary. These molecular orbitals and additional basis functions are further expanded in Cartesian Gaussian functions. With this choice of basis all of the matrix elements appearing in Eq. (3.1), except for the matrix elements of $V G_P^{(+)} V$, can be evaluated analytically. However, these matrix elements can also be obtained in closed form¹⁶⁻¹⁸ if an approximate closure relation is inserted around $G_P^{(+)}$; viz.,

$$\langle \Psi_m^{(-)} | V G_P^{(+)} V | \Psi_n^{(+)} \rangle$$

$$\cong \sum_{\gamma, \gamma', \delta, \delta'} \langle \Psi_m^{(-)} | V | \gamma \rangle O_{\gamma, \gamma'} \langle \gamma' | G_p^{(+)} | \delta \rangle O_{\delta, \delta'} \langle \delta' | V | \Psi_n^{(+)} \rangle, \quad (5.1)$$

where $(O^{-1})_{\gamma, \gamma'} = \langle \gamma | \gamma' \rangle$ and Cartesian Gaussian functions are again chosen for the insertion basis $|\gamma\rangle$. This insertion basis can be larger than the one used to expand $\Psi_n^{(+)}$. The form of the insertion used in Eq. (5.1) does not require that $|\gamma\rangle$ be an orthonormal set. Thus, we can include the SCF orbitals, additional scattering functions, and extra Gaussians used only for insertion to make up the $|\gamma\rangle$ basis. A criterion for the completeness of this insertion basis can be obtained by observing the way in which the scattering matrix approaches unitarity. Furthermore, the "residue" contribution to these matrix elements of $V G_p^{(+)} V$ can be obtained essentially exactly via insertion of a complete set of plane waves around $G_p^{(+)}$. This procedure results in an S-matrix that is very nearly unitary without resorting to large Cartesian Gaussian insertion basis sets.¹⁹

This formulation allows us to obtain an analytic approximation to the body-frame fixed-nuclei^{1,20,21} scattering amplitude f^B for molecules of arbitrary geometry. To generate the physical differential cross section, one needs the laboratory-frame¹ scattering amplitude f^L . As a first step to acquiring this quantity, we expand f^B in a partial wave series

$$f^B(\vec{k}_m, \vec{k}_n) = \sum_{\ell, m} F_{\ell, m}^B(k_m, \vec{k}_n) Y_{\ell}^m(\hat{k}_m). \quad (5.2)$$

Here, $F_{\ell, m}^B$ is given by

$$F_{\ell, m}^B(k_m, \vec{k}_n) = \int d\hat{k}_m Y_{\ell}^m(\hat{k}_m)^* f^B(\vec{k}_m, \vec{k}_n). \quad (5.3)$$

An N-point Gauss-Legendre quadrature is used to perform each of the angular integrations in Eq. (5.3); for given k_m and k_n this requires that $f^B(\vec{k}_m, \vec{k}_n)$ be determined at the appropriate set of angles. A straightforward application of the Wigner rotation matrices²² is then used to obtain f^L as a partial wave series expanded in terms of the laboratory-frame angles \hat{k}'_m ; *vis.*,

$$f^L(\vec{k}'_m, \vec{k}_n) = \sum_{L, m, \mu} F_{L, m}^B(k_m, \vec{k}_n) Y_L^\mu(\hat{k}'_m) D_{\mu m}^L(0, \beta, \alpha), \quad (5.4)$$

where D is the rotation matrix whose argument consists of the Euler angles relating the two reference frames. The random orientation of the target is accounted for by explicitly averaging over the angles \hat{k}_n . If the laboratory-frame angles \hat{k}'_m are denoted by (θ', ϕ') , the differential cross section can be written as

$$\sigma(\theta', \phi'; k_m, k_n) = \frac{1}{4\pi} \frac{k_m}{k_n} \int d\hat{k}_n |f^L(\vec{k}'_m, \vec{k}_n)|^2. \quad (5.5)$$

Again, Gauss-Legendre quadratures are used to perform the angular integrations. Finally, the physical cross section is obtained by averaging over the azimuthal angle ϕ' and performing the appropriate average over the initial and sum over final spin states for the transition of interest.

References

1. N. F. Lane, *Rev. Mod. Phys.* **52**, 29 (1980).
2. *Electron-Molecule Collisions*, edited by I. Shimamura and K. Takayanagi (Plenum, New York, 1984).
3. K. Takatsuka and V. McKoy, *Phys. Rev. A* **24**, 2473 (1981); K. Takatsuka and V. McKoy, *Phys. Rev. A* **30**, 1734 (1984).
4. M. A. P. Lima, T. L. Gibson, K. Takatsuka, and V. McKoy, *Phys. Rev. A* **30**, 1741 (1984).
5. T. L. Gibson, M. A. P. Lima, K. Takatsuka, and V. McKoy, *Phys. Rev. A* **30**, 3005 (1984).
6. M. A. P. Lima, T. L. Gibson, W. M. Huo, and V. McKoy, *Phys. Rev. A* **32**, 2696 (1985).
7. M. A. P. Lima, T. L. Gibson, W. M. Huo, and V. McKoy, *J. Phys. B: At. Mol. Phys.* **18** L865 (1985).
8. W. M. Huo, V. McKoy, M. A. P. Lima and T. L. Gibson, *Thermophysical Aspects of Reentry Flow*, edited by J. Moss and C. Scott, (AAIA, New York, 1986).
9. L. M. Brescansin, M. A. P. Lima, W. M. Huo, and V. McKoy, *Phys. Rev. B* **32**, 7122 (1985).
- 10 M. A. P. Lima, T. L. Gibson, W. M. Huo, L. M. Brescansin, and V. McKoy, *Swarm Studies and Inelastic Electron-Molecule Collisions*, edited by L. Pitchford, V. Mckoy, A. Chutjian, and S. Trajmar, Springer Ser. Atom.

- Plasm. (Springer, Berlin, Heidelberg, 1986).
11. S. Geltman, *Topics in Atomic Collision Theory* (Academic Press, New York, 1969), p. 99.
 12. N. Maleki and J. Macek, *J. Phys. Rev.* **21**, 1403 (1980).
 13. H. Feshbach *Ann. Phys.* **5**, 357 (1958); **19**, 287 (1962).
 14. B. Friedman, *Principles and Techniques of Applied Mathematics* (Wiley, New York, 1960), p. 45.
 15. See, for example, C. J. Joachain, *Quantum Collision Theory* (North Holland, Amsterdam, 1975), p. 233.
 16. N. S. Ostlund, *Chem. Phys. Lett.* **34**, 419 (1975).
 17. D. A. Levin, A. W. Fliflet, M. Ma, and V. McKoy, *J. Comp. Phys.* **28**, 416 (1978).
 18. D. K. Watson, R. R. Lucchese, V. McKoy, and T. N. Rescigno, *Phys. Rev. A* **21**, 738 (1980).
 19. T. L. Gibson (unpublished).
 20. A. Temkin and K. V. Vasavada, *Phys. Rev.* **160**, 109 (1967).
 21. A. Temkin, K. V. Vasavada, E. S. Chang, and A. Silver, *Phys. Rev.* **186**, 57 (1969).
 22. E. U. Condon and H. Odabasi, *Atomic Structure* (Cambridge, London, 1980).

IV. Applications to Elastic Electron-Molecule Collisions

1. H₂

To assess the accuracy with which polarization is represented in the Schwinger multichannel formulation, we have calculated elastic integral and differential scattering cross sections for e-H₂ collisions from 1 to 10 eV. Our *ab initio* results are found to be in good agreement with other recent theoretical studies and with a variety of experimental data including measured differential cross sections. Our method is designed to be applicable to electronically inelastic collisions and to closed-shell target molecules of arbitrary geometry.

1.1 Introduction

Polarization effects are known to be very important¹ for low-energy electron collisions with molecules which do not possess large permanent dipole moments. In these cases, the polarization interaction has a significant effect on the overall shape and magnitude of the scattering cross section as well as on the width and position of resonances. Hence, there is considerable need for computationally feasible methods which can reliably include these effects. Although substantial progress has been made for some systems (most notably H₂ and N₂), no single method has yet been demonstrated for general use; *i.e.*, for elastic and electronically inelastic collisions with both linear and nonlinear molecular targets.

We begin by reviewing briefly some of the commonly used approaches for including polarization effects. These effects arise from the distortion of the molec-

ular charge distribution by the electric field of the incident electron. In the adiabatic approximation,^{2,3} the polarization potential for a particular value of \vec{r} is calculated by allowing the molecular orbitals to fully relax in the presence of a negative charged fixed at \vec{r} . However, this approximation fails in the near vicinity of the molecule where nonadiabatic dynamic corrections⁴⁻⁶ become important. A widely used and semiempirical approach to these dynamical effects assumes the known asymptotic form¹ of the polarization potential and includes a parameter-dependent cutoff function to mimic the nonadiabatic corrections. This method is easy to implement, but more complete treatments^{2,3} have revealed some of its inherent inadequacies. A further drawback is the need for parameters which are usually obtained by "tuning" so as to reproduce known features in the cross sections. This last difficulty is avoided in the polarized orbital method⁴⁻⁹ where Temkin's criterion¹⁰ is used to include nonadiabatic effects in an approximate but parameter-free fashion. However, the utility of the polarized orbital approach depends considerably on the particular way in which the method is implemented.⁶ Recently, another parameter-free model of polarization¹¹ has been applied to elastic scattering by H₂ and N₂. This model used the free-electron-gas correlation energy to represent polarization effects¹² in the near vicinity of the molecule and the known asymptotic form to represent long-range polarization effects. Comparison of the results obtained by this approach with those of more elaborate studies indicates that this method overestimates polarization effects somewhat.

Polarization effects arise from virtual electronic excitation of the target and can be represented by the inclusion of energetically closed channels in the expansion of the scattering wave function. Such an expansion in actual target eigenstates can converge slowly. Expansion in pseudostates generally converges faster and hence these pseudostates are often used both in close-coupling expansions¹³ and in the optical potentials which represent the polarization effects.^{14,15} Although these methods have a firmer theoretical basis than those described above, their application generally requires considerably greater effort. These pseudostates are also known to lead to nonphysical or spurious resonances in the scattering cross section. The number of such spurious resonances increases with the number of pseudostates although the resonance widths become narrower. Techniques for smoothing the T-matrices across these resonances have been proposed.¹⁶

In two recent papers,^{17,18} we have detailed the formal development of a Schwinger multichannel (SMC) theory for use in electron-molecule scattering and its first application to electronically inelastic $e - H_2$ collisions. In these applications we neglected the contribution from closed channels for consistency in comparison with the results of previous theoretical studies. However, the formulation also allows for the inclusion of a substantial number of closed electronic channels to represent polarization effects¹⁹ and, due to the manner in which the open and closed channel spaces are coupled, the SMC formulation is free of singularities on the real energy axis above the inelastic threshold. Further,

as implemented, our method is designed to be applicable to closed-shell target molecules of arbitrary geometry.

In this chapter we report results obtained with this method for elastic $e - H_2$ scattering including closed channel effects. This system provides a good test of how effectively the formulation can represent the effects of polarization since accurate experimental and theoretical cross sections are available for comparison. The computational details of our study can be found in Sec. 1.2 together with a discussion of our results and a comparison with other studies. In Sec. 1.3 we summarize our results and conclusions.

1.2 Procedures and Results

To assess the effectiveness with which closed channel effects can be represented in our method, we have calculated elastic integral and differential cross sections for $e - H_2$ scattering from 1 to 10 eV. This constitutes a nontrivial test of our theory since the exact static exchange (ESE) integral cross sections are known to be quite different from measured values in this energy range (cf. Fig. 5). Further, the $e - H_2$ system has been extensively studied and accurate experimental²⁰ and theoretical^{6,15} results for elastic scattering are available.

Our calculations are performed within the framework of the fixed-nuclei approximation.^{1,21} Here, the nuclei are held fixed at their equilibrium values and the dependence of the scattering amplitude on internuclear separation is neglected. The rotational levels are treated as degenerate and the physical cross sections are obtained by averaging the fixed-nuclei results over all molecular

orientations. Unless otherwise stated, atomic units are used throughout.

For the ground state of H_2 we used a SCF wave function obtained with a [6s3p/4s3p] Cartesian Gaussian basis at an internuclear separation of a 1.4 a_0 . The exponents and contraction coefficients are from the [5s2p/3s2p] set given by Huzinaga²² together with an additional set of diffuse s- and p-type functions. For convenience, the exponents and contraction coefficients are given in Table I. With this basis we obtain an SCF energy of $-1.13295 E_h$ and values of $\alpha_{\perp} = 4.54 a_0^3$, $\alpha_{\parallel} = 6.53 a_0^3$ for the perpendicular and parallel components of the polarizability, respectively. These polarizabilities are obtained from an SCF finite-field calculation and can be compared to the accurate values of $\alpha_{\perp} = 4.58 a_0^3$, $\alpha_{\parallel} = 6.39 a_0^3$. A set of H_2^- orbitals calculated with the same SCF basis was Schmidt orthogonalized to the occupied $1\sigma_g$ orbital and the resulting pseudo-orbitals used to construct the (N+1) particle determinants in the expansion of $\Psi_1^{(\pm)}$. The use of these one-particle pseudo-orbitals reduces the number of terms needed in the expansion of the closed channel space compared to the number required if the regular SCF virtual orbitals are used. The Gaussian basis sets used as additional scattering functions and in the insertion basis are also shown in Table I. For the energies considered here, expansion of the scattering functions solely in a discrete basis should be adequate. Also, for the purpose of this study, we restrict the partial wave expansion of the scattering amplitude to values of $l \leq 3$.

In the body-frame, all calculated results include contributions from the

${}^2\Sigma_g, {}^2\Sigma_u, {}^2\Pi_u,$ and ${}^2\Pi_g$ symmetries in $\Psi_1^{(\pm)}$. Of the available scattering basis, no more than 18(12) spatial functions were used to construct the open channel determinant in the expansion of $\Psi_1^{(\pm)}$ for $\Sigma(\Pi)$ symmetries. For the Σ symmetries the scattering set consists of a mixture of pseudo-orbitals and additional functions chosen to improve the flexibility of the basis. However, since there are no π -orbitals in the pseudo-orbital set, the scattering basis for the Π symmetries is made up entirely of additional functions. The $(N+1)$ particle closed channel determinants are formed from a set of target pseudostates consisting of a $1\sigma_g$ orbital and a pseudo-orbital together with an associated set of "scattering" functions. For the closed channels of Σ symmetry we used 10 pseudostates, each of which has an associated set of 7 scattering functions. In the Π symmetries we used 6 scattering functions with each of the 8 pseudostates.

As an initial step in this study we obtained ESE cross sections for comparison both with the results obtained with closed channels and as a preliminary test of our scattering and insertion basis sets. Our ESE integral cross sections are shown in Fig. 1 together with the ESE result of Collins, Robb, and Morrison.²³ The excellent agreement between these two sets of results indicates that our basis provides an accurate description of static-exchange scattering. Hence, any differences between our static-exchange-polarization (SEP) cross sections and those of other studies should arise from the treatment of polarization.

In Figs. 2-4 we present our SEP integral cross sections for the ${}^2\Sigma_g, {}^2\Sigma_u,$ and ${}^2\Pi_u$ symmetries, respectively. Also shown are the SEP results of Schneider

and Collins¹⁵ in which an optical potential is used to include polarization effects and those of Gibson and Morrison⁶ whose treatment of polarization is based on a polarized orbital approach. For purposes of comparison, we have included our ESE results. The $^2\Sigma_u$ and $^2\Pi_u$ cross sections of Figs. 3 and 4 show that the triplet-coupled target contributions to these cross sections are by no means negligible for this energy range. For the Σ symmetries our SEP results are in quite reasonable agreement with those of the other two studies, and a comparison shows that, with the exception of the lowest energy in the $^2\Sigma_g$ symmetry, almost all of the closed channel effects are accurately taken into account. In Fig. 4 we see that our SEP results for the $^2\Pi_u$ symmetry are essentially identical to those of Schneider and Collins.¹⁵

Table II contains our total integral cross sections as well as those obtained by Gibson and Morrison⁶ and the measured values of Jones and Bonham.²⁴ The results of Schneider and Collins¹⁵ in Table II were interpolated onto an eV energy mesh using a cubic spline routine and include contributions from the $^2\Sigma_g$, $^2\Sigma_u$, and $^2\Pi_u$ symmetries. The total cross sections are also shown in Fig. 5 along with our ESE results. Again, comparison shows that most of the closed channel effects are properly accounted for by our method. In our calculated cross sections of Fig. 5, we did not include pseudo-orbitals of π symmetry in the closed-channel expansion for the $^2\Sigma$ symmetries. Thus, configurations of the type $1\sigma n\pi m\pi$, which can be important at lower energies, were not included. To indicate the importance of such configurations, Fig. 5 shows the elastic cross

section at 1 eV obtained in including these ${}^2\Sigma(1\sigma n\pi m\pi)$ contributions.

Differential cross sections can provide greater insight into the scattering process and are a more stringent test of the theory than the integral cross sections. Our SEP differential cross sections are shown in Figs. 6-8 for scattering energies of 1, 3, and 10 eV along with the corresponding ESE cross sections and the measured values of Linder and Schmidt,²⁵ Srivastava *et al.*,²⁶ and Shyn and Sharp.²⁷ Although Schneider and Collins¹⁵ did not report differential cross sections, we show results calculated from the T-matrix elements of Gibson and Morrison.⁶ For consistency, the results labelled Gibson and Morrison in Figs. 6-8 use the same partial wave expansion as the present study; *i.e.*, Σ and Π symmetries with $\ell \leq 3$. Although the differential cross sections so calculated are not highly converged in the extreme forward and backward directions at 10 eV, the associated integral cross section is converged to better than 1%. These figures show that the substantial differences in the cross sections due to the inclusion of polarization are reproduced by our method. Further, our SEP results are in very reasonable qualitative and quantitative agreement with measured values.

1.3 Conclusions

In this section we have reported a study designed to assess the effectiveness of our Schwinger multichannel formulation in representing polarization effects in low-energy electron-molecule collisions. We chose to obtain elastic integral and differential cross sections for $e - H_2$ collisions from 1 to 10 eV. It is worth noting that these calculations were implemented entirely in an L^2 basis. The integral

cross sections show that our method can effectively and accurately represent most polarization effects without resorting to a large pseudostate expansion. Further, our differential cross sections were found to be in reasonably good agreement with existing measured values.

References

1. N. F. Lane, *Rev. Mod. Phys.* **52**, 29 (1980).
2. M. A. Morrison and P. J. Hay, *Phys. Rev. A*, **20**, 740 (1979).
3. D. G. Truhlar, D. A. Dixon, and R. A. Eades, *J. Phys. B.* **12**, 1913 (1979);
D. A. Dixon, R.A. Eades, and D. G. Truhlar, *ibid.*, **12**, 2741, (1979); R. A.
Eades, D. G. Truhlar, and D. A. Dixon, *Phys. Rev. A* **20**, 867 (1979); R.
A. Eades, D. A. Dixon, and D. G. Truhlar, *J. Phys. B*, **15**, 2265 (1982).
4. N. F. Lane and R. J. W. Henry, *Phys. Rev.* **173**, 183 (1968); R. J. W. Henry
and N. F. Lane, *ibid.*, **183** 221 (1969).
5. S. Hara, *J. Phys. Soc. Jpn.* **27** 1262 (1969).
6. T. L. Gibson and M. A. Morrison, *Phys. Rev. A* **29**, 2497 (1984) and
references therein; T. L. Gibson and M. A. Morrison, *J. Phys. B* **15**, L221
(1982).
7. C. A. Weatherford, R. J. W. Henry and M. C. Bruels, *Proc. Indian Natl.
Sci. Acad. Part A* **39**, 437 (1973).
8. A. Jain and D. G. Thompson, *J. Phys. B* **15**, L631 (1982); A. Jain and D.
G. Thompson, *ibid.*, **17**, 443 (1983).
9. K. Onda and A. Temkin, *Phys. Rev. A* **28**, 621 (1983).
10. A. Temkin, *Phys. Rev.* **107**, 1004 (1957); A. Temkin and J. C. Lamkin,
ibid., **121**, 788 (1961).
11. N. T. Padial and D. W. Norcross, *Phys. Rev. A* **29**, 1742 (1984).
12. J. O'Connell and N. F. Lane, *Phys. Rev. A* **27**, 1893 (1983).

13. B.I. Schneider, *Chem. Phys. Lett.* **51**, 578 (1977).
14. A. Klonover and U. Kaldor, *J. Phys. B* **11**, 1623 (1978).
15. B. I. Schneider and L. A. Collins, *J. Phys. B* **15**, L335 (1982); B. I. Schneider and L. A. Collins, *Phys. Rev. A* **27**, 2847 (1983) (and private communication).
16. P. G. Burke, K. A. Berrington, and C. V. Sukumar, *J. Phys. B* **14**, 289 (1981).
17. K. Takatsuka and V. McKoy, *Phys. Rev. A* **30**, 1734 (1984).
18. M. A. P. Lima, T. L. Gibson, K. Takatuska, and V. McKoy, *Phys. Rev. A* **30**, 1741 (1984).
19. A preliminary form of this method has been applied to e-H scattering. See K. Takatsuka and V. McKoy, *Phys. Rev. A* **24**, 2473 (1981).
20. For a recent review of the experimental literature see S. Trajmar, D. F. Register, and A. Chutjian, *Phys. Repts.* **97**, 219 (1983).
21. A. Temkin and K. V. Vasavada, *Phys. Rev.* **160**, 109 (1967); A. Temkin, K. F. Vasavada, E. S. Chang, and A. Silver, *ibid.*, **186**, 57 (1969).
22. S. Huzinaga, *J. Chem. Phys.* **42**, 1293 (1965).
23. L. A. Collins, W. D. Robb, and M. A. Morrison, *Phys. Rev. A* **21**, 488 (1980).
24. R. Jones and R. A. Bonham. The results quoted here are from Table 2a of Reference 26.
25. F. Linder and H. Schmidt, *Z. Naturforsch.* **26a**, 1603 (1971). The results

shown here are the renormalized values given in Table 4a of Reference 26.

26. S. K. Srivastava, A. Chutjian and S. Trajmar, *J. Chem. Phys.* **63**, 2659 (1975).
27. T. W. Shyn and W. E. Sharp, *Phys. Rev. A* **24**, 1734 (1981).

Table I. Cartesian Gaussian Basis Set^a

Gaussian Center and type	Exponents (α)
H, ^{b,c} 4s	33.644, 5.05796, 1.4668, 0.321144, 0.101309, 0.06
H, ^b 3p _x	1.1142, 0.2592, 0.06
H, ^d 6p _x , 6p _y	1.08, 0.54, 0.18, 0.06, 0.02, 0.01
Midpoint, ^e 1s	0.01
Midpoint, 4p _x	0.25, 0.05, 0.01, 0.002
Midpoint, 3d _{xy}	0.4, 0.1, 0.025
H, ^f 3s	17.75, 9.34, 2.2926
H, 2p _x	3.2, 0.49248
H, 2p _x , 2p _y	2.16, 0.3118
Midpoint, ^f 1s	0.05
Midpoint, 2p _x	0.09, 0.01
Midpoint, 3d _{xy}	1.2, 0.2, 0.05

^a Defined by $X_{lmn}^{(\alpha)} = N_{lmn}(x - A_x)^l (y - A_y)^m (z - A_z)^n e^{-\alpha|\vec{r}-\vec{A}|^2}$, where \vec{A} is the position of the Gaussian center.

^b Basis set used for the $X^1\Sigma_g^+(1\sigma_g)^2$ state of H₂.

^c The first three basis functions are contracted with coefficients of 0.025374, 0.189683, 0.85293, respectively.

^d Additional functions used to expand the scattering functions for the $^2\Pi_{g,u}$ symmetries.

^e Same as *d* but for $^2\Sigma_{g,u}$ symmetries.

^f Additional functions used in the insertion around $VG_P^{(+)}V$.

Table II. Integral Cross Sections for e-H₂ ($\times 10^{-16} \text{cm}^2$)

Impact				
energy (eV)	JB^a	GM^b	SC^c	SMC^d
1	13.1	12.84	12.48	13.59
2	15.4	14.80	14.51	14.32
3	16.2	15.65	15.14	14.92
4	15.7	15.49	15.03	14.71
5	14.9	14.74	14.36	14.13
6	13.9	13.77	13.48	13.39
8	12.0	11.79	11.68	11.64
10	10.3	10.09	10.11	10.11

^a Experimental results of Reference 24.

^b Calculated results of Reference 6.

^c Interpolated from the results of Reference 15.

^d Present results.

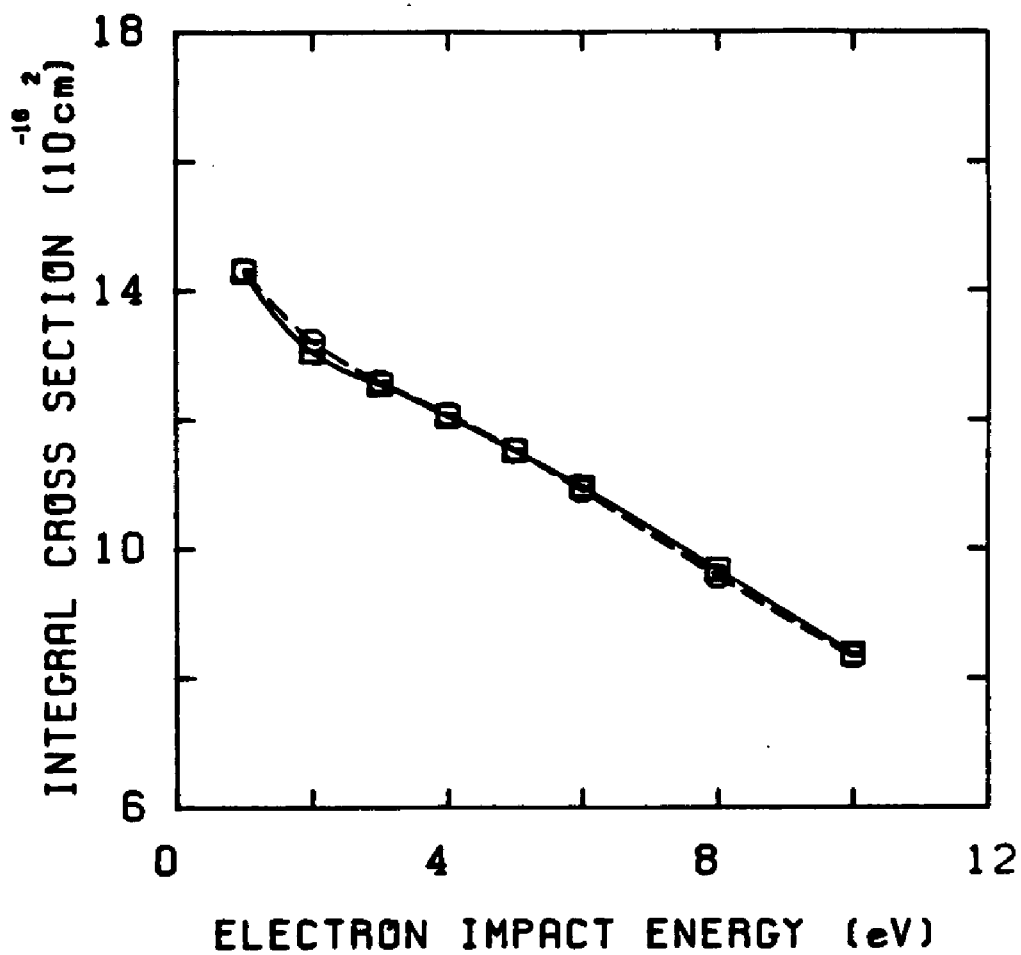


Figure 1: Elastic cross section for the $e - H_2$ scattering in the static-plus-exchange (SE) approximation: present results (□), SE results of Ref. 23 (○).

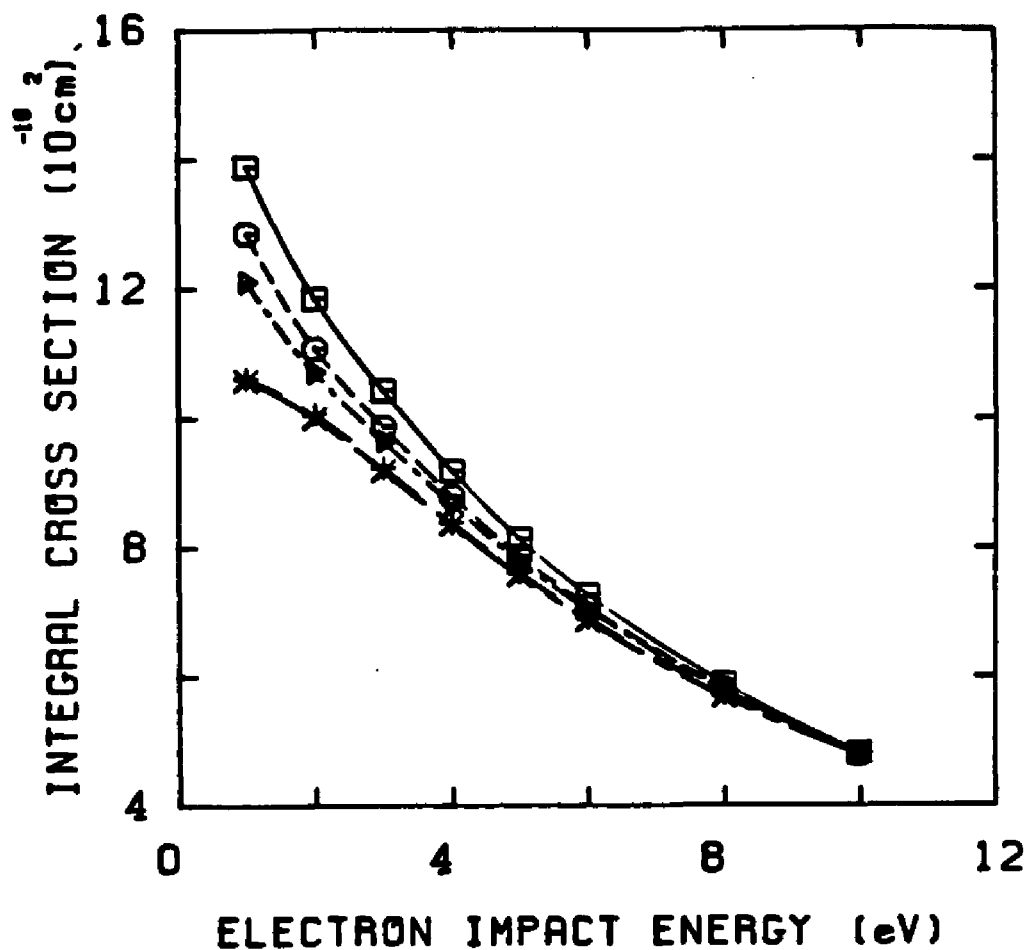


Figure 2: Elastic cross sections for the $^2\Sigma_g$ symmetry: present SE results (\square), present results including only singlet-coupled pseudo-states in the closed channel expansion (\circ), present results including singlet-coupled and triplet-coupled pseudo-states in the closed channel expansion (\triangle), static-plus-exchange-plus-polarization (SEP) results of Ref. 15 (\times), SEP results of Ref. 6 ($+$).

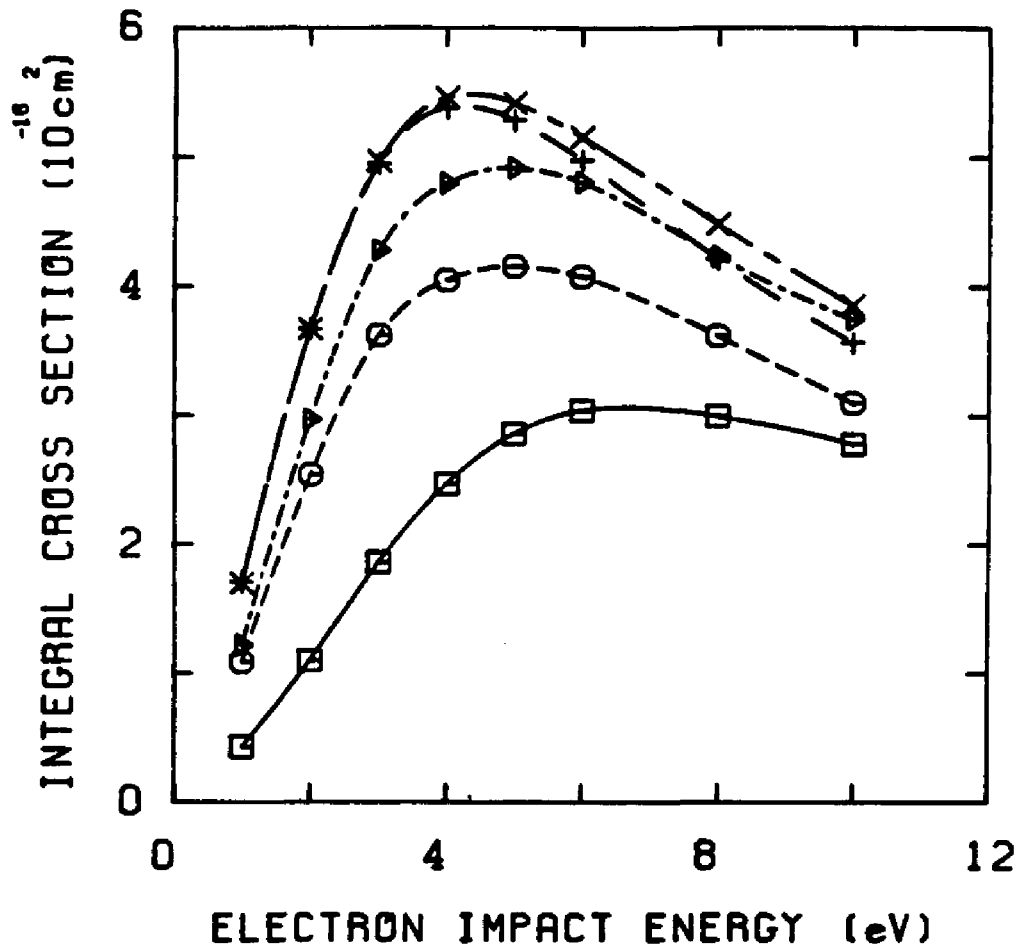


Figure 3: Elastic cross sections for the $^2\Sigma_u$ symmetry: same label as in Fig. 2.

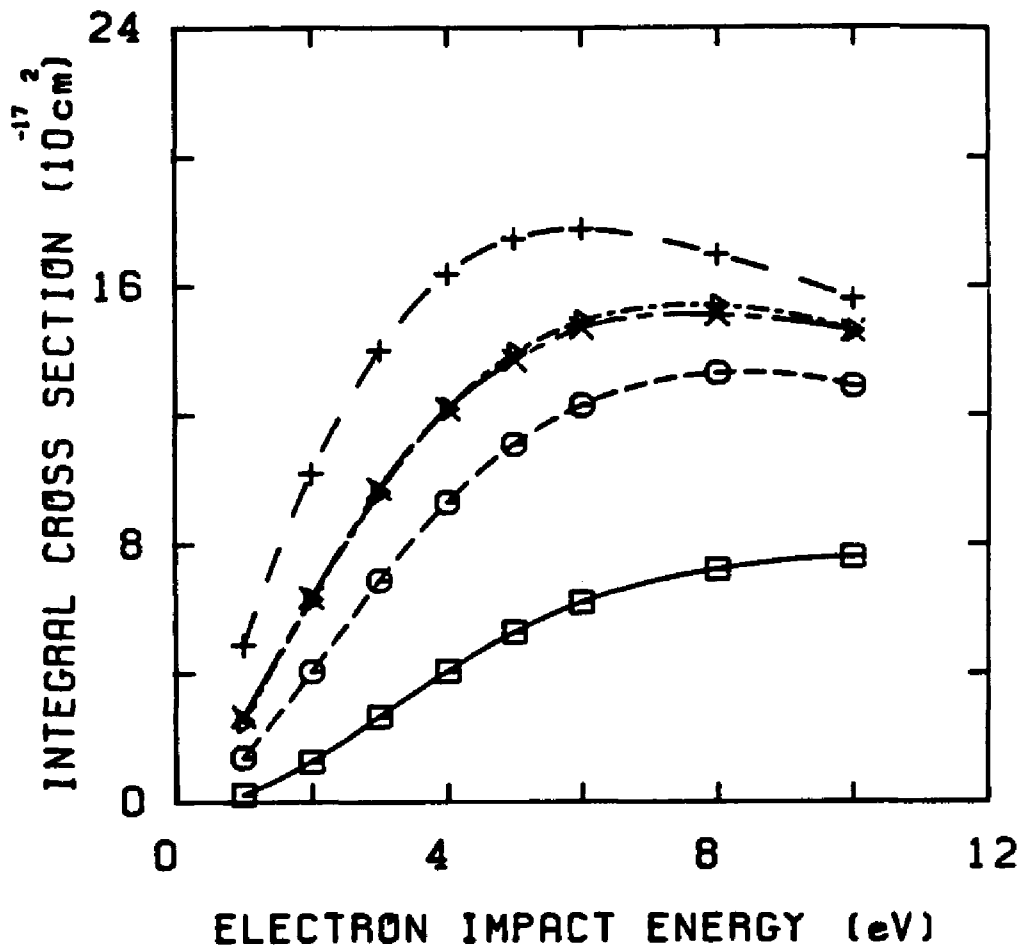


Figure 4: Elastic cross sections for the $^2\Pi_u$ symmetry: same label as in Fig. 2.

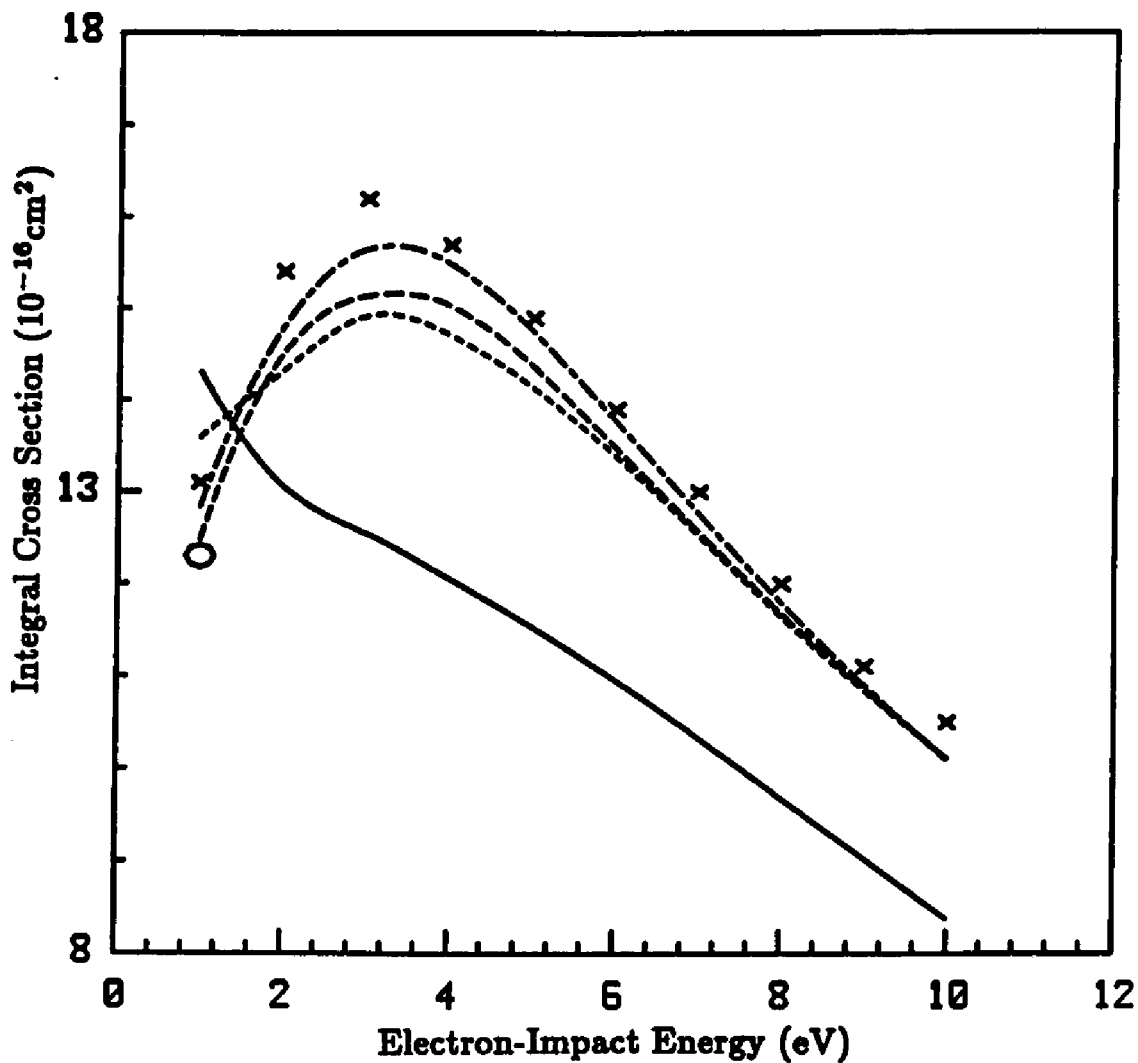


Figure 5: Elastic cross section for $e - \text{H}_2$ scattering: present SE results (solid line), present SEP results (short dashed line), SMEP results of Ref. 15 (long-short dashed line), SMEP results of Ref. 6 (long dashed line), measured values of Ref. 24 (\times), present SEP result at 1 eV including $^2\Sigma$ ($1\sigma n\pi m\pi$) contributions (O).

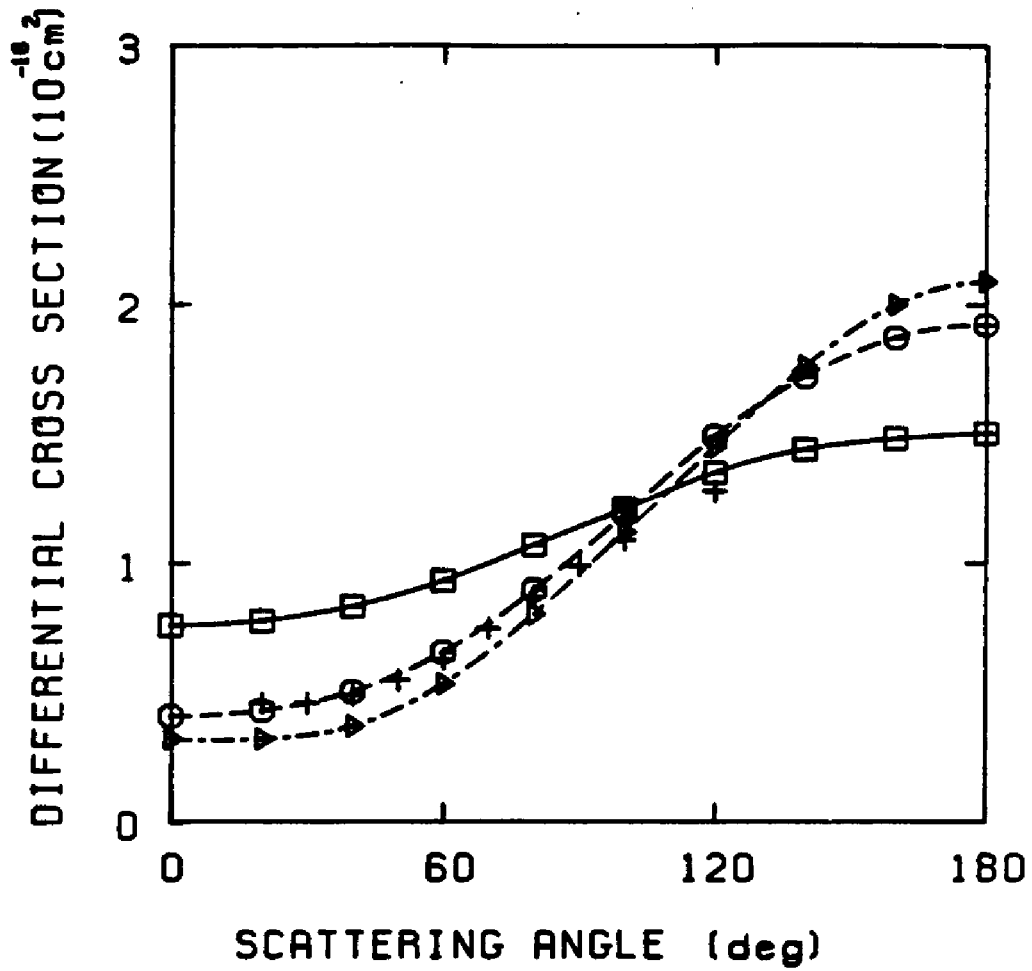


Figure 6: Elastic differential cross section (DCS) for $e - H_2$ scattering at 1 eV: present SE results (□), present SEP results (○), SEP results of Ref. 6 (△), measured values of Ref. 25 (+).

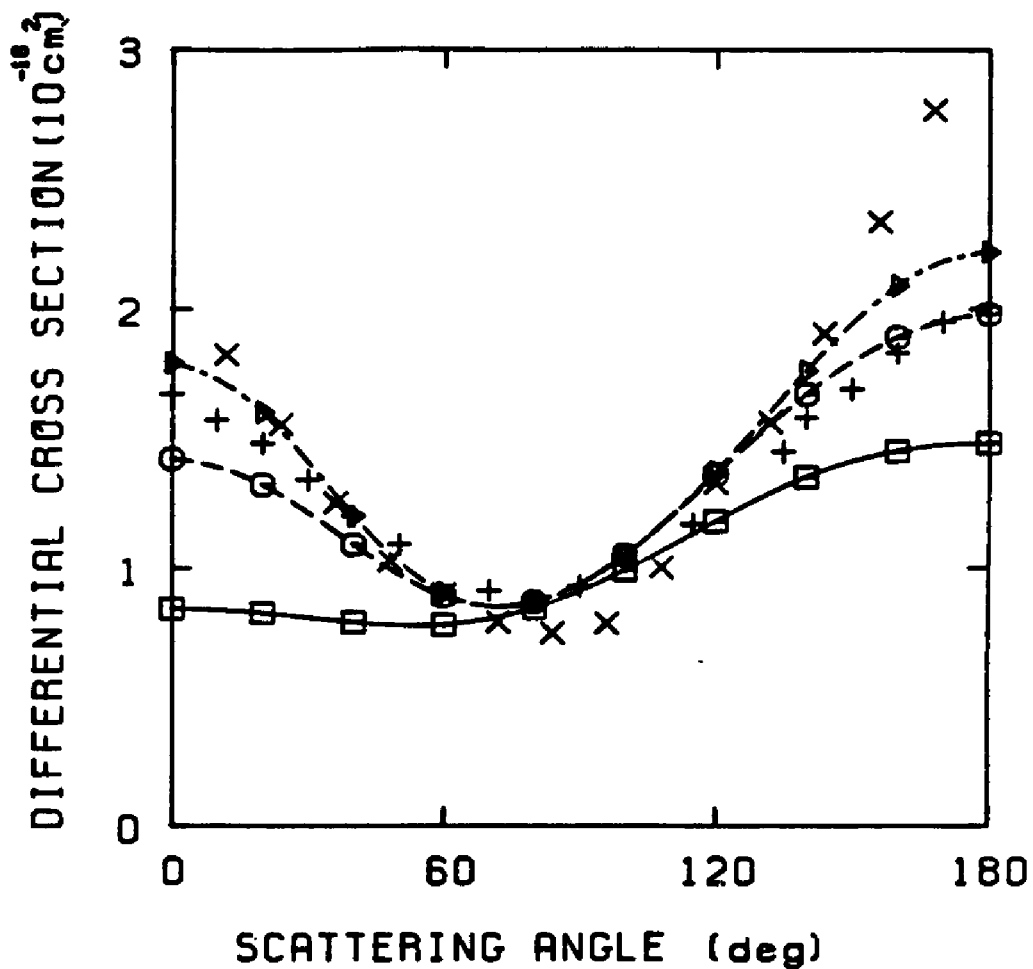


Figure 7: Elastic differential cross section (DCS) for $e-H_2$ scattering at 3 eV: present SE results (\square), present SEP results (\circ), SEP results of Ref. 6 (\triangle), measured values of Ref. 26 (+). measured values of Ref. 27 (\times).

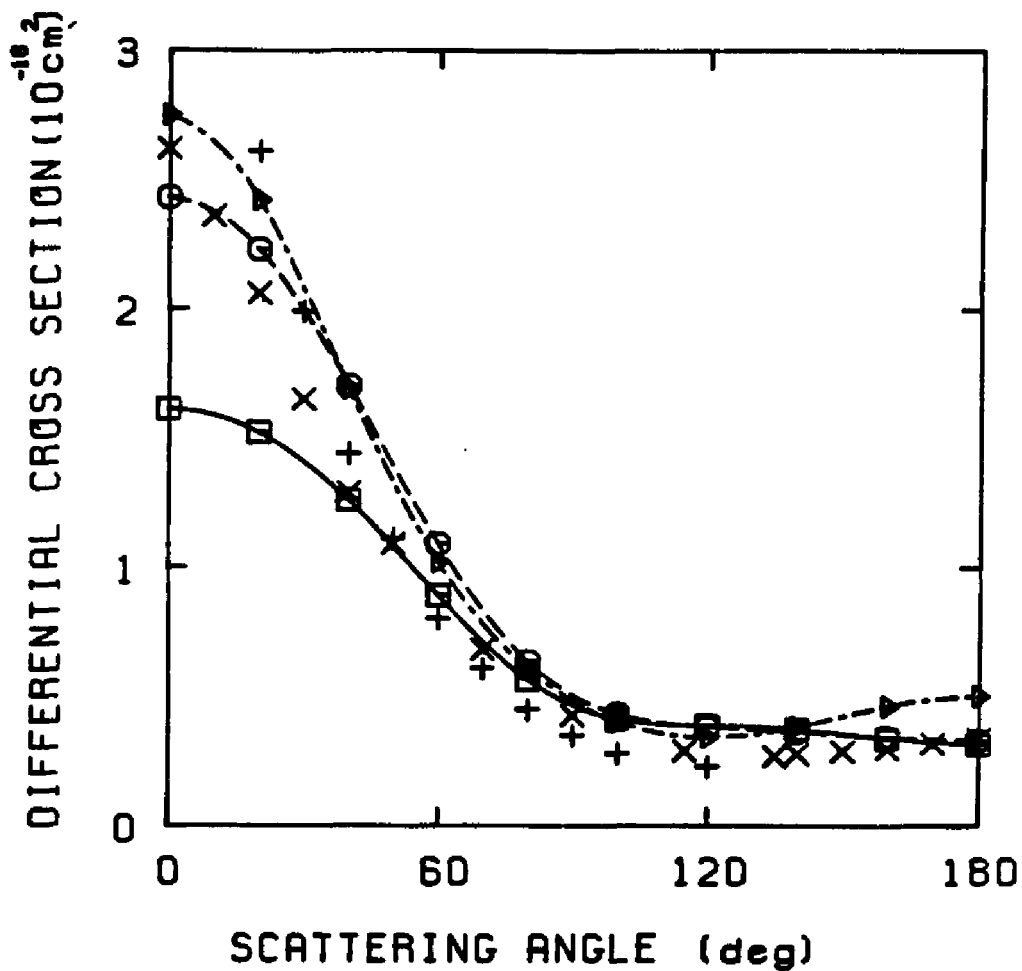


Figure 8: Elastic differential cross section (DCS) for $e - H_2$ scattering at 10 eV: present SE results (\square), present SEP results (\circ), SEP results of Ref. 6 (\triangle), measured values of Ref. 25 ($+$), measured values of Ref. 26 (\times).

2. N₂

In the following we present the first application of the Schwinger Multi-channel Collisions (SMC) formulation to the study of a shape resonance. We discuss the results obtained for $^2\Pi_g$ resonance in N₂ scattering. This resonance has received much attention due to its role in the vibrational excitation of N₂ by electron impact and in electron transport properties. Considering the sensitivity of theoretical calculations of cross sections near shape resonances, we use the present studies to discuss some criteria of convergence of our procedures.

2.1 Introduction

Low-energy electron-molecule collisions play an important role in the modelling of planetary atmosphere, gas lasers, and swarm and plasma etching processes. Among such systems, the $^2\Pi_g$ channel of N₂ has received much attention as a result of its role in the vibrational excitation of N₂ by electron impact and electron transport properties. Experimental and theoretical studies on this resonance have been reviewed by Schulz,¹ Trajmar *et al.*,² and Lane.³ The first *ab initio* determination of the width of the 2.3 eV shape resonance in this channel was carried out by Schneider *et al.*,⁴ using the R-matrix method. Width calculations have also been carried by Hazi and co-workers^{5,6} using the Stieltjes technique. More recent R-matrix calculations include the work of Burke *et al.*⁷ and Le Dourneuf *et al.*⁸ In addition, this channel has been studied using an iterative close-coupling method,⁹ a many-body optical-potential approach,¹⁰ a noniterative partial-differential-equation method,^{11,12} a linear algebraic method,^{13,14} a

complex coordinate SCF technique,¹⁵ as well as a standard bound-state configuration interaction (CI) method with noninteger nuclear charges.^{16,17} The importance of electron correlation (polarization) is amply demonstrated in these calculations.

The Schwinger multichannel (SMC) formulation^{18,19} is a general method for the calculation of elastic and electronically inelastic electron-molecule collision cross sections at low and intermediate energies for molecules of arbitrary symmetry. It has been applied to the treatment of elastic scattering by H₂, CH₄, and H₂O with good success.²⁰⁻²² Its applicability to inelastic collisions has been demonstrated in recent studies of the electron impact excitation of H₂, both in the gas phase²³ and as an oriented molecule to simulate surface scattering.²⁴ In this section, we apply the SMC formulation to the study of the ²Π_g resonance in low-energy e-N₂ scattering. The purpose of this study is twofold. First, this is the first application of the SMC formulation to the study of a shape resonance. While our previous study of e-H₂ system²⁰ demonstrated that polarization can be treated reliably by the SMC method, the important correlation effects in that system are of the long-range type.¹⁴ On the other hand, short-range correlations dominate in the ²Π_g resonance in N₂. It is of interest to test how well this kind of correlation can be treated in the SMC method. Secondly, for the design of the next generation of space vehicles, the modelling of the flowfield upon their re-entry into the earth's atmosphere requires the knowledge of elastic and inelastic collision cross section between low-energy electrons and ro-vibrationally hot

molecules. Such data are not available experimentally due to the difficulty in preparing targets at high ro-vibrational temperatures. The SMC formulation is well suited to provide such data, since it does not encounter additional computational difficulty when the molecule is near dissociation. Also, since the method can treat both elastic and inelastic collisions, the plane-wave integrals obtained in the elastic calculation can, at least in principle, be used as part of the input in the inelastic calculation to achieve computational economy. A calculation of vibrational excitation cross sections of ro-vibrationally hot N_2 , based on the widths deduced from the present work, has been reported elsewhere.²⁵

In the following section we discuss details of the calculations. Particular attention is paid to the choice of the insertion basis set used in the L^2 representation of the free-particle Green's function and in the choice of closed channel configurations to represent the polarization effects. Our results are summarized in Sec. 2.3.

2.2 Computational Procedure and Results

In the present calculation, the incident electron energy is below the excitation energy of the lowest excited electronic state of N_2 . Thus the elastic channel is the only open channel. The total wavefunction $\Psi_1^{(+)}$ is expanded in a basis of $(N+1)$ -particle Slater determinants,

$$T_{\vec{k}_f, \vec{k}_i} = \sum_{ij} \langle S_{\vec{k}_f} | V | \psi_i \rangle A_{ij}^{-1} \langle \psi_j | V | S_{\vec{k}_i} \rangle. \quad (1)$$

The Slater determinants, ψ_i , are constructed from an orthogonal set of molecu-

lar orbitals which are in turn expanded in a set of Cartesian Gaussian functions. With this choice of basis, all the matrix elements appearing in Eq. (1), except for those of $VG_P^{(+)}V$, can be evaluated for molecules of arbitrary geometry.²¹ Furthermore, the $VG_P^{(+)}V$ matrix elements can be obtained in closed form using the following procedure. The principal value contribution to the $VG_P^{(+)}V$ matrix element is obtained by inserting a large set of Cartesian Gaussian functions around $G_P^{(+)}$, whereas the contribution from the poles of $G_P^{(+)}$ is evaluated exactly. This procedure results in an S matrix which is very nearly unitary without resorting to an enormous quadrature basis.²⁶

a. Gaussian Basis set for $\Psi_1^{(+)}$

A Gaussian basis set with 11s8p3d basis functions on each nucleus is used in the representation of $\Psi_1^{(+)}$. We started with the 9s5p2d/5s3p2d basis set used by Langhoff *et al.*,²⁷ in their calculation of the static polarizability of N_2 . Their values for $\alpha_{||}$ calculated with an SCF and CI wavefunctions at the experimental R_e are 14.908 and 14.868 a.u., respectively, to be compared with the experimental values of 15.05²⁸ and 14.76.²⁹ The SCF and CI values for α_{\perp} are 9.514 and 10.196 a.u., versus experimental values of 10.35²⁸ and 10.25.²⁹ We uncontracted this basis set and added diffuse s, p, and d functions. The need for diffuse s and p functions was demonstrated in a static-exchange calculation with a (s,p) basis set. It is found that the inclusion of diffuse functions changed both the position and width of the resonance. The final 11s8p3d basis set is given in Table I. Using the SCF wavefunction calculated with this basis set, the quadrupole moment of

N_2 is determined at the SCF R_e to be -0.936 a.u., versus an experimental³⁰ value of -1.04 ± 0.07 .

b. Insertion Basis set for $G_p^{(+)}$

While the choice of the Gaussian basis set, molecular orbitals, and Slater determinants in the representation of $\Psi_1^{(+)}$ can be made based on certain physical assumptions and previous calculations of other physical properties, the L^2 -representation of $G_p^{(+)}$ is a more mathematical approximation. The reliability of the solution of Eq. (1) depends on the completeness of this insertion basis and care must be exercised on its choice. In our earlier application of the SMC method,^{20,31} all the contributions to the $VG_p^{(+)}V$ matrix element were determined using the quadrature (α insertion), and the unitarity of the calculated S matrix was used as the criterion for the completeness of the insertion basis. We have since adapted the practice of calculating the contribution from the poles of $G_p^{(+)}$ exactly and have used the insertion basis only for the principal value contribution (k insertion), resulting in an S matrix which is almost exactly unitary. However, due to the lack of a better criterion, we reverted to α insertion in testing the insertion basis and depended on the unitarity of the S matrix as a guide, even though our final results were calculated using the k insertion technique. This practice was based on the rationale that the representation of $G_p^{(+)}$ near its poles should also be important to the principal value part of $VG_p^{(+)}V$. There was some numerical support for this conjecture since we found that the insertion functions which did not improve the unitarity condition also had little

effect on the T matrix, as discussed further below.

Our insertion basis always includes the original Gaussian basis set used for $\Psi_1^{(+)}$, since all the necessary integrals have already been calculated. Table II presents two sets of additional d_{xx} functions used in the ${}^2\Pi_{g,x}$ channel calculation. It is noticed that none of the insertion basis contains very diffuse functions. This is somewhat surprising because normally such functions are expected to be important in an L^2 representation of $G_P^{(+)}$. Our original trial basis did include very diffuse d_{xx} functions, but they were eliminated based on the unitarity criterion discussed above. We think this result may be a reflection of the quasi-bound state character of the ${}^2\Pi_g$ channel and is not generally applicable to all insertion calculations. We also found that the calculations near the resonance to be particularly sensitive to the choice of insertion basis. Figure 1 presents the eigenphase sum, δ_{sum} , as a function of incident electron energy at the target internuclear distance, $R = 1.9$ bohr, calculated using insertion basis I and II and the k insertion technique. Calculations using the α insertion showed that basis I failed the unitarity condition completely at 0.25-0.27 Ry, but at other energies the unitarity condition was rather well satisfied, whereas for basis II the largest deviation from unitarity was 9%. It is seen that the two curves are in good agreement except in the region where unitarity fails for basis I. It should be remembered that the data used in the figure were actually calculated using k insertion with perfect unitarity, even for basis I. We consider that the results in Fig. 1 justify our use of the α insertion technique and unitarity condition as a guide in the

choice of the insertion basis. Figure 1 also demonstrates the importance of a good insertion basis in a Schwinger-type calculation, since an erroneous width would be deduced using basis I.

c. Choice of molecular orbitals and closed channel configurations

In our calculation, an SCF wavefunction is used to represent the target in the asymptotic region. In the static exchange approximation, the (N+1)-particle wavefunction is expanded in terms of the following set of Slater determinants

$$\Psi_1^{(+)} = \sum_k c_k \mathcal{A}\{\phi_1 \phi_2 \dots \phi_n \phi_k\}, \quad (2)$$

where \mathcal{A} is the antisymmetrization operator, $\phi_1, \phi_2, \dots, \phi_n$ are target SCF orbitals, and ϕ_k is an orbital generated from the Gaussian set for $\Psi_1^{(+)}$ and orthogonalized to the target orbitals. Since the full set of ϕ_k is used, the result is independent of the choice of orbitals. However, in a polarization (correlation) calculation, $\Psi_1^{(+)}$ is represented by a POLCI-type wavefunction,

$$\begin{aligned} \Psi_1^{(+)} = & \sum_k c_k \mathcal{A}\{\phi_1 \phi_2 \dots \phi_n \phi_k\} \\ & + \sum_{i,j,k} c_{i,j,k} a_j a_i^\dagger \mathcal{A}\{\phi_1 \phi_2 \dots \phi_n \phi_k\}, \end{aligned} \quad (3)$$

where the operator a_i^\dagger annihilates an electron occupying one of the target orbitals ϕ_i and a_j creates an electron in orbital ϕ_j and $c_{i,j,k}$ is the coefficient associated with this closed channel configuration. The closed channel configurations describe the mutual distortion of the incoming electron and the target. Our present computer code is limited in the total number of Slater determinants

used in $\Psi_1^{(+)}$. Since this is far from the size of the full set of all possible closed channel configurations, a judicial choice of the orbital basis and closed channel configurations must be made to achieve reliable results. While our code is being extended, we believe the procedure used in the N_2 calculation is physically meaningful and a description is given here. Two different orbital sets were tried: virtual orbitals from the target SCF calculation with the π_g orbitals replaced by the corresponding set obtained from an IVO calculation of N_2^- and the set of natural orbitals obtained from a standard POLCI calculation for N_2^- using a bound-state code. Within the limitation of our code, we were not able to obtain any correlation effects using the first set. We believe this is due to the inadequacy of the virtual orbitals to describe the distortion of the target. On the other hand, a bound-state POLCI calculation (including all possible configurations) can be used efficiently in describing the relaxation of the target in the presence of an extra electron. Of course, the use of a bound-state code to calculate N_2^- , without imposing any stabilization constraint nor the correct boundary condition, results in a N_2^- wavefunction which is a mixture of continuum and bound states. Nevertheless, the natural orbitals from such a calculation, ordered according to their occupation in the density matrix, enables us to truncate the set of orbitals used for the closed channel configurations in the SMC calculation. While we cannot carry out the full expansion in Eq. (3) to establish convergence, we find that, cutting back the orbitals used in the second expansion in Eq. (3) by half, results in 3% change in the calculated cross section near resonance, giving us confidence

that the truncation of the orbitals based on the natural orbitals is indeed valid. It should be noted that the full set of orbitals is used in the first sum in Eq. (3) (static-exchange terms) and that orbital truncation deals only with the second sum (polarization terms). Table III presents the truncated orbital basis used in the polarization calculations.

The closed channel configurations describe the correlation effects between the continuum electron and the bound electrons. The pair functions, used to describe the correlation, can be divided into two types: radial correlation (or in-out correlation) where each electron is promoted (or demoted) into an orbital of the same symmetry, and angular correlation where each electron is promoted to an orbital of different symmetry. Schneider and Collins¹⁴ have discussed the effect of such terms in their study of e-N₂ scattering using the linear-algebraic-optical potential method. They identified the radial correlation as a short-range correlation. The angular correlation, with electron promotion limited to dipole-allowed configurations, is identified as a long-range correlation since it reduces to the r^{-4} potential at large r . Nevertheless, the angular correlation terms include a short-range component also. The effect of these correlations terms was studied in our determination of important closed channel configurations. We started by studying the effect of correlating individual pairs, *e.g.*, the $3\sigma_g$ electron with the continuum electron, with all possible radial and correlation terms included. We found virtually no effect in correlating the $1\sigma_g$, $1\sigma_u$, and $2\sigma_g$ electrons and a small effect in correlating the $2\sigma_u$. The most important contribution comes from

correlating the six outermost electrons in $3\sigma_g$, $1\pi_{u_x}$, and $1\pi_{u_y}$ orbitals. Also, we see very small correlation effects from the dipole allowed angular correlation terms. Based on our results for the individual pair correlations, we choose two set of closed channel configurations, set I with radial correlation terms only, and set II with both radial and angular correlations. The closed channel configurations can be obtained from Table III by combining the ϕ_i , ϕ_j , and ϕ_k tabulated there. In both sets, only six of the target electrons are correlated. Nevertheless, there are certain residual correlation effects from the $2\sigma_g$ and $2\sigma_u$ electrons since we use the set of natural orbitals from a CI calculation which included the correlation of those electrons, and the ordering of the natural orbital is affected by their correlation. It is also noted that the term "radial correlation" is a misnomer. Since the closed shell configurations are expressed in terms of Slater determinants, the configuration $c_{i,j,k} a_j a_i^\dagger \mathcal{A}\{\phi_1 \phi_2 \dots \phi_n \phi_k\}$ can also be written as $c_{i,k,j} a_k a_i^\dagger \mathcal{A}\{\phi_1 \phi_2 \dots \phi_n \phi_j\}$. In the terminology of Schneider and Collins,¹⁴ Set I corresponds to a 13-reference calculation and set II is a 21-reference calculation. Fig. 2 compares the eigenphase sums calculated at $R=2.068$ bohr using the two sets of closed channel configurations. It is seen that set II lowers the resonance energy by 0.3 eV. This result is reminiscent of those obtained by Schneider and Collins.¹⁴ It is interesting to note that the effect of angular correlation terms for each individual electron pair is very small, but their combined effect, when all six target electrons are correlated with the continuum electron, is much stronger than the sum of their individual contributions.

Finally, in Fig. 3 we present the eigenphase sums at $R=2.608$ bohr, calculated using configuration set I, along with the results of Berman and Domcke¹⁰ and Gibson.³²

Conclusions

We presented a study of the shape resonance in $e - N_2$ scattering. We also presented some criteria of convergence of our results with respect to the Gaussian representation of the principal value of the Green's function. We found that the k insertion yields relatively good results at all energies except in the near vicinity of the resonance. However, in the vicinity of the resonance, when more elaborate Gaussian basis sets are used for the α insertion, we also obtain very good results.

References

1. G. J. Schulz, *Rev. Mod. Phys.* **45**, 423 (1973).
2. S. Trajmar, D. F. Register, and A. Chutjian, *Phys. Repts.* **97**, 219 (1983).
3. N. F. Lane, *Rev. Mod. Phys.* **52**, 29 (1980).
4. B. I. Schneider, M. Le Dourneuf, and Vo Ky Lan, *Phys. Rev. Lett.* **43**, 1926 (1979).
5. A. U. Hazi, T. N. Rescigno, and M. Kurilla, *Phys. Rev. A* **23**, 1089 (1981).
6. A. U. Hazi, *Electron-Atom and Electron-Molecule Collisions*, edited by J. Hinze (Plenum, New York, 1983) p. 103.
7. P. G. Burke, C. J. Noble, and S. Salvini, *J. Phys. B* **16**, L113 (1983).
8. M. Le Dourneuf, V. K. Lan, and B. I. Schneider, in *Electron-Atom and Electron-Molecule Collisions*, edited by J. Hinze (Plenum, New York, 1983) p. 135.
9. L. A. Collins, W. D. Robb, and M. A. Morrison, *Phys Rev. A* **21**, 488 (1980).
10. M. Michael Berman and W. Domcke, *Phys. Rev. A* **29**, 2485 (1984).
11. K. Onda and A. Temkin, *Phys. Rev. A* **28**, 621 (1983).
12. C. A. Weatherford, K. Onda, and A. Temkin, *Phys. Rev. A* **31**, 3620 (1985).
13. B. I. Schneider and L. A. Collins, *Phys. Rev. A* **27**, 2847 (1983).
14. B. I. Schneider and L. A. Collins, *Phys. Rev. A* **30**, 95 (1984).
15. T. N. Rescigno, A. E. Orel, and C. W. McCurdy, *J. Chem. Phys.* **73**, 6347 (1980).
16. B. Nestmann and S. D. Peyerimhoff, *J. Phys. B* **18**, 615 (1985).

17. B. Nestmann and S. D. Peyerimhoff, *J. Phys. B* **18**, 4309 (1985).
18. K. Takatsuka and V. McKoy, *Phys. Rev. A* **24**, 1267 (1981).
19. K. Takatsuka and V. McKoy, *Phys. Rev. A* **30**, 2473 (1984).
20. T. L. Gibson, M. A. P. Lima, K. Takatsuka, and V. McKoy, *Phys. Rev. A* **30**, 3005 (1984).
21. M. A. P. Lima, T. L. Gibson, W. M. Huo, and V. McKoy, *Phys. Rev. A* **32**, 2696 (1985).
22. L. M. Brescansin, M. A. P. Lima, T. L. Gibson, W. M. Huo, and V. McKoy, *J. Chem. Phys.* (submitted for publication, 1986).
23. M. A. P. Lima, T. L. Gibson, W. M. Huo, and V. McKoy, *J. Phys. B* **18**, L865 (1985).
24. L. M. Brescansin, M. A. P. Lima, W. M. Huo, and V. McKoy, *Phys. Rev. B* **32**, 7122 (1985).
25. W.M. Huo, V. McKoy, M.A.P. Lima and T.L. Gibson, *Thermophysical Aspects of Reentry Flow*, edited by J. Moss and C. Scott (AAIA, New York, 1986).
26. T. L. Gibson (to be published).
27. S. R. Langhoff, C. W. Bauschlicher, Jr., and D. P. Chong, *J. Chem. Phys.* **78**, 5287 (1983).
30. N. J. Bridge and A. D. Buckingham, *Proc. R. Soc. London Ser A* **295**, 334 (1966).
28. G. R. Alms, A. W. Burham, and W. H. Flygare, *J. Chem. Phys.* **63**, 3321

(1975).

29. G. Herzberg, *Spectra of Diatomic Molecules* (Litton, New York, 1950).
31. M. A. P. Lima, T. L. Gibson, K. Takatsuka, and V. McKoy, *Phys. Rev. A* **30**, 1741 (1984).
32. T. L. Gibson (private communication, 1986).

Table I. Gaussian basis set used in the representation of $\Psi_1^{(+)}$. All basis functions are centered at the nucleus.

Type	Exponent
s	5909.0, 887.5, 204.7, 59.84, 20.0, 7.193, 2.686, 0.7, 0.2133, 0.07, 0.03
p_x, p_y, p_z	26.79, 5.956, 1.707, 0.5314, 0.1654, 0.06, 0.02, 0.01
d_{xx}, d_{yy}, d_{zz}	0.95, 0.2639, 0.06
d_{xy}	0.95

Table II. Gaussian basis set used in the representation of $G_P^{(+)}$

Basis set	Exponent of mid-point d_{x_2} functions
Set I: Basis set from Table I plus 10 d_{x_2} functions at midpoint	240, 120, 60, 30, 15, 8, 4, 2, 1, 0.25
Set II: Basis set from Table I plus 15 d_{x_2} functions at midpoint	4800, 2400, 1200, 600, 480, 240, 120, 60, 30, 15, 8, 4, 2, 1, 0.25

Table III. Closed channel configurations used for the $^2\Pi_{g^{\pm}}$ channel

ϕ_i	ϕ_j	ϕ_k
Set I		
$3\sigma_g$	4, 5, 6, $7\sigma_g$	1, 2, 3, 4, $5\pi_{g^{\pm}}$
$1\pi_{uz}$	2, 3, 4, $5\pi_{uz}$	1, 2, 3, 4, $5\pi_{g^{\pm}}$
$1\pi_{uy}$	2, 3, 4, $5\pi_{uy}$	1, 2, 3, 4, $5\pi_{g^{\pm}}$
Set II		
$3\sigma_g$	4, 5, $6\sigma_g$	1, 2, $3\pi_{g^{\pm}}$
$1\pi_{uz}$	2, 3, $4\pi_{uz}$	1, 2, $3\pi_{g^{\pm}}$
$1\pi_{uy}$	2, 3, $4\pi_{uy}$	1, 2, $3\pi_{g^{\pm}}$
$3\sigma_g$	3, 4, $5\sigma_u$	2, 3, $4\pi_{uz}$
$3\sigma_g$	$1\delta_{uzv}$	2, 3, $4\pi_{uy}$
$1\pi_{uz}$	4, 5, $6\sigma_g$	3, 4, $5\sigma_u$
$1\pi_{uy}$	$1\delta_{gzv}$	4, 5, $6\sigma_g$
$1\pi_{uy}$	3, 4, $5\pi_{gv}$	2, 3, $4\pi_{uy}$

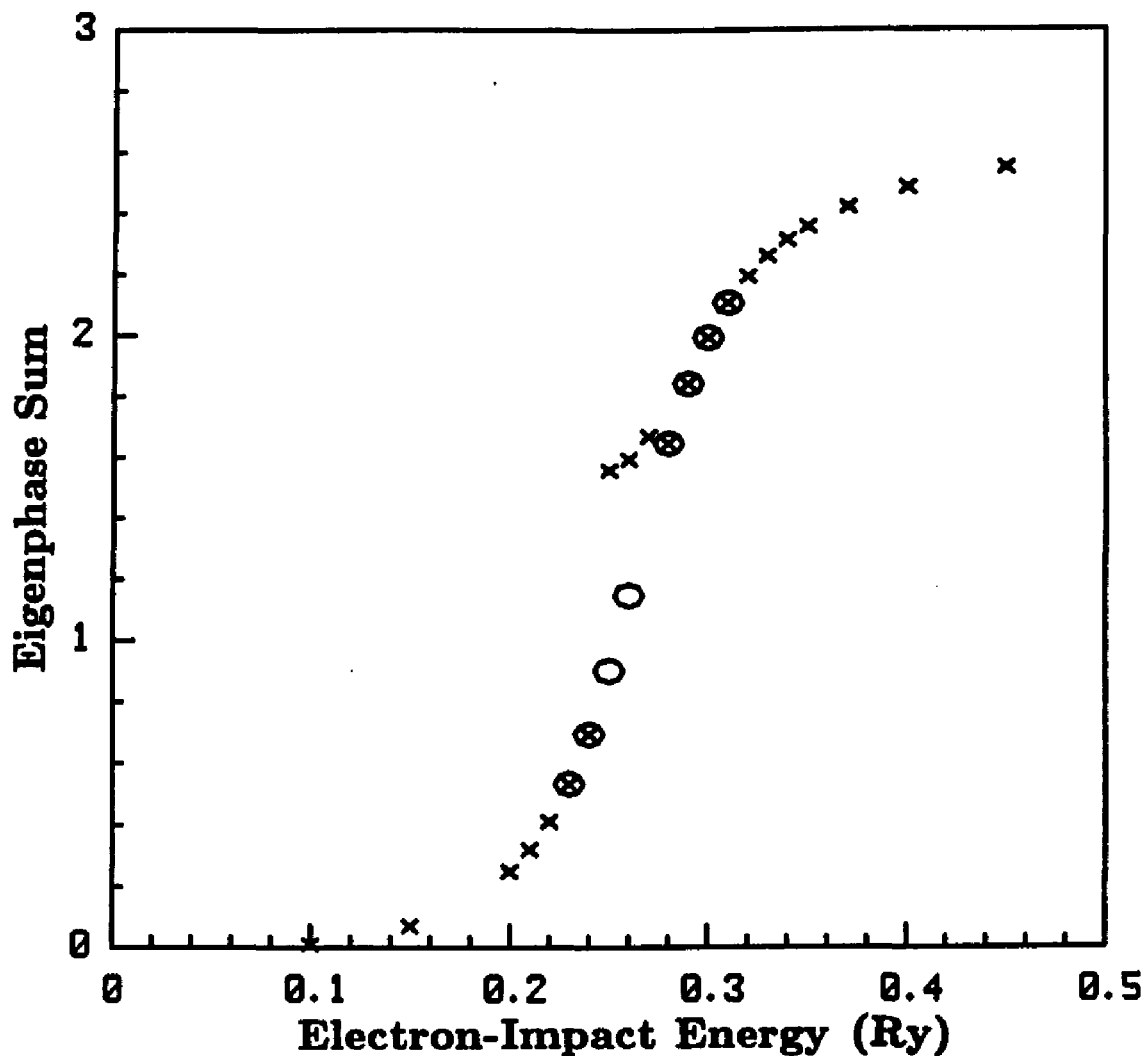


Figure 1: Eigenphase sum for the $2\Pi_g$ in $e-N_2$ scattering at target internuclear distance, $R=1.9 a_0$: present static-plus-exchange (SE) results using insertion basis I (\times), present SE results using insertion basis II (\circ). Insertion basis I and II are shown in Table II.

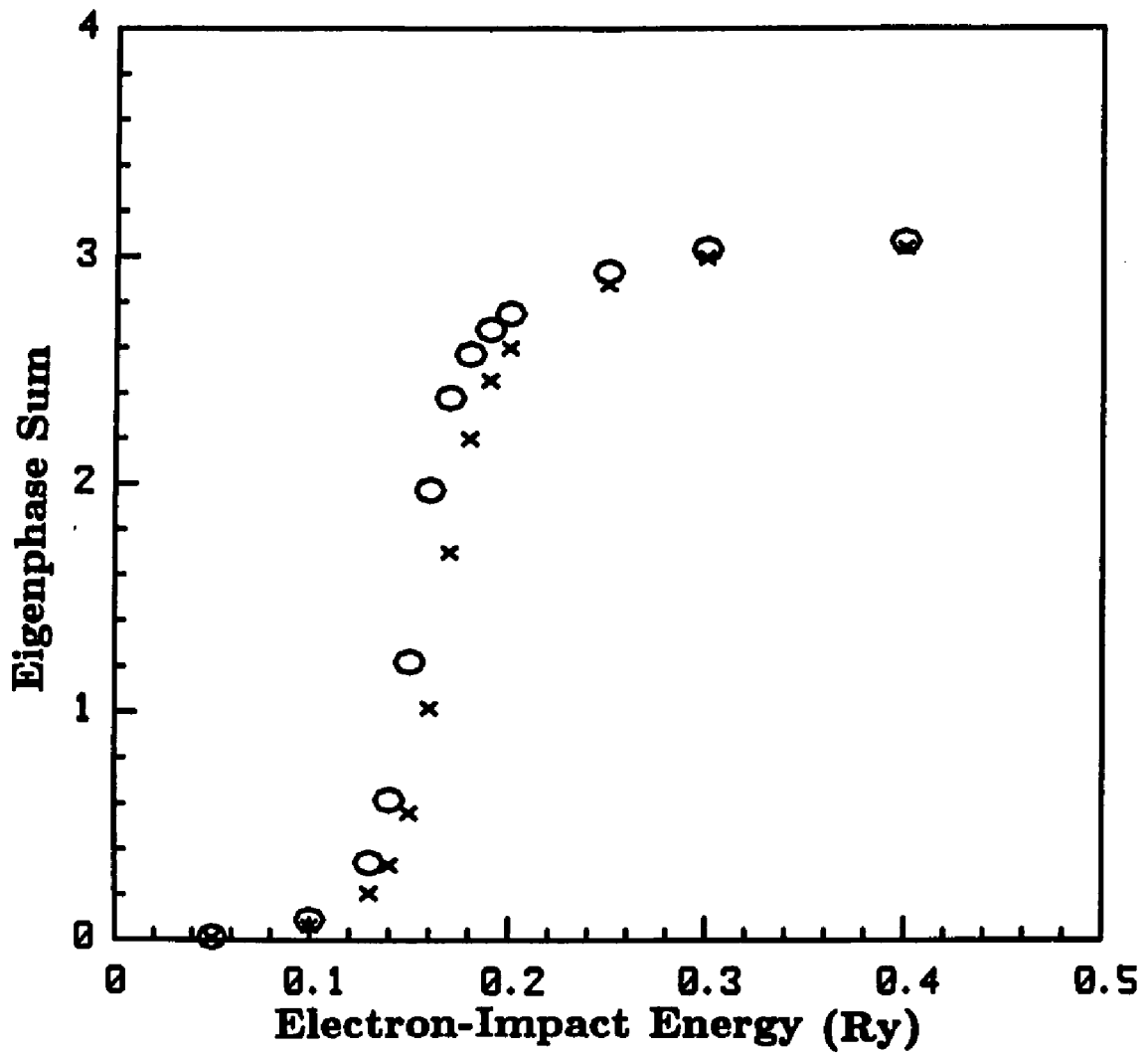


Figure 2: Eigenphase sum for the $^2\Pi_g$ in $e - N_2$ scattering at target internuclear distance, $R=2.068 a_0$: present static-plus-exchange-plus-polarization (SEP) results using set I of closed channel configurations (\times), present SEP results using set II of closed channel configurations (\circ). Sets I and II of closed channel configurations are shown in Table III.

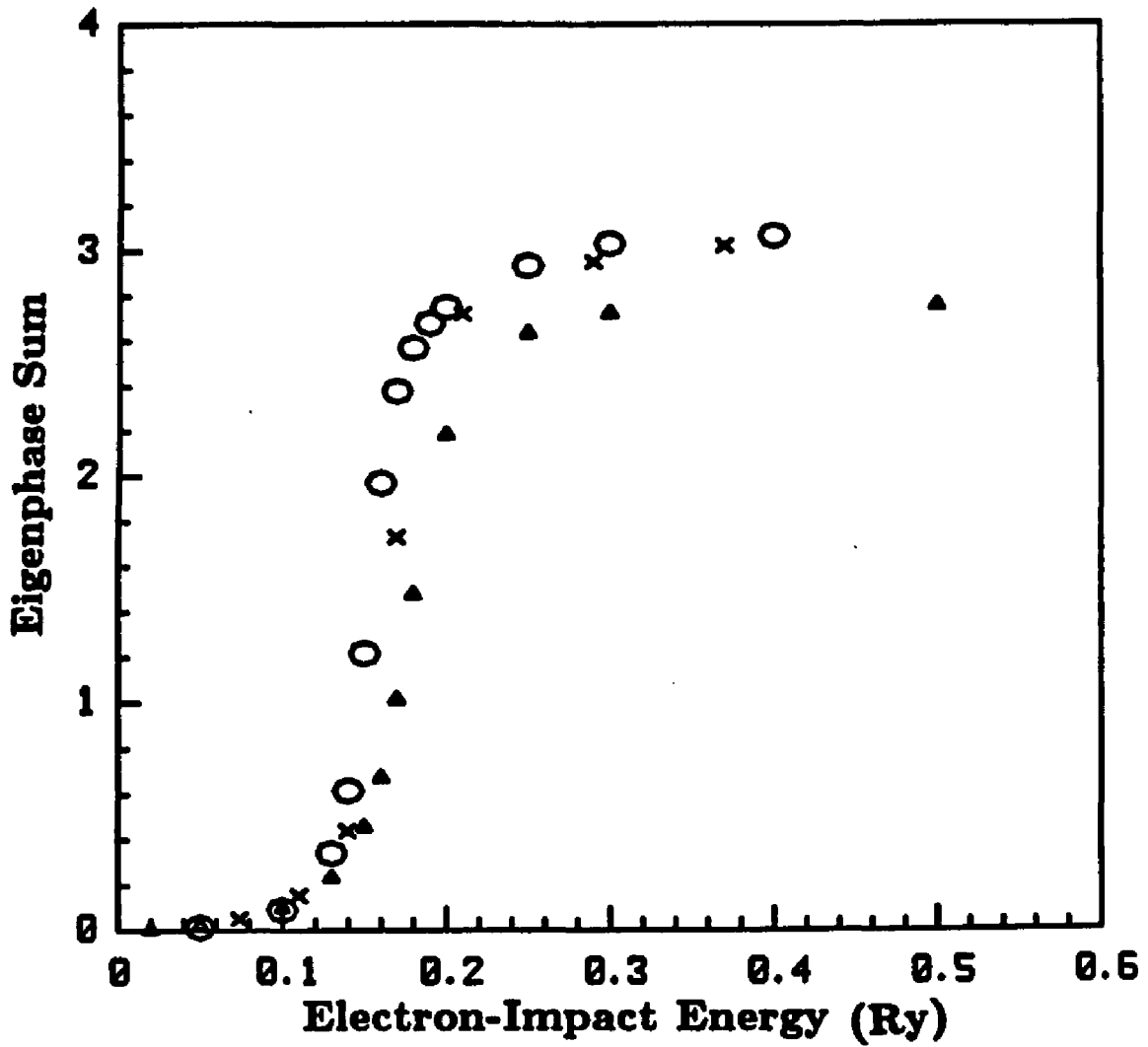


Figure 3: Eigenphase sum for the ${}^2\Pi_g$ in $e - N_2$ scattering at target internuclear distance, $R=2.068 a_0$: present SEP results (O), SEP results of Ref. 10 (x), SEP results of Ref. 32 (Δ).

3. CO

We report the results of a preliminary study on the shape resonance of low-energy e -CO scattering using the Schwinger multichannel method. We obtained integral cross sections and eigenphase sums for the resonant symmetry ${}^2\Pi$ from 0.5 to 5 eV. Our results were obtained with a relatively small basis set and are in very good agreement with previous theoretical results.

3.1 Introduction

The knowledge of cross sections for low-energy e -CO scattering is of great importance in several areas, *e.g.*, in the modeling of electrical conductivity in plasmas,¹ studies of adsorbed CO molecule on surface,² and rate coefficients of e -CO under interstellar conditions,³ etc. In Analogy to the isoelectronic molecule N_2 , the cross sections for low-energy e -CO are governed by a shape resonance.

In this chapter, we study e -CO elastic scattering cross section for overall ${}^2\Pi$ symmetry. This symmetry exhibits a shape resonance⁴ similar to the ${}^2\Pi_g$ resonance of e - N_2 , which was studied in the previous chapter. As we will see in the following section, we obtain cross sections and related parameters (position and width of the resonance) in good agreement with other theoretical results.⁵⁻⁷

3.2 Procedures and Results

To further assess the accuracy with which polarization is represented in our formulation, we have calculated elastic cross sections for the overall ${}^2\Pi$ symmetry in e -CO scattering from 0.5 to 5 eV. This constitutes a good test since the shape

resonance is very sensitive to polarization effects,⁸ and several other theoretical results⁵⁻⁷ are available.

For the ground state of CO we used a self-consistent-field (SCF) wave function obtained with a [11s6p1d] uncontracted Cartesian Gaussian basis on each nucleus and a [5p_x5p_y4d_{xx}4d_{yy}] basis on the center of mass. The Gaussian exponents were taken from the basis given by Dunning,⁹ augmented with diffuse π -functions shown in Table I. For the Ground state we obtained an electronic energy of -135.285 a.u. for an internuclear separation of 2.132 a_0 . A set of CO⁻ natural orbitals calculated with the same SCF basis was obtained with a configuration interaction program followed by the diagonalization of the density matrix for the ² Π symmetry.¹⁰ These orbitals were then used to construct the (N+1)-particle determinants in the expansion of $\Psi_1^{(\pm)}$. As discussed before, the use of the "ion natural orbitals" (INO) reduces the number of pseudoexcitations needed to represent $\Psi_1^{(\pm)}$ compared to the number that would be required if the standard SCF virtual orbitals were used.¹⁰ The partial wave expansion of the scattering amplitude is restricted to $\ell \leq 5$.

In Fig. 1 we show our static-plus-exchange (SE) and static-plus-exchange-plus-polarization results for the eigenphase sum as a function of energy. Note that the resonance position is shifted from ~ 3.8 for the SE results to ~ 1.8 eV for the SEP results. Also shown in Fig. 1 are the SEP and SE results of Salvini *et al.*,⁵ in which the R-matrix method is used, along with the SE results of Levin *et al.*⁶ and Collins *et al.*,⁷ obtained using the T-matrix discrete-basis-set approach and

the iterative close-coupling method, respectively. Our SE results lie between the results of Salvini *et al.*⁵ and results of Collins *et al.*⁷ It is also seen that our SEP results and the R-matrix results of Salvini *et al.*⁵ are in very good agreement.

Figures 2 and 3 display the eigenphase sums and the cross sections, respectively, for different combinations of closed channels in the the description of polarization effects. These figures show clearly the convergence of our results with respect to the number of configurations. the net contribution to the cross sections becomes less important. This study also shows that the contribution of the "singlet-coupled target" configurations to the cross sections are substantially more important than the "triplet-coupled target" contributions. Finally, our best results including polarization for the position (E_r) and width (Γ) of the resonance estimated from Fig. 4 are ~ 1.8 and ~ 1.2 eV, respectively. They should be compared to $E_r = 2.08$ and $\Gamma = 0.9$ eV obtained with the R-matrix method by Salvini *et al.*⁵ function.

3.3 Conclusions

We have presented preliminary results for elastic e-CO scattering for impact energies 1-5eV. We used a relatively small basis set and obtained results in good agreement with previous theoretical studies.

References

1. See, for example, J. E. Land, *J. App. Phys.* **49**, 5716 (1978).
2. G. D. Billing, *Chem. Phys.* **86**, 349 (1984); M. H. Tsai, T. N. Rhodin, R. V. Kasowski, *J. Vac. Sci. & Technol. A* **2**, 1016 (1984).
3. See, for example, S. Saha, S. Ray, B. Bhatlacharyya, and A.K. Barva, *Phys. Rev. A* **23**, 2926 (1981).
4. N. Chandra, *Phys. Rev. A* **16**, 80 (1977).
5. S. Salvini, P. G. Burke and C. J. Noble, *J. Phys. B* **17**, 2549 (1984).
6. D. A. Levin, A. W. Fliflet and V. Mckoy, *Phys. Rev. A* **21**, 1202 (1980).
7. L. A. Collins, W. D. Robb and M. A. Morrison, *Phys. Rev. A* **21**, 488 (1980).
8. *Electron-Molecule Collisions*, edited by I. Shimamura and K. Takayanagi (Plenum, New York, 1984).
9. T. H. Dunning, Jr., *J. Chem. Phys.* **53**, 5716 (1978).
10. A more detailed explanation of these procedures was given in the previous section.

Table I. Cartesian Gaussian Basis Set^{a,b}

Gaussian Center ^c and type	Exponents (α)
C, 11s	5240.635, 782.2848, 178.3508, 50.81594, 16.82356, 6.175776, 2.418049, 0.5119, 0.15659, 0.036, 0.009
C, 6p	18.8418, 4.15924, 1.20671, 0.38554, 0.12194, 0.03
C, 1d _{zx} , 1d _{yz}	0.75
O, 11s	10662.28, 1599.71, 364.7253, 103.6518, 33.90581, 12.28747, 4.756803, 1.004271, 0.300686, 0.072, 0.018
O, 6p	34.85646, 7.843131, 2.308269, 0.723164, 0.214882, 0.054
O, 1d _{zx} , 1d _{yz}	0.85
Center of mass, 5p _x , 5p _y	0.243, 0.081, 0.027, 0.009, 0.003
Center of mass, 5d _{zx} , 5d _{yz}	0.027, 0.009, 0.003, 0.001

^a Defined by $X_{lmn}^{(\alpha)} = N_{lmn}(x - A_x)^l (y - A_y)^m (z - A_z)^n e^{-\alpha|r - \vec{A}|^2}$, where \vec{A} is the position of the Gaussian center.

^b Basis set used for the ground and excited states of H₂, in the expansion of the scattering functions, and for insertion around $V G_P^{(+)} V$.

^c At the equilibrium internuclear distance of $R_e = 2.132a_0$

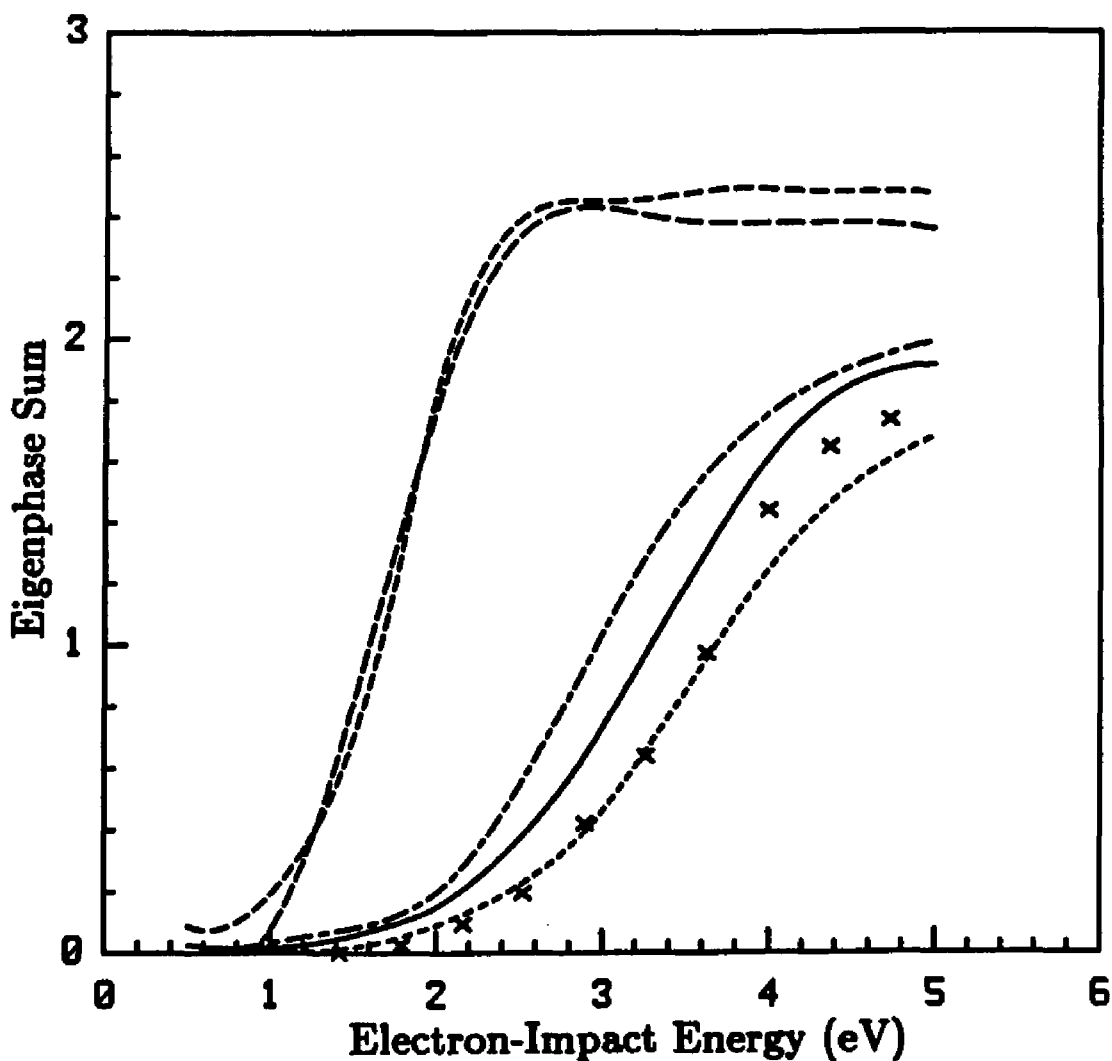


Figure 1: Eigenphase sum for the $^2\Pi$ symmetry in e - CO scattering: present static-plus-exchange (SE) results (solid line), SE results of Ref. 5 (short-long dashed line), SE results of Ref. 6 (\times), SE results of Ref. 7 (short dashed line), static-plus-exchange-plus-polarization (SEP) results of Ref. 5 (long dashed line), present SEP results (dashed line).

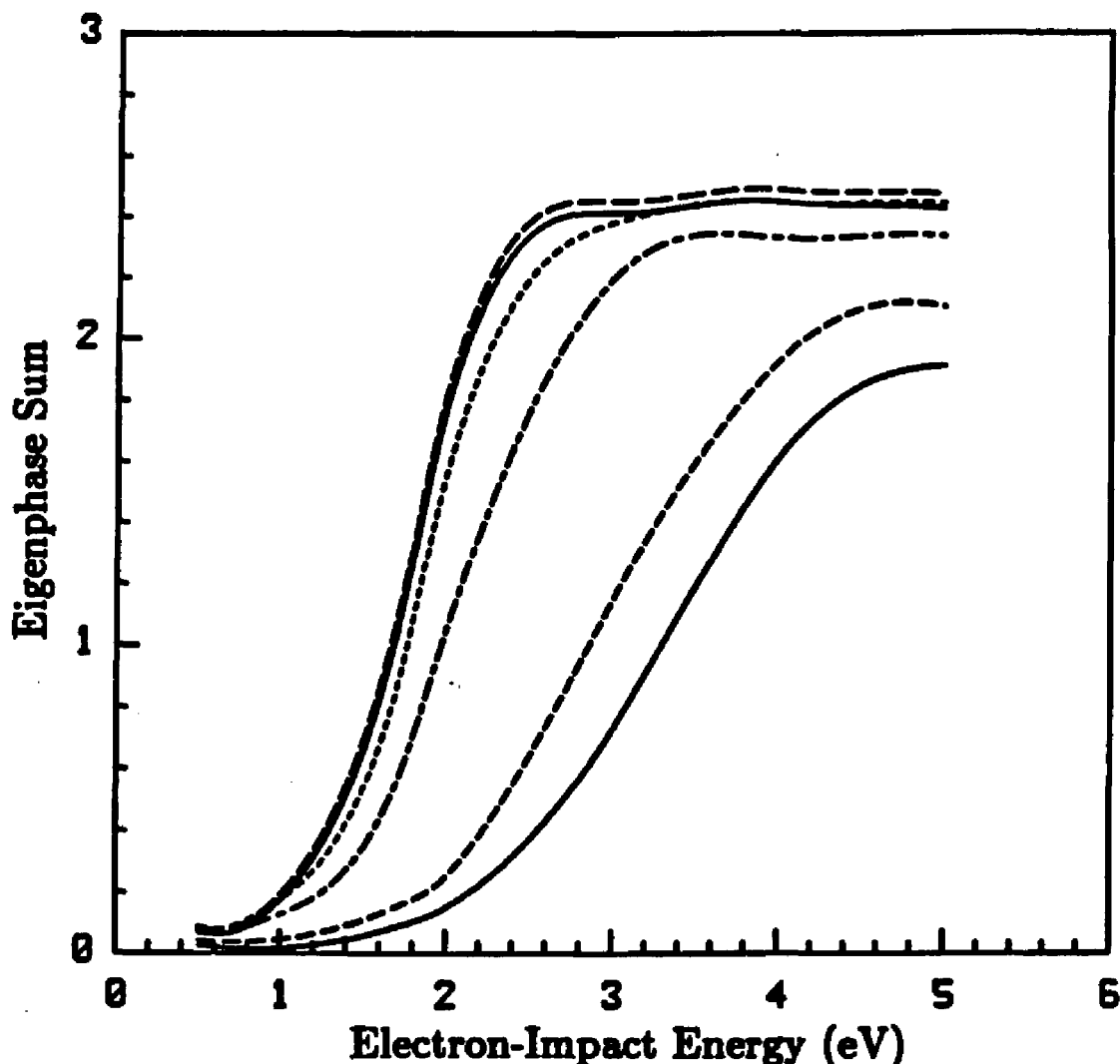


Figure 2: Eigenphase sum for the $^2\Pi$ symmetry in e - CO scattering: present SE results (solid line), present results including 4 triplet-coupled pseudostates with 4 scattering basis functions associated to each pseudostate in the closed channel expansion (dashed line), present results including 4 singlet-coupled pseudostates with 4 scattering basis functions (short-long dashed line), present results including 4 singlet-coupled and 4 triplet-coupled pseudostates with 4 scattering basis functions (short dashed line), present results including 5 singlet-coupled pseudostates with 6 scattering basis functions (solid line), present results including 5 singlet-coupled and 1 triplet-coupled pseudostates with 6 scattering basis functions (long dashed line).

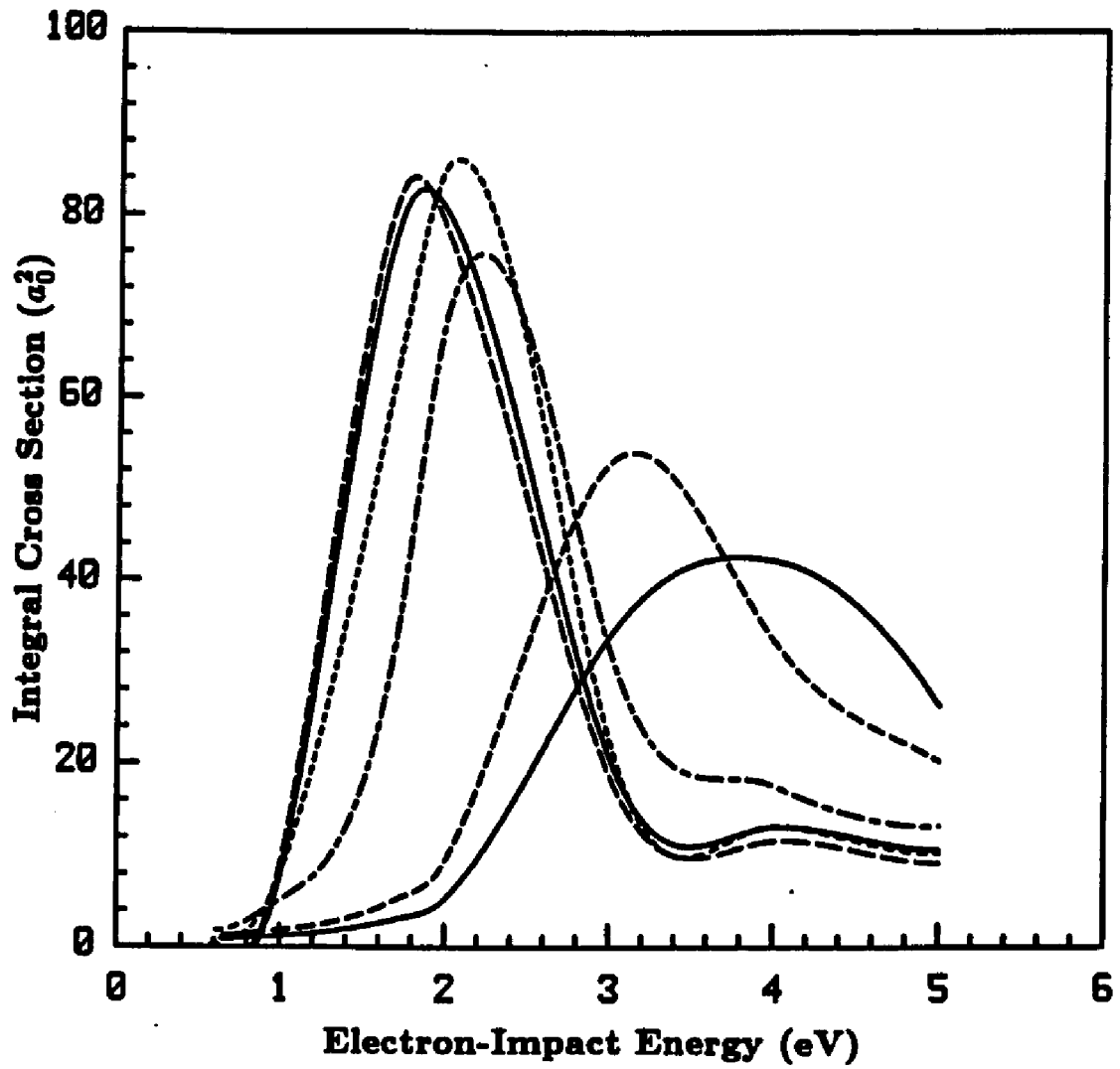


Figure 3: Elastic cross section for the $^2\Pi$ symmetry in e - CO scattering: same label as in Fig. 2.

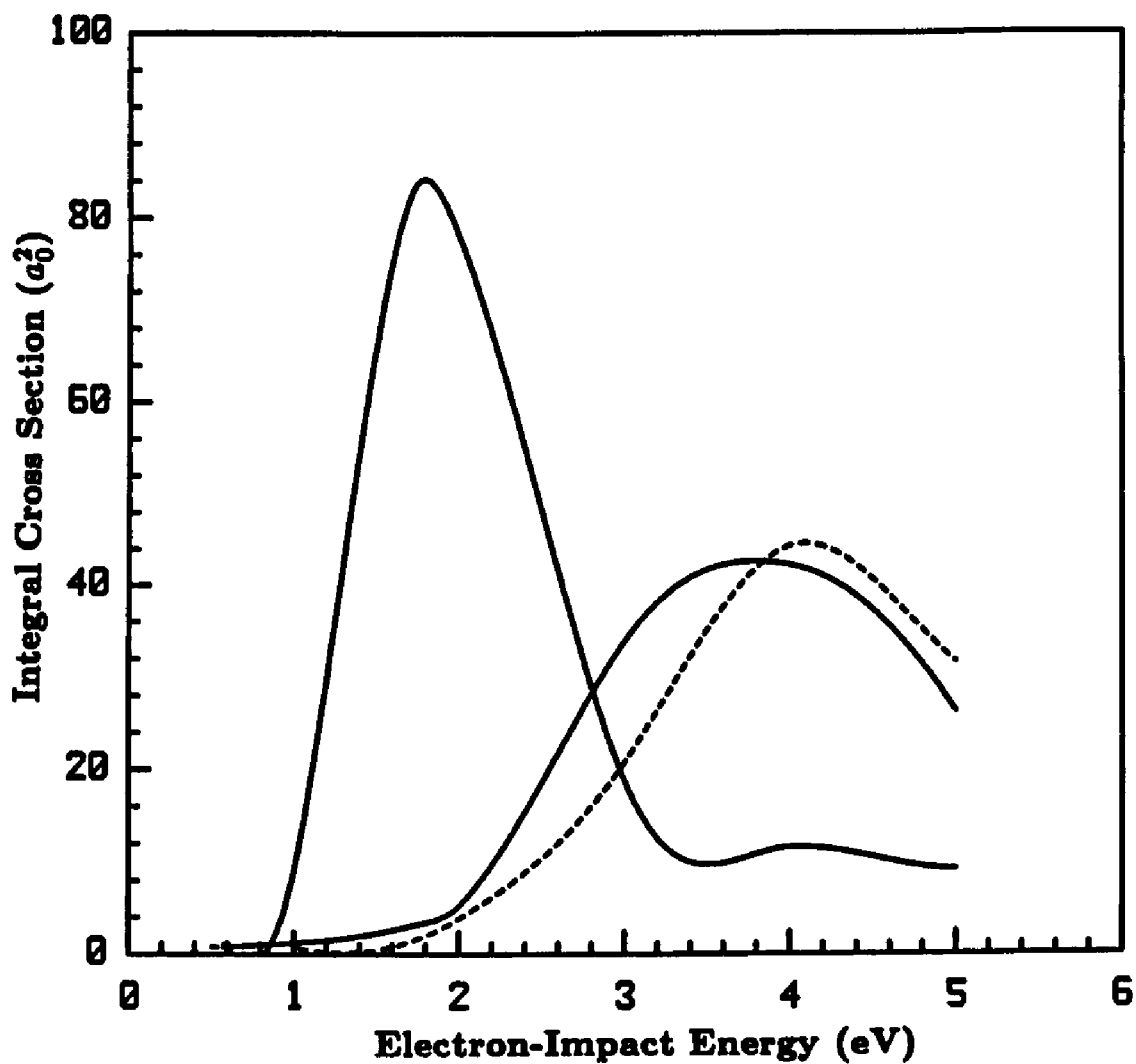


Figure 4: Elastic cross section for the $^2\Pi$ symmetry in e-CO scattering: present SE results (solid line), SE results of Ref. 7 (dashed line), SEP results of Ref. 5 (long dashed line), present SEP results (solid line showing a maximum at ~ 1.8 eV).

4. CH₄

We report the first application of the Schwinger multichannel formulation to low-energy electron collisions with a nonlinear polyatomic target. Integral and differential cross sections are obtained for $e - \text{CH}_4$ collisions from 3 to 20 eV. Inclusion of closed channels in the expansion of the total wave function shows that an interesting feature in the small-angle cross section is due to polarization. In these studies the exchange potential is directly evaluated and not approximated by local models. Our differential cross sections are found to be in very good agreement with existing measurements at 7.5 eV and higher energies. Below 7.5 eV, polarization effects become important. A preliminary study on these effects gives the correct trend for the differential cross sections at 3 and 5 eV. We have also studied the 2A_1 symmetry cross sections in the energy range from 0.2 to 5 eV. This symmetry is known to lead to a Ramsauer-Townsend minimum in the integral cross sections for incident electron energies below 1 eV. In our calculations this minimum is not seen in the static-exchange approximation. Our preliminary studies including polarization effects do not show the minimum but do lead to significant changes in the right direction in these cross sections.

4.1 Introduction

To date, most *ab initio* studies of electron-molecule collisions have concentrated on linear target molecules where single-center expansion techniques¹ are particularly well suited to exploit the cylindrical symmetry of such systems. However, a true multicenter method designed to be applicable to target molecules of

arbitrary geometry would dramatically widen the range of interesting problems² amenable to theoretical treatments. Moreover, such a multicenter method can be readily applied to electron collisions with molecules adsorbed on surfaces³ in which the surface effects are simulated by small clusters of atoms.

The behavior of cross sections for low-energy electron-molecule collisions is governed by static, polarization, and exchange interactions.¹ Polarization effects are known to be important for low-energy electron collisions with molecules which do not possess a large permanent dipole moment. Recently, there has been considerable progress in the development of accurate methods⁴⁻⁹ for including the effects of polarization. In addition to the static and polarization interactions, a reliable treatment of low-energy electron-molecule scattering must incorporate the effects of antisymmetry on the total scattering wave function. This requirement gives rise to energy-dependent exchange terms in the scattering equations. The nonlocal character of these terms makes the numerical solution of the resulting equations arduous. These difficulties have justifiably stimulated attempts to model the effects of exchange by including approximate local terms¹⁰⁻¹² in the interaction potential. The traditional test for local models of exchange is to compare the static-model-exchange cross sections with exact-static-exchange results. Such a comparison is even more important if, in addition, one is trying to assess the utility of an approximate treatment of polarization. So far, essentially exact treatments of the exchange terms have been restricted to linear systems.¹³⁻¹⁷ Thus, a set of accurate static-exchange cross sections for poly-

atomic systems would be useful and a logical first step for more complete studies including polarization effects.

Recently, we have presented two different applications of the Schwinger Multichannel theory^{18,19} (SMC) to $e - H_2$ collisions. In one paper²⁰ we reported results for the inelastic process $X^1\Sigma_g^+ \rightarrow b^3\Sigma_u^+$ within the two-state approximation and in the other⁹ we demonstrated the ability of the theory to account for polarization effects in a *ab initio* manner for elastic scattering. Here we report the application of the SMC theory to elastic $e - CH_4$ scattering in the static-plus-exchange (SE) and static-plus-exchange-plus-polarization (SEP) approximations. Due to its presence in planetary atmospheres, methane is an important system for study. As a result one needs cross section data for modeling and understanding these planetary atmospheres. Theoretical²¹⁻²⁶ and experimental²⁷⁻³¹ $e - CH_4$ collision results are available for comparison. However, to our knowledge this is the first study of electron-polyatomic molecule scattering without the use of a local exchange potential.

In Sec. 4.2 we report differential cross sections for elastic $e - CH_4$ scattering at the static-exchange level for selected energies in the 3-20 eV range. A preliminary study of polarization effects in this system is given in Sec. 4.3. We summarize our results and conclusions in Sec. 4.4

4.2 Procedures and results for the static-exchange calculations

As a first application of our formulation to polyatomic systems we have calculated differential and integral cross sections for elastic $e - CH_4$ collisions

for incident energies of 3-20 eV. This polyatomic system provides a convenient test for our procedures because it has 5 centers and possesses no permanent dipole or quadrupole moment. There have been several static model-exchange polarization (SMEP) studies²¹⁻²⁶ of this system and measured cross sections are available.²⁷⁻³¹

Our calculations are performed within the framework of the fixed-nuclei approximation. Here, the nuclei are held at their equilibrium positions and the dependence of the scattering amplitude on internuclear separation is neglected. The rotational levels are treated as degenerate and the physical cross sections are obtained by averaging the fixed-nuclei results over all molecular orientations. Unless otherwise stated, atomic units are used throughout.

For the ground state of CH₄ we used a self-consistent-field (SCF) wave function obtained with a [12s8p4d] uncontracted Cartesian Gaussian basis on the carbon and a [7s] basis on each hydrogen. The Gaussian exponents shown in Table I are from the [9s5p] basis given by Huzinaga³² together with an additional set of d-functions and diffuse s- and p-type functions. A set of CH₄ virtual orbitals calculated with the same SCF basis and Schmidt-orthogonalized to the occupied orbitals $1a_1$, $2a_1$, $1t_{2x}$, $1t_{2y}$, and $1t_{2z}$ were used to expand the scattering functions and to satisfy the closure relation in the insertion technique. The use of totally uncontracted Gaussian functions permits greater flexibility in the scattering and insertion basis set. With this basis we obtain an SCF energy of $-40.2029E_h$ at a carbon-hydrogen nuclear distance of $2.050a_0$ to be compared

with $-40.2124E_h$ obtained by Meyer³³ at the same geometry.

Our calculations in the body frame include contributions from the 2A_1 , 2T_2 , and 2E symmetries in $\Psi_1^{(\pm)}$. Indeed, all 83 available virtual (scattering) orbitals from the molecular SCF calculation, $21a_1$, $18t_{2x}$, $18t_{2y}$, $18t_{2z}$ and $8e$, were used in the expansion of $\Psi_1^{(\pm)}$; i.e., $\Psi_1^{(\pm)}$ is constructed from linear combinations of (N+1)-Slater determinants

$${}^2A_1 : 1a_1^2 2a_1^2 1t_{2x}^2 1t_{2y}^2 1t_{2z}^2 ka_1$$

$${}^2T_{2x} : 1a_1^2 2a_1^2 1t_{2x}^2 1t_{2y}^2 1t_{2z}^2 kt_{2x}$$

$${}^2T_{2y} : 1a_1^2 2a_1^2 1t_{2x}^2 1t_{2y}^2 1t_{2z}^2 kt_{2y}$$

$${}^2T_{2z} : 1a_1^2 2a_1^2 1t_{2x}^2 1t_{2y}^2 1t_{2z}^2 kt_{2z}$$

$${}^2E : 1a_1^2 2a_1^2 1t_{2x}^2 1t_{2y}^2 1t_{2z}^2 ke,$$

with ka_1 , kt_2 and ke being continuum functions represented by the virtual orbitals. We have shown in an earlier paper¹⁹ that this type of expansion reduces the SMC expression for the scattering amplitude to the static exchange level of approximation. Finally, for the partial wave expansion of the scattering amplitude we include values of $l \leq 5$.

In Figures 1-6 we present the calculated differential cross sections for incident energies of 3, 5, 7.5, 10, 15 and 20 eV, respectively. Also shown at each energy are the experimental results of Tanaka *et al.*²⁸ At 10 eV the theoretical results of Abusalbi *et al.*,²⁴ obtained using two different SMEP potentials, are also

included. At 20 eV the experimental data of Vušković *et al.*²⁹ and the calculations of Jain²⁸ are presented with our results and the measurements of Tanaka *et al.*²⁸

The differential cross sections in this range of energies are characterized by forward peaking, a minimum around 120° , and a backward peak. The minimum is rather sharp at low energies and becomes broader with increasing energy. In addition, experiment shows a secondary minimum occurring near 45° at 3 eV. As the incident energy is increased to 7.5 eV, the minimum moves to 60° and becomes a much less pronounced shoulder-like structure. The present calculations reproduce both the forward and backward peaks as well as the primary minimum near 120° . However, at low energies the calculated forward peak is much stronger than in the experiment. The secondary minimum is also missing, indicating, as we will see in the next section, that this feature is due to polarization effects and cannot be reproduced at the present level of approximation.

The sensitivity of the low-energy differential cross section to the particular way in which polarization effects are modeled has been demonstrated by Gianturco *et al.*²¹ They used a semiempirical polarization potential^{8,21} with the correct asymptotic form but with a short range cut-off parameter r_0 chosen by calibration to experimental data. These studies showed that even small changes in the cut-off parameter substantially affect the differential cross sections. Moreover, when the cut-off parameter is increased from 0.84 to 0.92, which makes the inner region of the potential look more like the static-exchange potential, the shoulder at low energy becomes less pronounced, indirectly supporting our con-

jecture that the secondary minimum is a polarization effect. The secondary minimum is also reproduced by the model polarization potential studies of Abusalbi *et al.*,²⁴ at 10 eV. However, at this energy the polarization effect is relatively small so that the difference between their "best" polarization curve and our static-exchange curve is rather small.

4.3 Procedures and results for inclusion of polarization effects

In this section we present a very preliminary study of $e - \text{CH}_4$ collisions in which the polarization effects have been included through closed channels. For the ground state of CH_4 we used a SCF wave function obtained with the the same Cartesian Gaussian basis set of our SE calculation. In addition to the ground state orbitals a set of CH_4^- natural orbitals was obtained from a configuration interaction (CI) calculation³⁴ and diagonalization of the density matrix³⁵ for the 2A_1 and 2T_2 symmetries. These orbitals were then used to construct the $(N + 1)$ -particle determinants in the expansion of $\Psi_1^{(\pm)}$. The use of the "ion natural orbitals" (INO) reduces the number of pseudo-excitations needed to represent $\Psi_1^{(\pm)}$ compared to the number that would be required if the standard SCF virtual orbitals are used.³⁵

Our calculations in the body frame include contributions from the 2A_1 , 2T_2 , and 2E symmetries in $\Psi_1^{(\pm)}$. When including polarization effects the expansion of $\Psi_1^{(\pm)}$ is done in terms of two types of configurations (Slater determinants). One is the SE-configuration which was described in the previous section and has

the form

$${}^2A_1 : 1a_1^2 2a_1^2 1t_{2x}^2 1t_{2y}^2 1t_{2z}^2 k a_1,$$

and the other, hereafter referred to as SEP-configuration, is characterized by a pseudoexcitation of the target core; *e.g.*,

$${}^2A_1 \quad 1a_1^2 2a_1^1 1t_{2x}^2 1t_{2y}^2 1t_{2z}^2 m a_1 n a_1.$$

All 83 available orbitals from the molecular INO calculation, $21a_1$, $18t_{2x}$, $18t_{2y}$, $18t_{2z}$, $4e_1$ and $4e_2$, are used to construct the SE-configurations in the expansion of $\Psi_1^{(\pm)}$. However, no more than 180 SEP-configurations (~ 20 target pseudostates) out of the many thousand possible configurations are used to describe polarization effects for each symmetry. In spite of this limited number of SEP-configurations the results, as we will see, are very encouraging. Finally, for the partial wave expansion of the scattering amplitude we again include values of $l \leq 5$.

Figure 7 shows our SE and SEP integral cross sections along with the theoretical results of Salvini and Thompson²² for the 2A_1 symmetry in the energy range from 0.2 to 5 eV. This symmetry is known²¹ to lead to the Ramsauer-Townsend minimum in the integral cross sections for incident energies below 1 eV. Salvini and Thompson²² obtained the Ramsauer-Townsend minimum with a model-exchange potential at the SE level of approximation. In our calculations this minimum is not seen at this level of approximation. Our preliminary studies including polarization effects, shown in Fig. 7, do not show this minimum but

lead to changes in the cross sections in the right direction. Figures 8 and 9 show our differential cross sections at 3 and 5 eV along with the experimental data of Tanaka *et al.*²⁸ and the SMEP results of Jain and Thompson.²³ We note that our present SEP calculations qualitatively reproduce the secondary minimum occurring near 40° seen in the experimental differential cross sections at 3 and 5 eV.

In Fig. 10, our integral cross sections are shown along with the SMEP calculations of Jain and Thompson²³ and the measurements of Tanaka *et al.*²⁸, Ferch *et al.*,³⁰ and Jones.³¹ There are clearly significant differences between the electron-molecule beam data of Tanaka *et al.*²⁸ and those obtained by electron transmission experiments by Ferch *et al.*³⁰ and Jones.³¹ Compared with the experiment, the maximum in our total cross section is shifted to higher energies by about 2.5 eV. When polarization effects are included in our calculations, we observe a substantial improvement in the integral cross section for incident energies below 5 eV but only a slight shift in the position of the maximum. Some of the discrepancy between our calculated integral cross sections and the experimental data of Tanaka *et al.*²⁸ can arise from uncertainties in extrapolating the measured differential cross sections to small (< 30°) and large(> 140°) angles. Above the maximum the qualitative agreement between the calculated and measured cross sections is reasonable. In Fig. 11 we show our calculated momentum transfer cross sections along with those of the SMEP calculations of Jain and Thompson²³ and the values derived from the data of Tanaka *et al.*²⁸ The differ-

ences between our calculated momentum transfer cross sections and the derived values of Tanaka *et al.*,²⁸ particularly at higher energies, are again probably due to uncertainties in extrapolating the measured differential cross sections to larger angles. The values of the differential cross sections at higher angles, *e.g.*, beyond 120° , are heavily weighted in the calculation of the momentum transfer cross sections.

4.4 Conclusions

In this chapter we have reported the first application of the Schwinger multichannel formulation to low-energy electron impact collisions with a nonlinear polyatomic target. Integral and differential cross sections have been obtained for $e - \text{CH}_4$ collisions for incident energies between 3 and 20 eV. Our differential cross sections are seen to be in very reasonable agreement with existing measurements at 7.5 eV and above. Below 7.5 eV a very interesting feature in the small angle differential cross section is ascribed to polarization effects. Furthermore, preliminary studies give the correct trend in the differential cross sections at 3 and 5 eV. We also studied the 2A_1 symmetry cross sections in the energy range from 0.2 to 5 eV. The Ramsauer-Townsend minimum expected in this symmetry is not seen in the static-exchange approximation. Our preliminary studies including polarization effects do not show the minimum but do lead to the expected changes in these cross sections. Integral cross sections and momentum transfer cross sections are compared with experimental data. In spite of the good agreement between our differential cross sections and the experimental

data of Tanaka *et al.*,²⁸ we find some differences between the momentum transfer data. Some of this discrepancy may be due to poor extrapolation of the experimental differential cross sections beyond 120°, which are heavily weighted in the calculation of the momentum transfer cross sections. The present study helps to demonstrate the utility of this approach and represents considerable progress toward obtaining accurate *ab initio* cross sections for a variety of polyatomic targets.

References

- ¹ N. F. Lane, *Rev. Mod. Phys.* **52**, 29 (1980).
- ² For a recent review of experimental progress see S. Trajmar, D. F. Register, and A. Chutjian, *Phys. Rep.* **97**, 219 (1983).
- ³ L. M. Brescansin, M. A. P. Lima, W. M. Huo, and V. Mckoy, *Phys. Rev. B* **32**, 7122 (1985); J. W. Davenport, W. Ho, and J. R. Schrieffer, *Phys. Rev. B* **17**, 3115 (1978).
- ⁴ B. I. Schneider, *Chem. Phys. Lett.* **51**, 578 (1977); B. I. Schneider and L. A. Collins, *Phys. Rev. A* **27**, 2847 (1983).
- ⁵ A. Klonover and J. Kaldor, *J. Phys. B* **11**, 1623 (1978).
- ⁶ D. J. Truhlar, D. A. Dixon, and R. A. Eades, *J. Phys. B* **12**, 1913 (1979).
- ⁷ M. A. Morrison and P. J. Hay, *Phys. Rev. A* **20**, 740 (1979); T. L. Gibson and M. A. Morrison, *Phys. Rev. A* **29**, 2497 (1984).
- ⁸ F. H. M. Faisal, *J. Phys. B* **3**, 636 (1970); P. G. Burke and A. L. Sinfailam, *J. Phys. B* **3**, 641 (1970); P. G. Burke and N. Chandra, *J. Phys. B* **5**, 1696 (1972); P. G. Burke, N. Chandra, and F. A. Gianturco, *J. Phys. B* **5**, 2212 (1972).
- ⁹ T. L. Gibson, M. A. P. Lima, K. Takatsuka, and V. Mckoy, *Phys. Rev. A* **30**, 3005 (1984), and references therein.
- ¹⁰ S. Hara, *J. Phys. Soc. Japan* **22**, 710 (1967).
- ¹¹ M. E. Riley and D. G. Truhlar, *J. Chem. Phys.* **63**, 2182 (1975).
- ¹² T. L. Gibson and M. A. Morrison, *J. Phys. B* **14**, 727 (1981), and references

therein.

- ¹³ M. A. Morrison and B. I. Schneider, *Phys. Rev. A* **16**, 1003 (1977).
- ¹⁴ L. A. Collins, and W. D. Robb, and M. A. Morrison, *Phys. Rev. A* **21**, 488 (1980).
- ¹⁵ D. K. Watson, R. R. Lucchese, V. Mckoy, and T. N. Rescigno, *Phys. Rev. A* **21**, 738 (1980).
- ¹⁶ D. A. Levin, A. W. Fliflet, and V. Mckoy, *Phys. Rev. A* **21**, 1202 (1980); see also References 9 and 20.
- ¹⁷ T. N. Rescigno and A. E. Orel, *Phys. Rev. A* **24**, 1267 (1981)
- ¹⁸ K. Takatsuka and V. Mckoy, *Phys. Rev. A* **24**, 2473 (1981).
- ¹⁹ K. Takatsuka and V. Mckoy, *Phys. Rev. A* **30**, 1734 (1984).
- ²⁰ M. A. P. Lima, T. L. Gibson, K. Takatsuka, and V. Mckoy, *Phys. Rev. A* **30**, 1741 (1984).
- ²¹ F. A. Gianturco and D. G. Thompson, *J. Phys. B* **9**, L383 (1976); F. A. Gianturco and D. G. Thompson, *J. Phys. B* **13**, 613 (1980).
- ²² S. Salvini and D. G. Thompson, *J. Phys. B* **14**, 3797 (1981).
- ²³ A. Jain and D. G. Thompson, *J. Phys. B* **15**, L631 (1982); private communication (1985).
- ²⁴ N. Abusalbi, R. A. Eades, T. Nam, D. Thirumalai, D. A. Dixon and D. G. Truhlar, *J. Chem. Phys.* **78**, 1213 (1983).
- ²⁵ A. Jain, *J. Chem. Phys.* **81**, 724 (1984).
- ²⁶ J. E. Bloor, *Wavefunctions and Mechanisms from Electron Scattering Proc-*

- esses*, edited by F. A. Gianturco and G. Stefani (Springer-Verlag, New York, 1984), p.85.
- ²⁷ K. Rohr, *J. Phys. B* **13**, 4897 (1980).
- ²⁸ H. Tanaka, T. Okada, L. Boesten, T. Suzuki, T. Yamamoto, and M. Kubo, *J. Phys. B* **15**, 3305 (1982).
- ²⁹ L. Vušković and S. Trajmar, *J. Chem. Phys.* **78**, 4947 (1983).
- ³⁰ J. Ferch, B. Granitza and W. Raith, *J. Phys. B* **18**, L445 (1985).
- ³¹ R. K. Jones, *J. Chem. Phys.* **82**, 12 (1985).
- ³² S. Huzinaga, *J. Chem. Phys.* **42**, 1293 (1965).
- ³³ W. Meyer, *J. Chem. Phys.* **58**, 1017 (1973).
- ³⁴ See, for example, *Methods of Electronic Structure Theory*, edited by H. F. Schaefer III (Plenum, New York, 1977).
- ³⁵ P. Löwdin, *Phys. Rev.* **97**, 1474 (1955). See also discussion in Sec. 2.

Table I. Cartesian Gaussian Basis Set^{a,b}

Gaussian center ^c and type	Exponents (α)
C, 12s	4233, 634.9, 146.1, 42.5, 14.19, 5.148, 1.967, 0.4962, 0.1533, 0.0496, 0.02, 0.01
C, 8p	18.16, 3.986, 1.143, 0.3594, 0.1146, 0.046, 0.018, 0.0072
C, 4d	2.4, 0.6, 0.15, 0.0375
H, 7s	19.24056, 7.45, 2.899152, 0.65341101, 0.1775765, 0.071, 0.025

^a Defined by $X_{lmn}^{(\alpha)} = N_{lmn} (x - A_x)^l (y - A_y)^m (z - A_z)^n e^{-\alpha|\vec{r}-\vec{A}|^2}$, where \vec{A} is the position of the Gaussian center.

^b Basis set used for the ground state of CH₄, in the expansion of the scattering functions, and for insertion around $V G_p^{(+)} V$.

^c At the equilibrium internuclear distance of $R_{CH} = 2.05a_0$

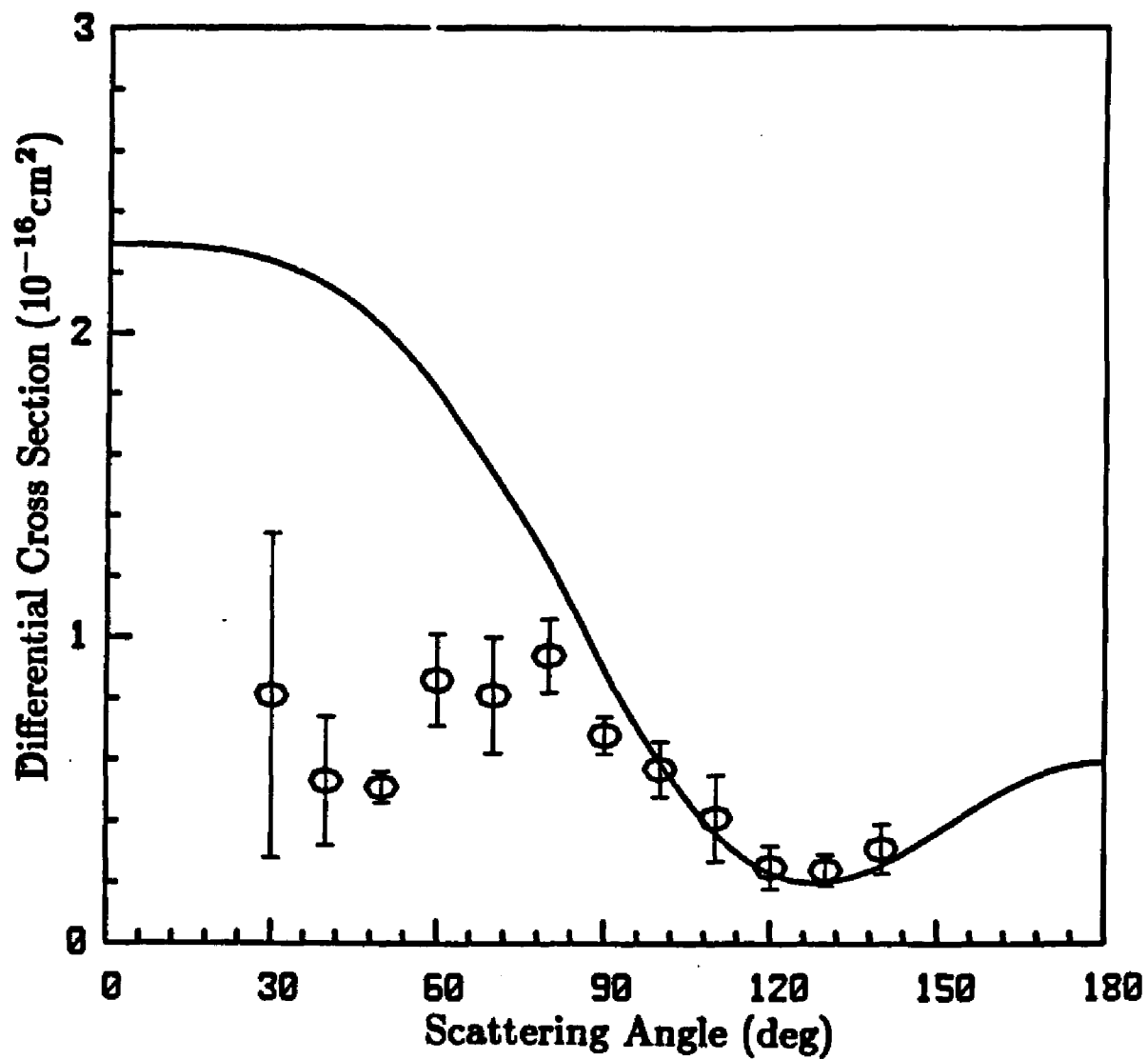


Figure 1: Differential cross sections (DCS) for $e - \text{CH}_4$ scattering at 3 eV: present static-plus-exchange (SE) results (solid line), measured values of Ref. 28 (\circ).

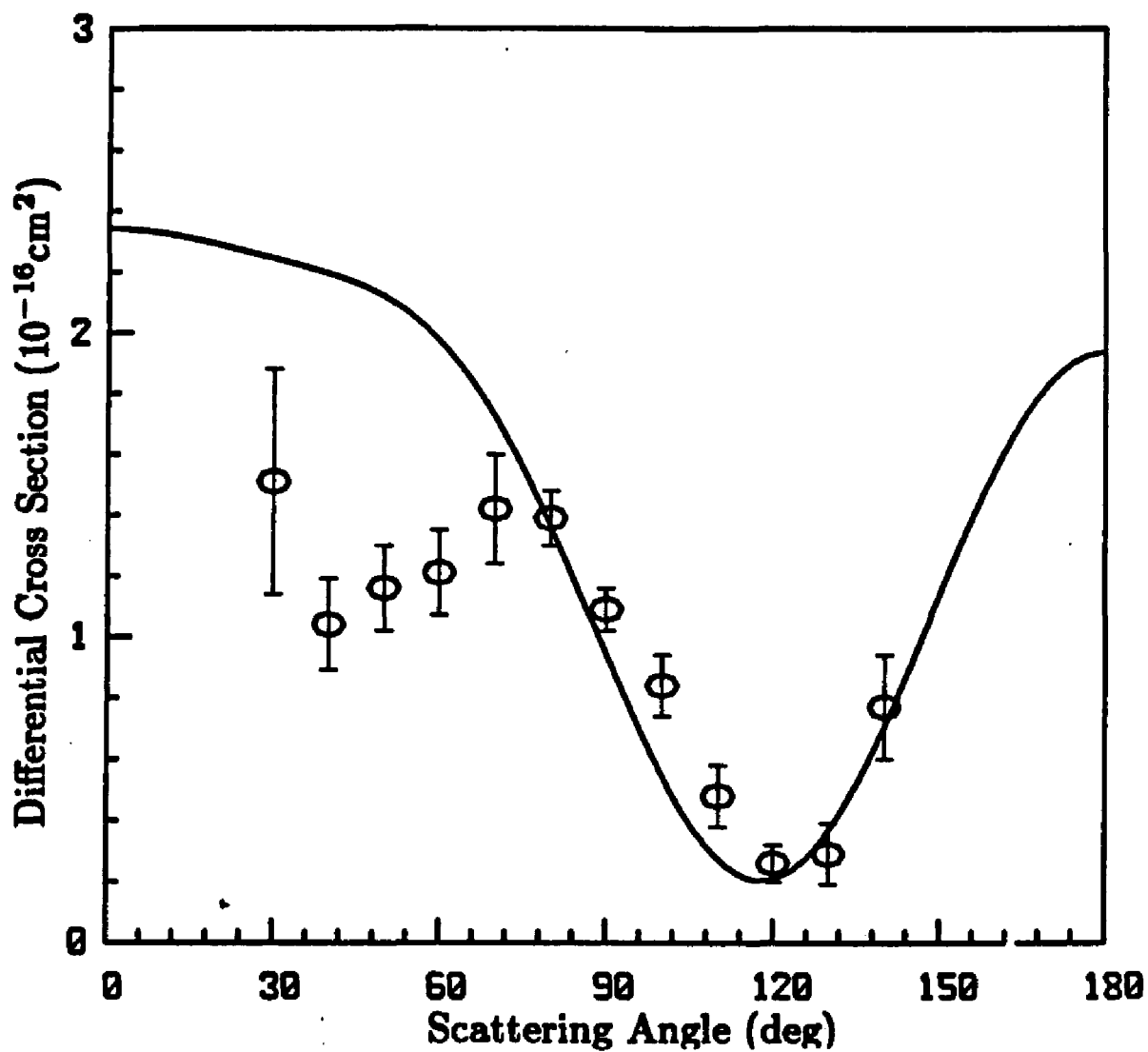


Figure 2: DCS for $e - \text{CH}_4$ scattering at 5 eV: present SE results (solid line), measured values of Ref. 28 (○).

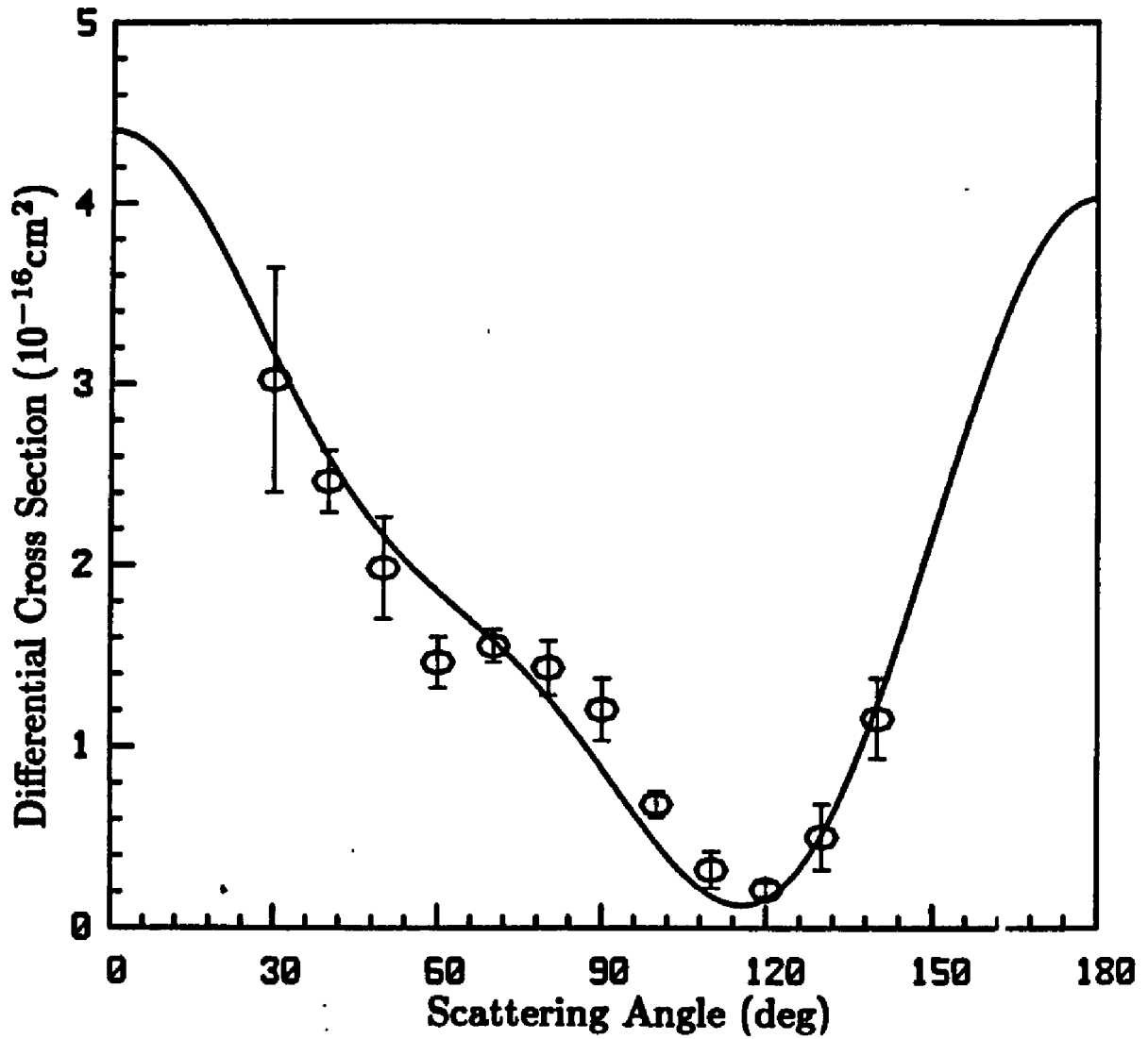


Figure 3: DCS for $e - \text{CH}_4$ scattering at 7.5 eV: present SE results (solid line), measured values of Ref. 28 (○).

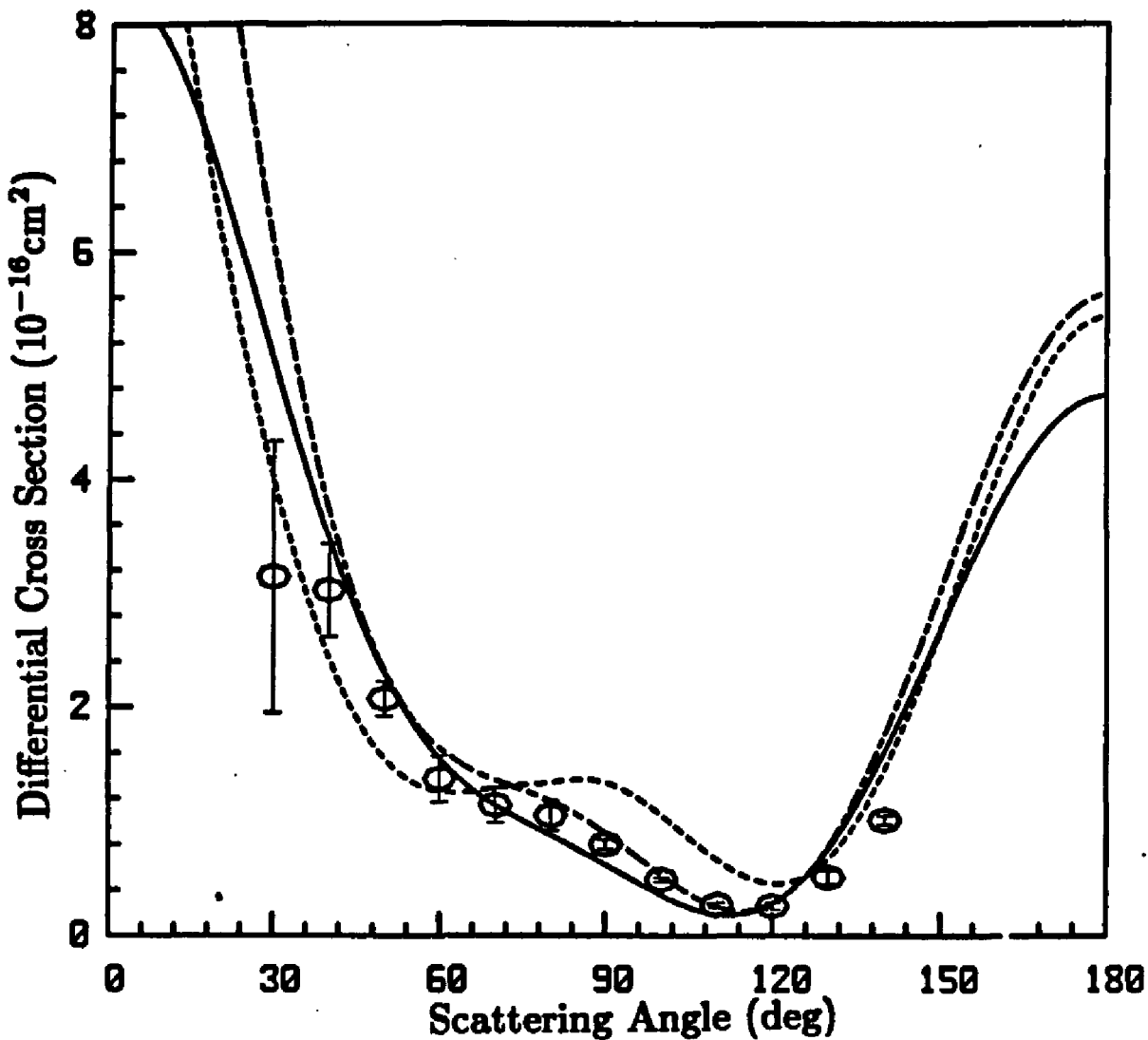


Figure 4: DCS for $e - \text{CH}_4$ scattering at 10 eV: present SE results (solid line), static model-exchange polarization (SMEP) results of Ref. 24 using an adiabatic polarization potential (dashed line), SMEP results of Ref. 24 using a local-kinetic energy semi-classical potential (long-short dashed line), measured values of Ref. 28 (O).

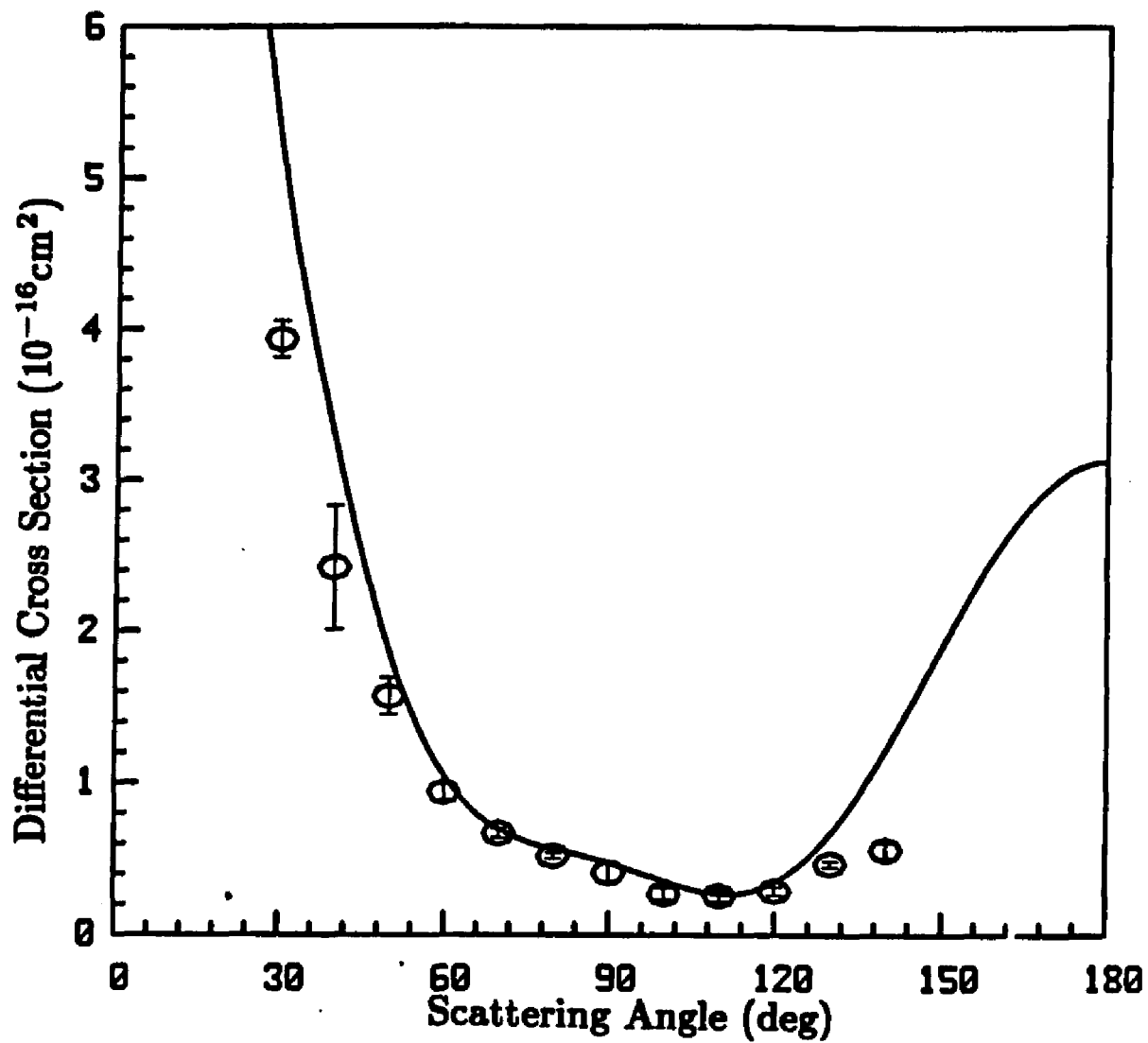


Figure 5: DCS for $e - \text{CH}_4$ scattering at 15 eV: present SE results (solid line), measured values of Ref. 28 (O).

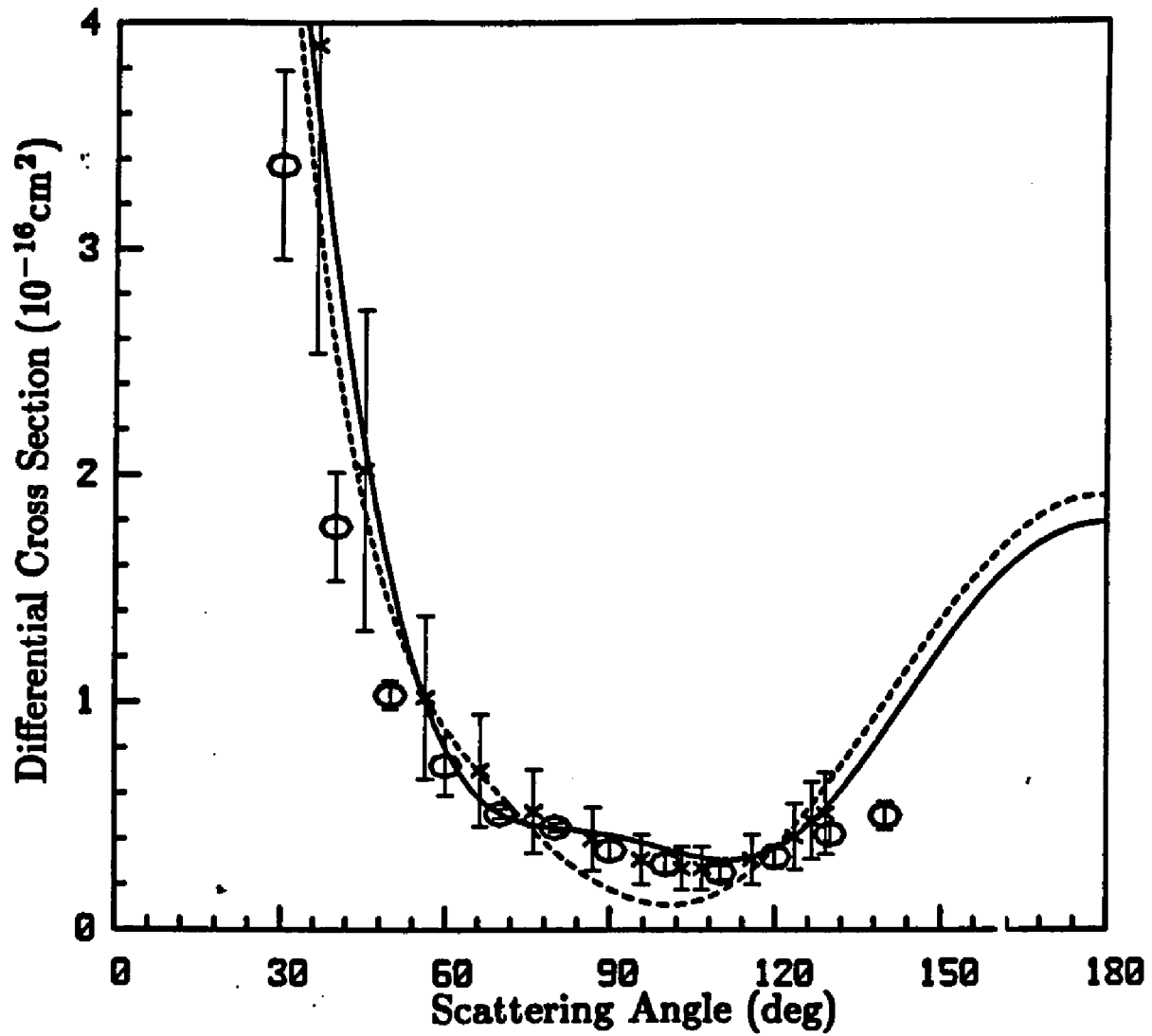


Figure 6: DCS for $e - \text{CH}_4$ scattering at 20 eV: present SE results (solid line), theoretical results of Ref. 25, measured values of Ref. 28 (\circ), measured values of Ref. 29 (\times).

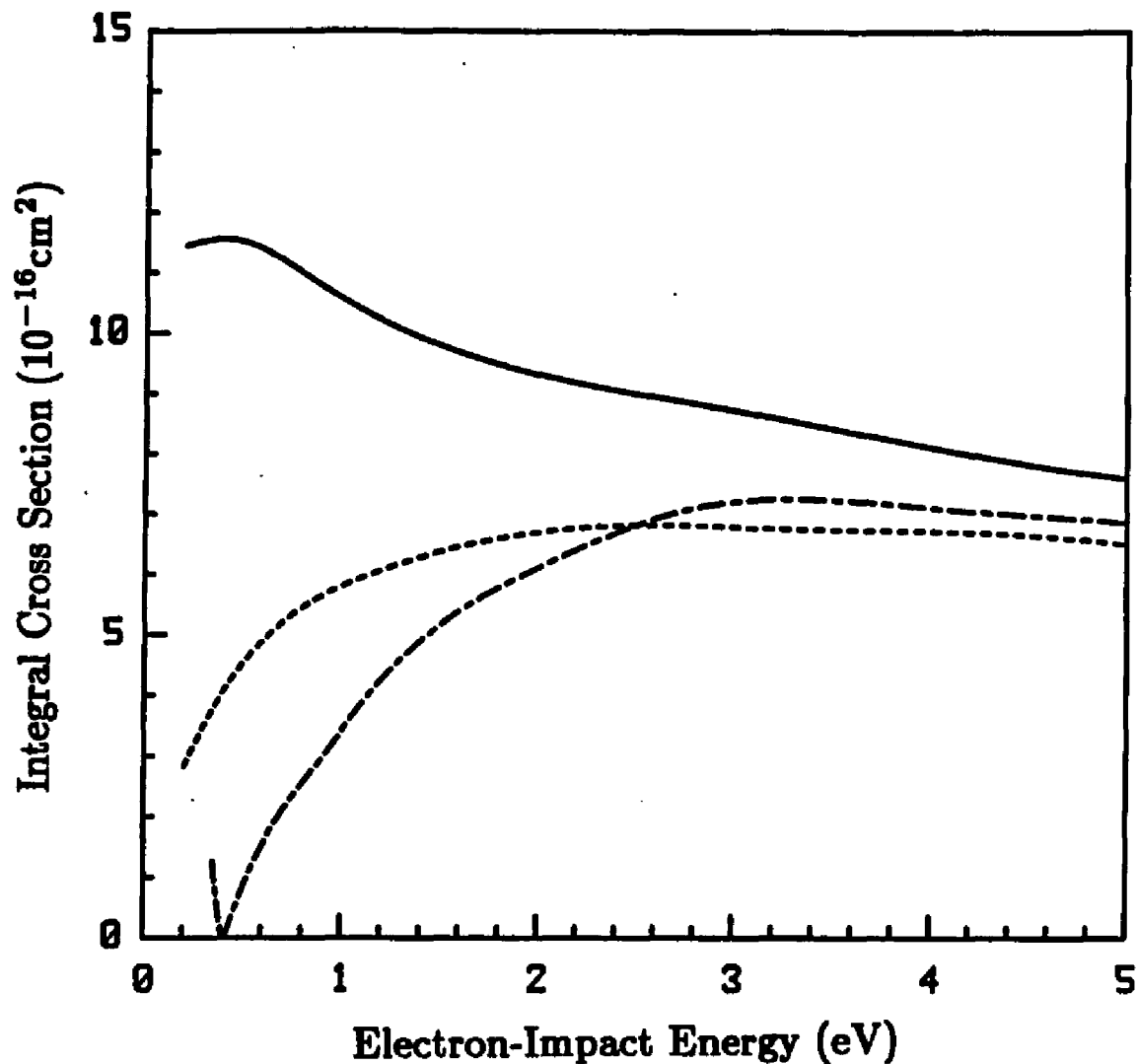


Figure 7: Elastic cross section for the 2A_1 symmetry: present SE results (solid line), present static-plus-exchange-plus-polarization (SEP) results (dashed line), static model-exchange (SME) results of Ref.22 (long-short dashed line).

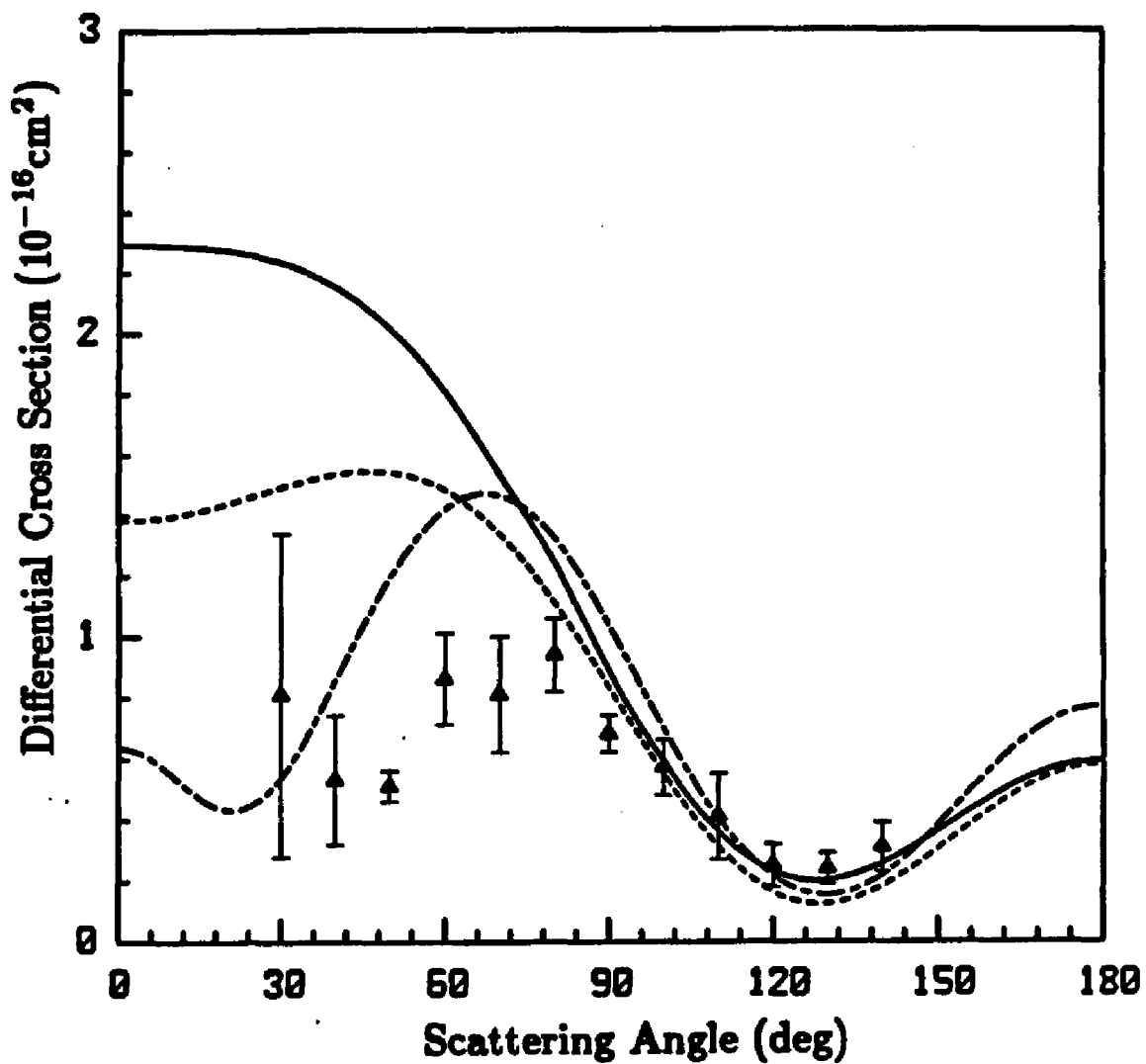


Figure 8: DCS for $e-\text{CH}_4$ scattering at 3 eV: present SE results (solid line), present SEP results (dashed line), SMEP results of Ref. 23 (long-short dashed line), measured values of Ref. 28 (Δ).

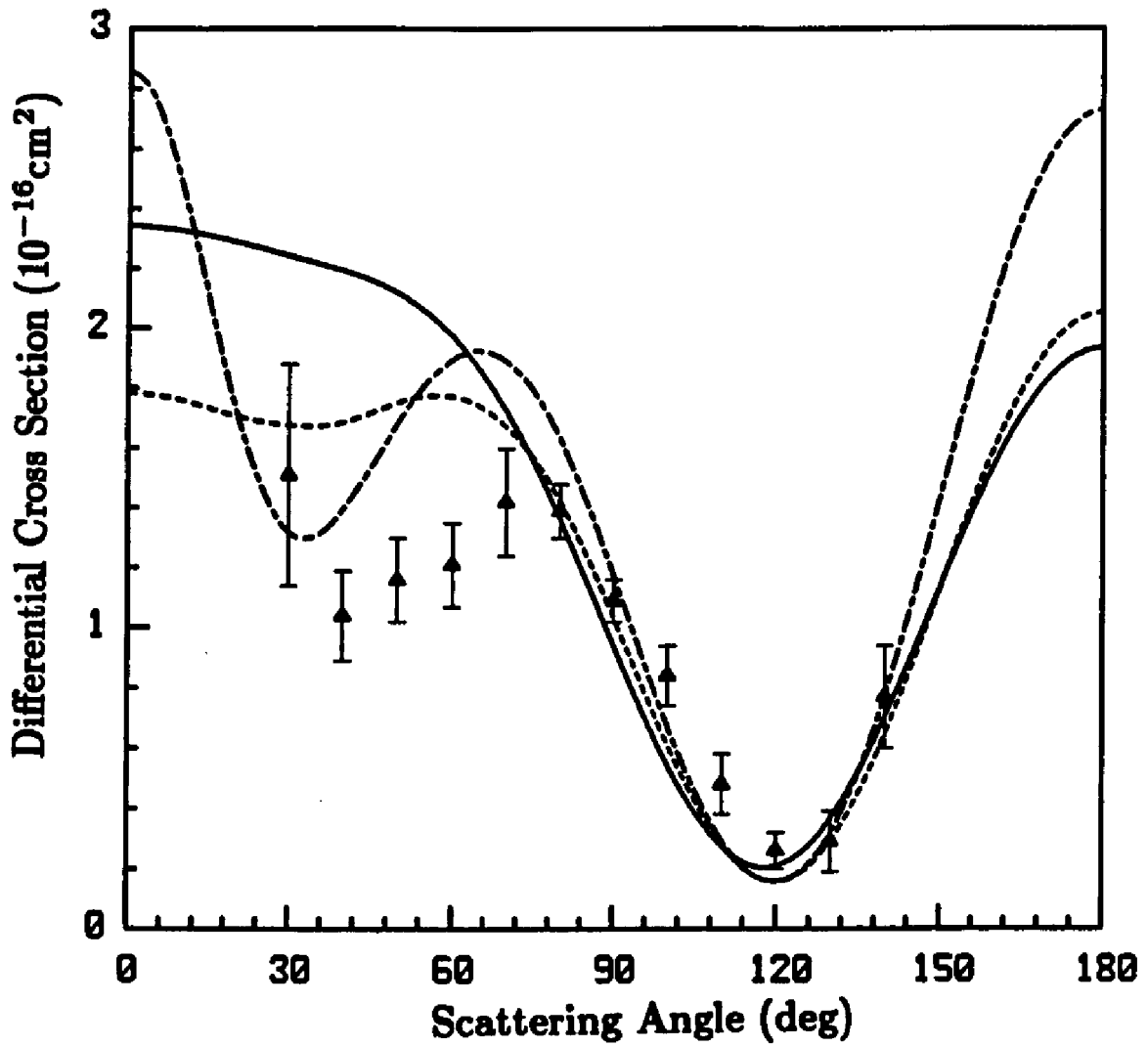


Figure 9: DCS for $e - CH_4$ scattering at 5 eV: same labels as in Fig.8.

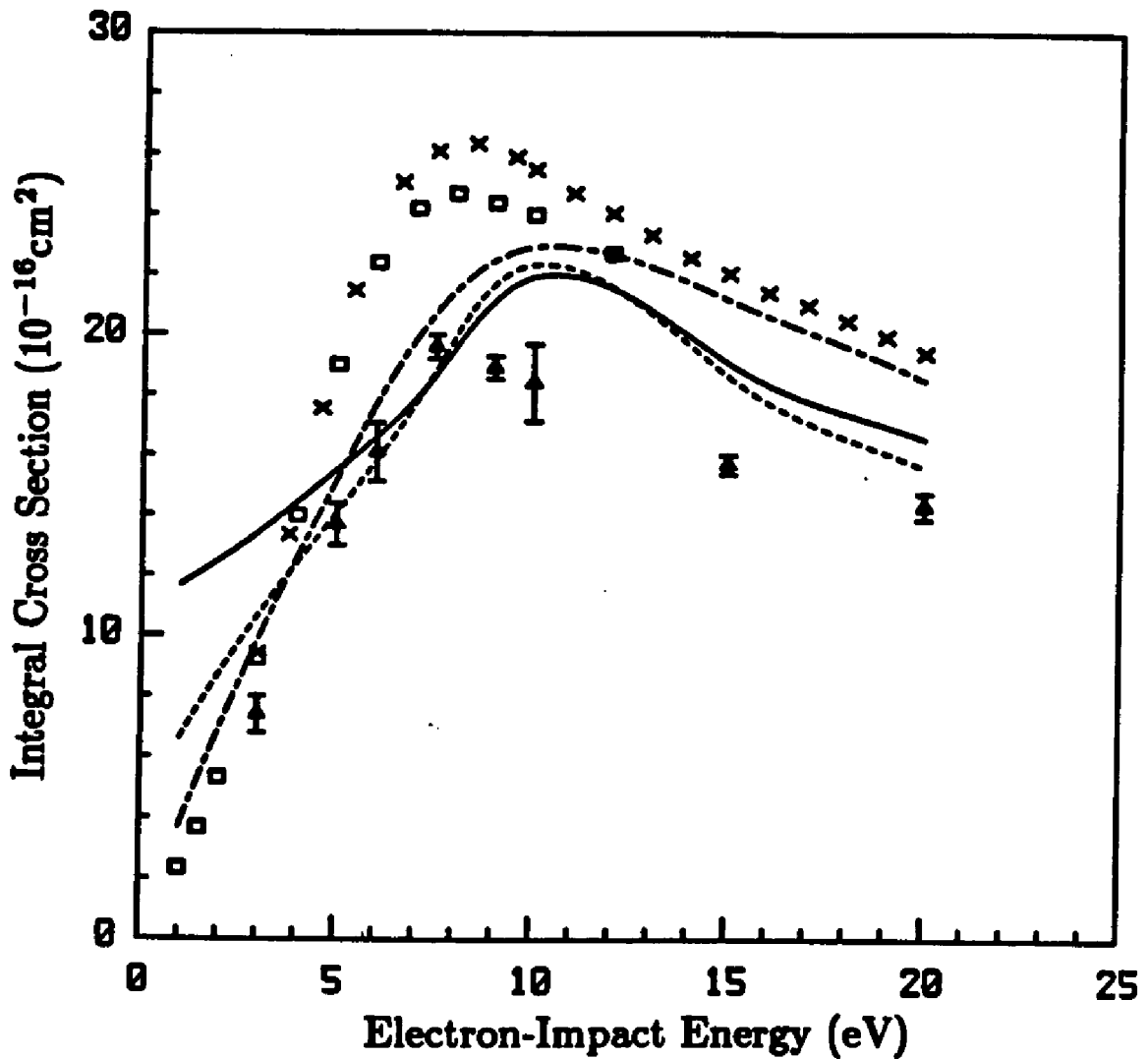


Figure 10: Elastic cross section for $e - \text{CH}_4$ scattering: present SE results (solid line), present SEP results (dashed line), SMEP results of Ref. 23 (long-short dashed line), measured values of Ref. 28 (Δ), measured values of Ref. 30 (\square), measured values of Ref. 31 (\times).

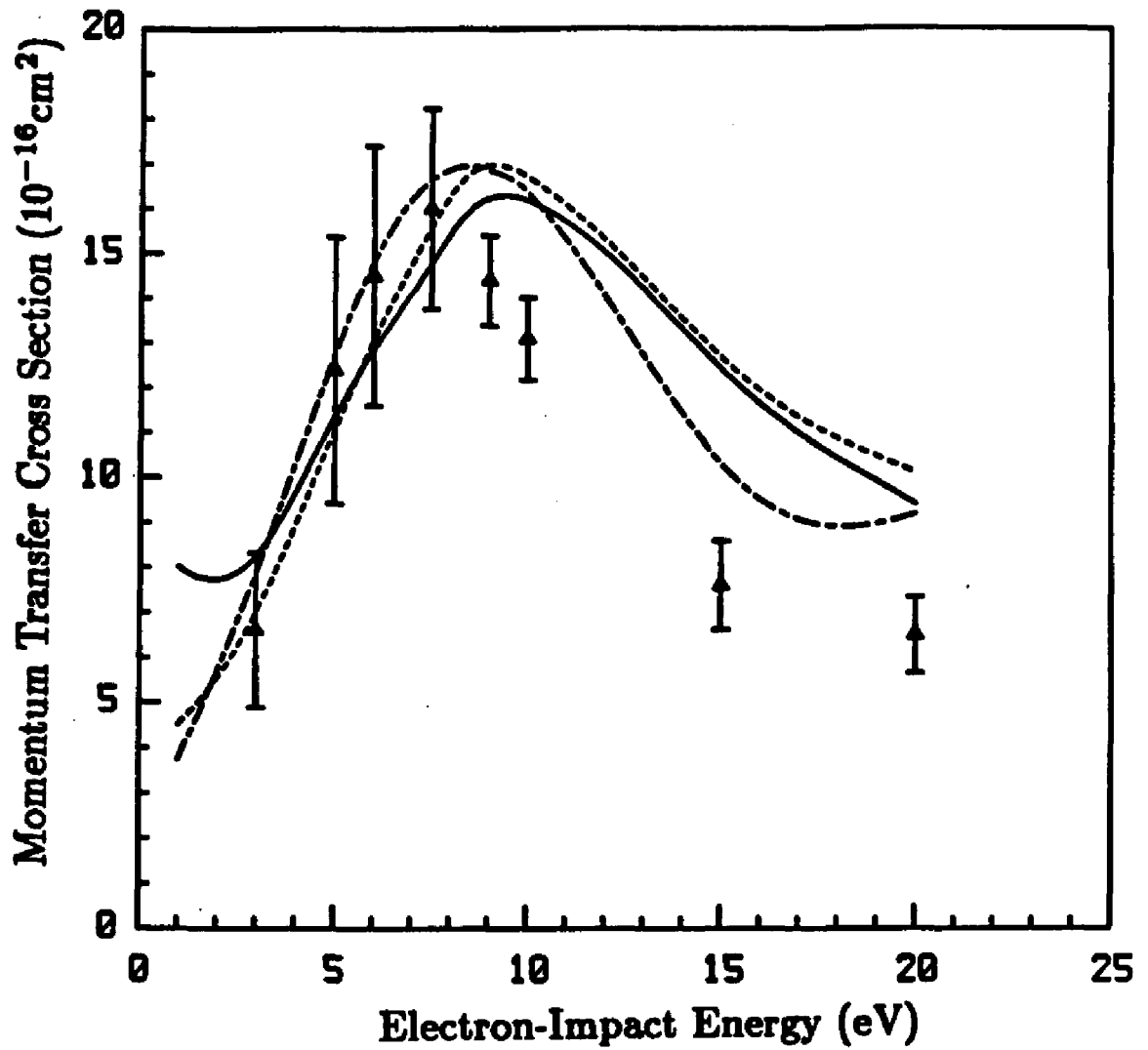


Figure 11: Elastic momentum transfer cross section for $e - \text{CH}_4$ scattering: present SE results (solid line), present SEP results (dashed line), SMEP results of Ref. 23 (long-short dashed line), measured values of Ref. 28 (Δ).

5. H₂O

We report elastic differential and momentum transfer cross sections for the elastic scattering of electrons by H₂O for collision energies from 2 to 20 eV. These fixed-nuclei static-exchange cross sections were obtained using the Schwinger variational approach. In these studies the exchange potential is directly evaluated and not approximated by local models. The calculated differential cross sections, obtained with a basis set expansion of the scattering wave function, agree well with available experimental data at intermediate and large angles. As used here, the results cannot describe adequately the divergent cross sections at small angles. An interesting feature of the calculated cross sections, particularly at 15 and 20 eV, is their significant backward peaking. This peaking occurs in the experimentally inaccessible region beyond a scattering angle of 120°. The implication of this feature for the determination of momentum transfer cross sections is discussed.

5.1 Introduction

Cross sections for the scattering of low-energy electrons by molecules play an important role in the modeling of gas lasers, planetary atmospheres, and swarm and plasma etching systems. In contrast to the related atomic problem, progress in both the experimental and theoretical studies of low-energy electron-molecule collisions has been limited.¹ On the theoretical side, this situation is primarily due to the additional complexities arising from the nonspherical potential fields of molecular targets. To date, most *ab initio* studies of electron-molecule colli-

sions have hence concentrated on linear molecules, where single-center expansion techniques are particularly well suited to exploit the cylindrical symmetry of such a system.²⁻⁴ A multicenter method designed to be applicable to target molecules of arbitrary geometry would dramatically widen the range of problems amenable to theoretical study.

In this section we present results of our studies of the cross sections for the elastic scattering of electrons by H_2O for incident energies from 2 to 20 eV. These cross sections were obtained in the fixed-nuclei and static-exchange approximations using a multichannel extension of the Schwinger variation principle which we have recently formulated. Such elastic fixed-nuclei cross sections are well-known to diverge in the forward direction for polar molecules.⁵ This divergence arises from the contribution of higher partial waves to the cross section which, in turn, are due to the long-range dipole potential. These higher partial waves can be well represented by a simple scattering approximation such as the Born.⁶ For these and other reasons, in the present studies we do not attempt to describe the strong forward peak of these differential cross sections but instead concentrate on obtaining the differential cross sections in the dynamically important region of intermediate and higher scattering angles. As the scattering angle is increased, the effect of low partial waves, which can be greatly affected by the short-range potential field, becomes more pronounced. The static-exchange potential, which we use in these studies, is known to account well for the scattering in this angular range. We will, in fact, see that a comparison of our calculated cross sections with

data over the experimentally accessible angular region, *i.e.* less than about 120° , bears this out particularly well. Furthermore, and more importantly, we will also see that our calculated differential cross sections rise significantly beyond 120° and are quite different from values which may be inferred from any extrapolation of the experimental data beyond 120° . Such differences in the differential cross sections can influence the derived values of momentum transfer cross sections.

In the next section we present several details of the applications of this theory to low-energy $e - \text{H}_2\text{O}$ scattering and compare the resulting cross sections with available experimental data.

5.2. Results and Procedures

In this section we discuss the results of our studies of the elastic static-exchange $e - \text{H}_2\text{O}$ scattering cross sections obtained using the Schwinger formulation. We will present elastic differential and momentum transfer cross sections for impact energies from 2 to 20 eV. These cross sections are obtained in the fixed nuclei approximation.

It is convenient to construct the ground state SCF wave function using a large uncontracted (15s10p3d) Cartesian Gaussian basis on the oxygen nucleus and a (6s1p) basis on the hydrogen nuclei. The exponents of these basis functions are shown in Table I. At the experimental equilibrium geometry⁶ of $R(\text{O-H}) = 1.81$ a.u. and $\theta(\text{H-O-H}) = 104.5^\circ$, this basis gives an SCF energy of -76.0545 a.u. This basis provides a large number of virtual orbitals ($39a_1$, $4a_2$, $13b_1$, $20b_2$), which are used to expand the trial scattering wave function and to satisfy

the closure relation assumed in the quadrature insertion technique for evaluating matrix elements $VG_P^{(\pm)}V$. In the body frame all calculated amplitudes include contribution from $(N+1)$ electron Slater determinants of 2A_1 , 2A_2 , 2B_1 and 2B_2 symmetries. In the partial wave decomposition of the scattering amplitude we included terms with $\ell \leq 5$.

In Figs. 1-5 we show our calculated fixed-nuclei elastic differential cross sections for collision energies of 2, 6, 10, 15, and 20 eV along with the theoretical results of Jain and Thompson⁷ and the experimental data of Danjo and Nishimura⁸ and of Jung *et al.*⁹, where available. We report differential cross sections for angles beyond about 30° because, as discussed earlier, the scattering solutions are obtained with a large discrete basis which, although containing some very diffuse functions, cannot describe the higher partial waves which lead to the divergence in this region.

Although there are no experimental data at 2 eV with which to compare, our differential cross sections at this energy do show a shallow minimum around 130° with a slight increase at higher angles. This behavior is quite similar to what is seen in related studies of e-LiF by Norcross and Collins.⁵ A comparison with the calculated results of Jain and Thompson,⁷ using a static model-exchange polarization potential, is not very meaningful since their cross sections are available at only two angles. At 6 eV our differential cross section between 30° and about 80° differ considerably from the data of Danjo and Nishimura⁸ which, in turn, are very different from the experimental values of Jung *et al.*⁹ Reasons for

either of these disagreements are not apparent at present. Our calculated cross sections between 80° and 120° agree well in both shape and magnitude, with the measurements of Danjo and Nishimura.⁸ The results of Jain and Thompson⁷ at 60° and 90° are in good agreement with the data of Danjo and Nishimura.⁸

The calculated differential cross sections at 10, 15, and 20 eV, shown in Figs. 3-5, agree well with the experimental data of Danjo and Nishimura.⁸ The experimental data again extend only to 120° . Beyond 120° our cross sections show a significant backward peak, which becomes more pronounced as the energy increases. This is probably the most important feature in these results. This backward peaking will obviously contribute significantly to the momentum transfer cross sections derived from these cross sections via the usual relationship; *i.e.*,

$$\sigma^M = 2\pi \int_0^\pi \frac{d\sigma}{d\theta} (1 - \cos\theta) \sin\theta d\theta. \quad (1)$$

Furthermore, a smooth extrapolation of the measured data beyond 120° would very likely underestimate greatly the differential cross sections. Momentum transfer cross sections of Danjo and Nishimura,⁸ assuming a smooth extrapolation of the data beyond 120° , are shown in Fig. 6. The larger discrepancies, between the calculated and "measured" momentum transfer cross sections seen at the higher energies in Fig. 6 are due to differences in the differential cross sections at larger angles. In fact, contribution from these angles dominates the momentum transfer cross sections. We expect that calculated differential elastic cross sections will generally prove very useful in the extrapolation of measured

data to high, and experimentally inaccessible, angular regions.¹⁰

5.3. Conclusions

In this section we have discussed the results of applications of the Schwinger variational method to the elastic scattering of low-energy electron by H_2O . We have studied these differential and momentum transfer cross sections at the static-exchange level and for collision energies from 2 to 20 eV. Although these results were obtained using an expansion of the scattering wave function in a large discrete basis and hence cannot describe small angle scattering adequately, the calculated cross sections agree quite well with available experimental data. Furthermore, our differential cross sections show significant backward peaking, particularly at 15 and 20 eV. This behavior lies in the experimentally inaccessible region beyond 120° , where any usual extrapolation of the experimental data below 120° would lead to estimates of the cross sections very different from the calculated results. This feature can be particularly important in the determination of momentum transfer cross sections from beam measurements.

References

1. See, for example, S. Trajmar, D. F. Register, and A. Chutjian, *Phys. Repts.* **97**, 219 (1983).
2. N. F. Lane, *Rev. Mod. Phys.* **52**, 29 (1980).
3. See, for example, B. I. Schneider and L. A. Collins, *Phys. Rev. A* **27**, 2847 (1983); *J. Phys. B* **18**, L857 (1985).
4. R. R. Lucchese, K. Takatsuka, and V. McKoy, *Phys. Repts.* **131**, 147 (1986).
5. See, for example, D. W. Norcross and L. A. Collins, *Adv. in Atomic and Molecular Phys.* **118**, 341 (Academic, New York, 1982).
6. See, for example, L. C. Snyder and H. Basch, *Molecular Wave Functions and Properties* (Wiley, New York, 1972).
7. A. Jain and D. G. Thompson *J. Phys. B* **15**, L631 (1982).
8. A. Danjo and H. Nishimura, *J. Phys. Soc. Japan* **54**, 1224 (1985).
9. K. Jung, T. Antoni, R. Muller, K. H. Kochen, and H. Ehrhardt, *J. Phys. B* **15**, 3535 (1982).
10. See, for example, M. A. P. Lima, T. L. Gibson, W. M. Huo, and V. McKoy, *Phys. Rev. A* **32**, 2696 (1985).

Table I. Cartesian Gaussian Basis Set^{a,b}

Gaussian center ^c and type	Exponents (α)
O, 15s	7816.54, 1175.82, 273.88, 81.1696, 27.1836, 9.5322, 3.4136, 0.9398, 0.2846, 0.0712, 0.0178, 0.00445, 0.0012, 0.0003, 0.0001,
O, 10p	35.1832, 7.904, 2.3051, 0.7171, 0.2137, 0.054, 0.0135, 0.00338, 0.00084, 0.00021
O, 3d	1.2188, 0.3610, 0.09
H, 6s	13.3615, 2.0133, 0.4538, 0.123, 0.02, 0.002
H, 1p	0.8371

^a Defined by $X_{lmn}^{(\alpha)} = N_{lmn} (x - A_x)^l (y - A_y)^m (z - A_z)^n e^{-\alpha|\vec{r}-\vec{A}|^2}$, where \vec{A} is the position of the Gaussian center.

^b Basis set used for the ground state of H₂O, in the expansion of the scattering functions, and for insertion around $V G_P^{(+)} V$.

^c At the equilibrium position of $R_{OH} = 1.814a_0$ and $\theta_{HOH} = 104.5^\circ$

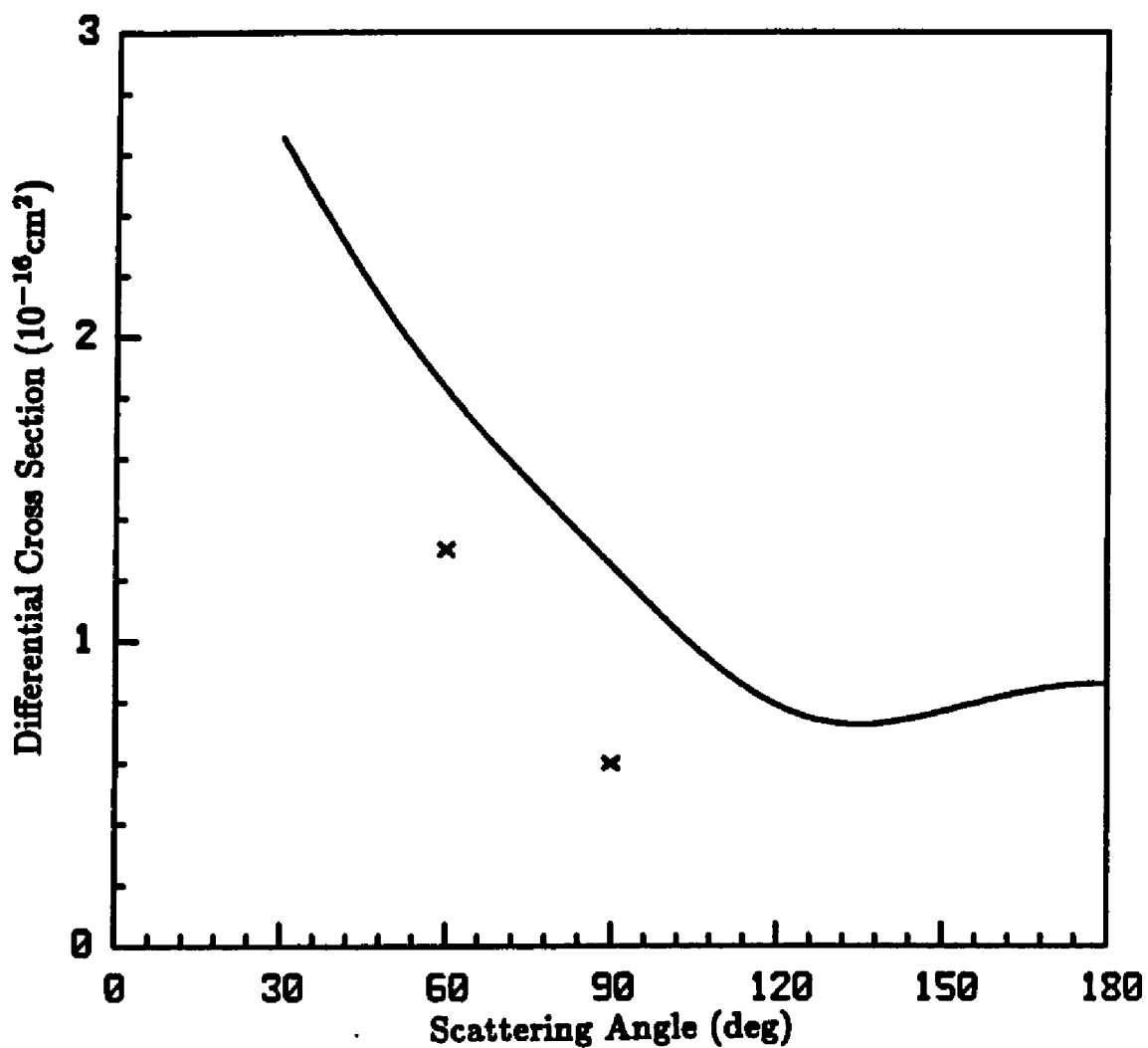


Figure 1: Differential cross sections (DCS) for $e-H_2O$ scattering at 2 eV: present static-plus-exchange (SE) results (solid line), static model-exchange polarization (SMEP) results of Ref. 7 (x).

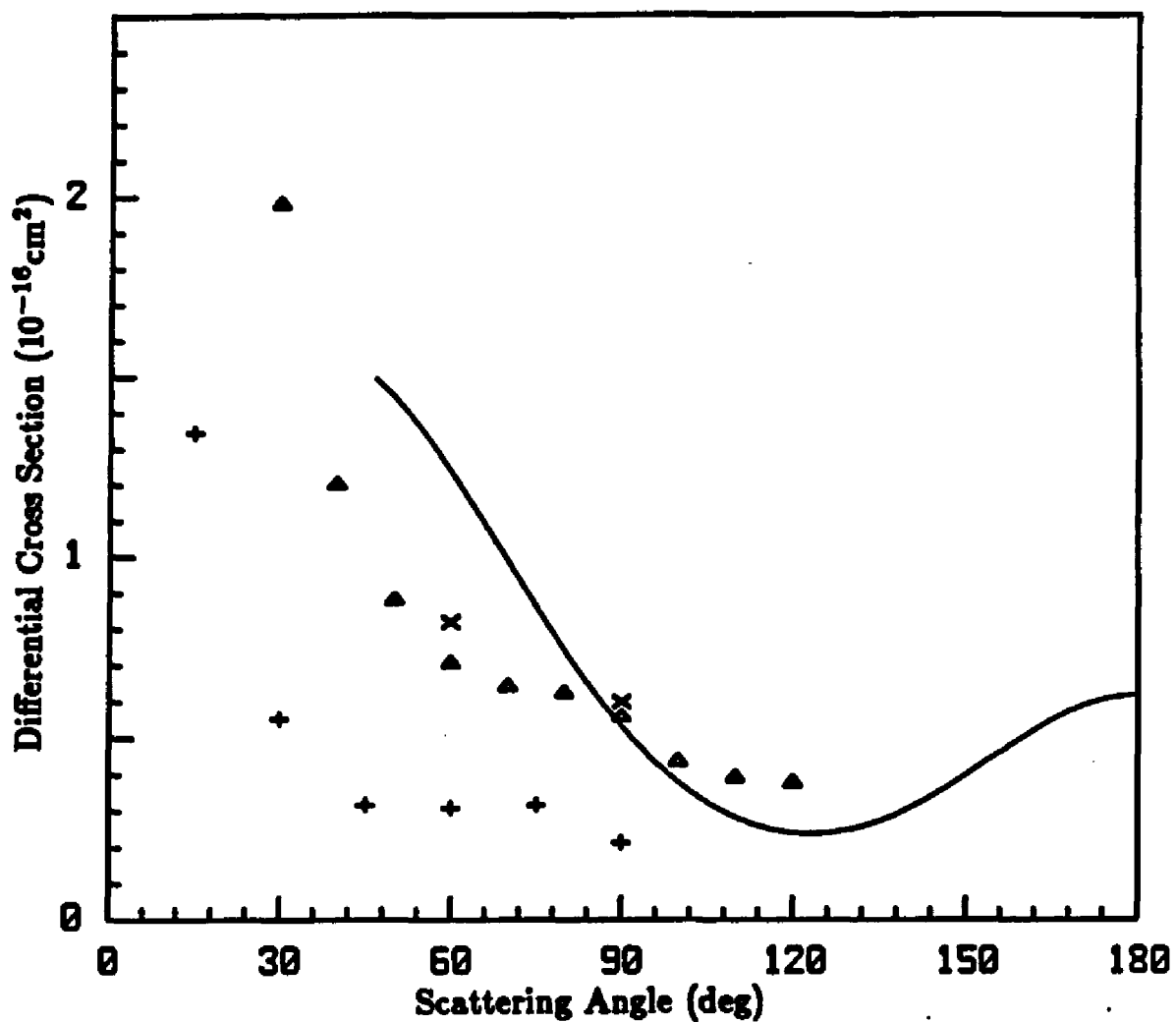


Figure 2: DCS for $e-H_2O$ scattering at 6 eV: present SE results (solid line), SMEP results of Ref. 7 (\times), measured values of Ref. 8 (Δ), measured values of Ref. 9 (+).

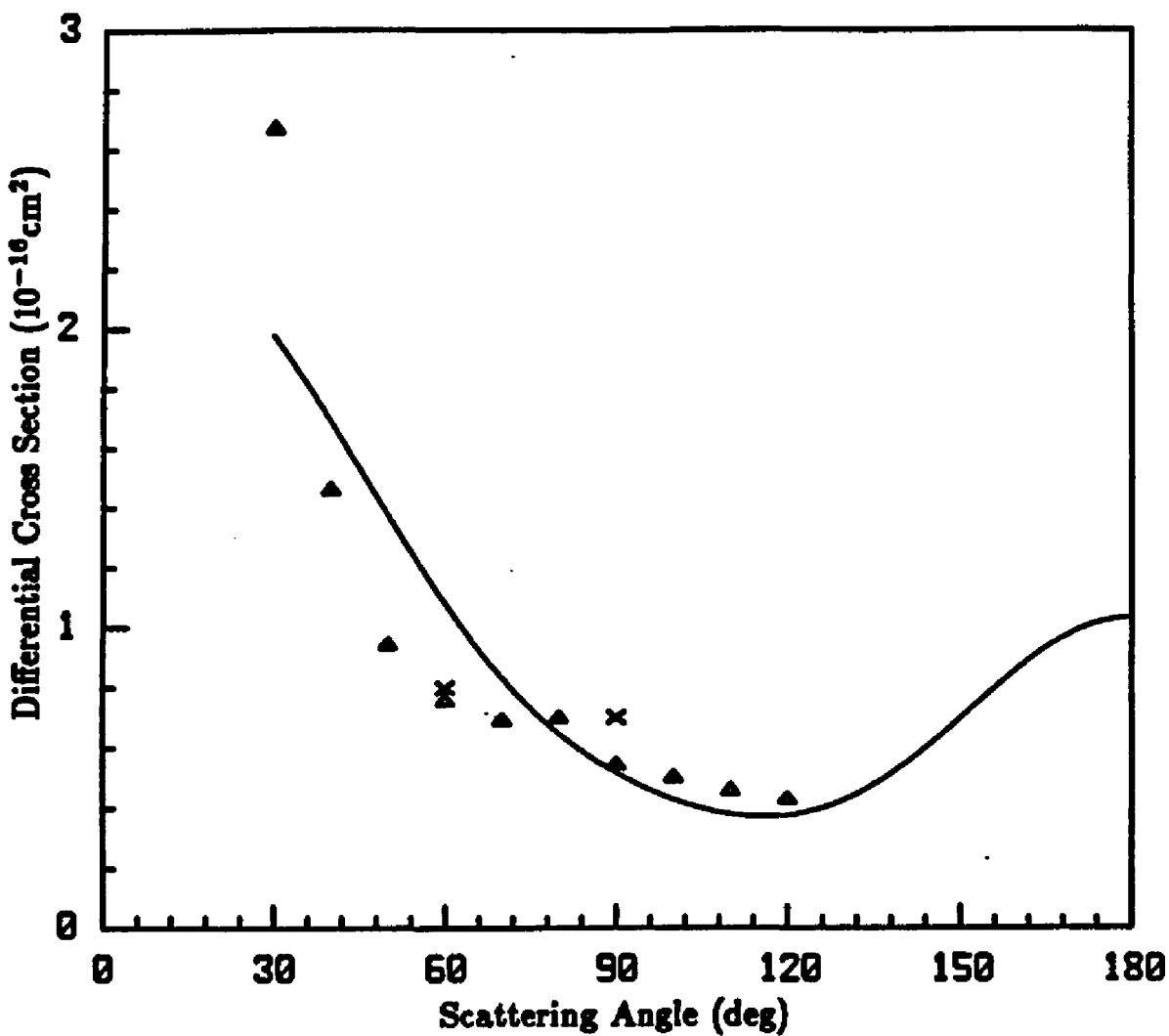


Figure 3: DCS for $e - H_2O$ scattering at 10 eV: present SE results (solid line), SMEP results of Ref. 7 (x), measured values of Ref. 8 (Δ).

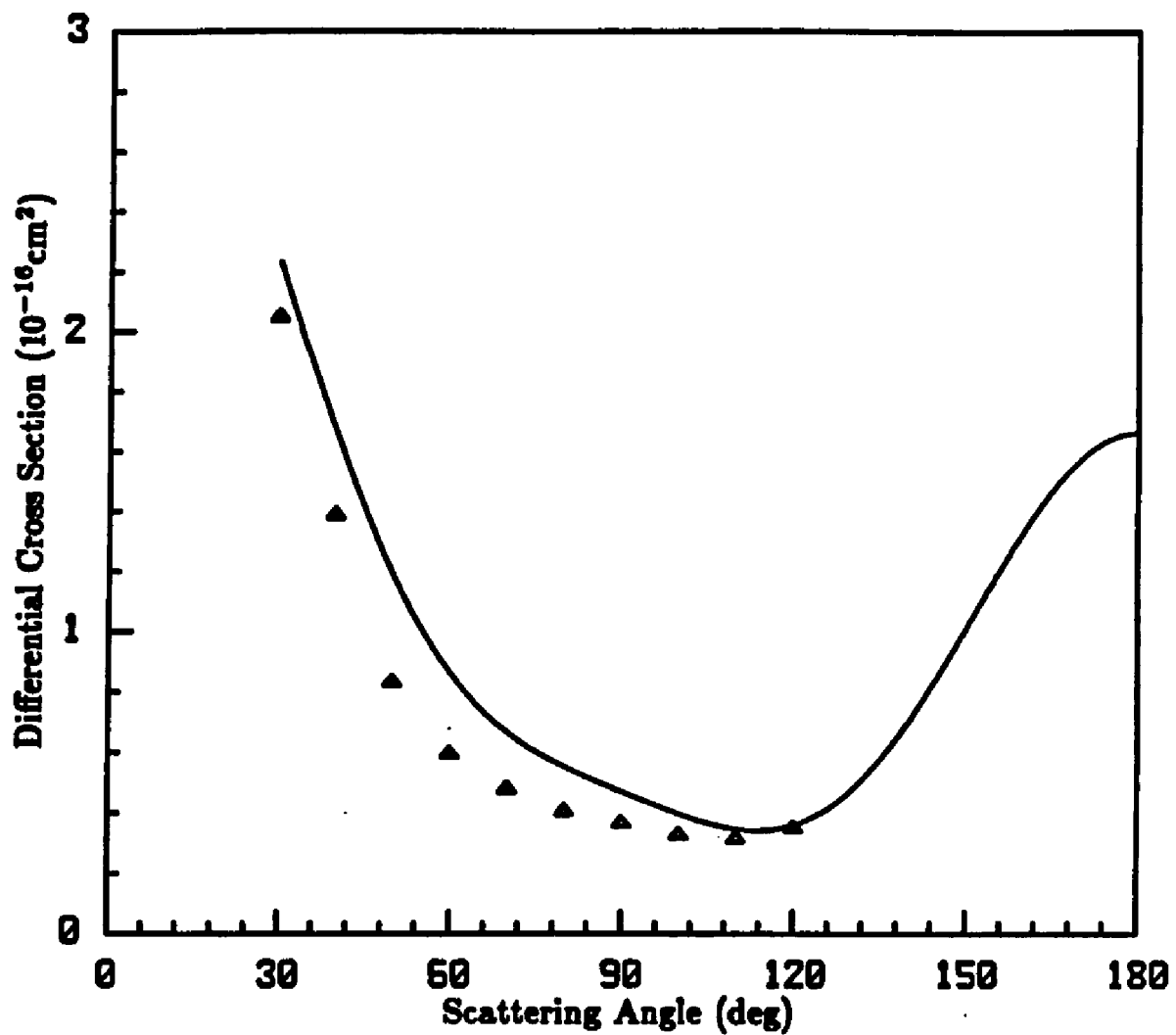


Figure 4: DCS for $\epsilon - \text{H}_2\text{O}$ scattering at 15 eV: present SE results (solid line), measured values of Ref. 8 (Δ).

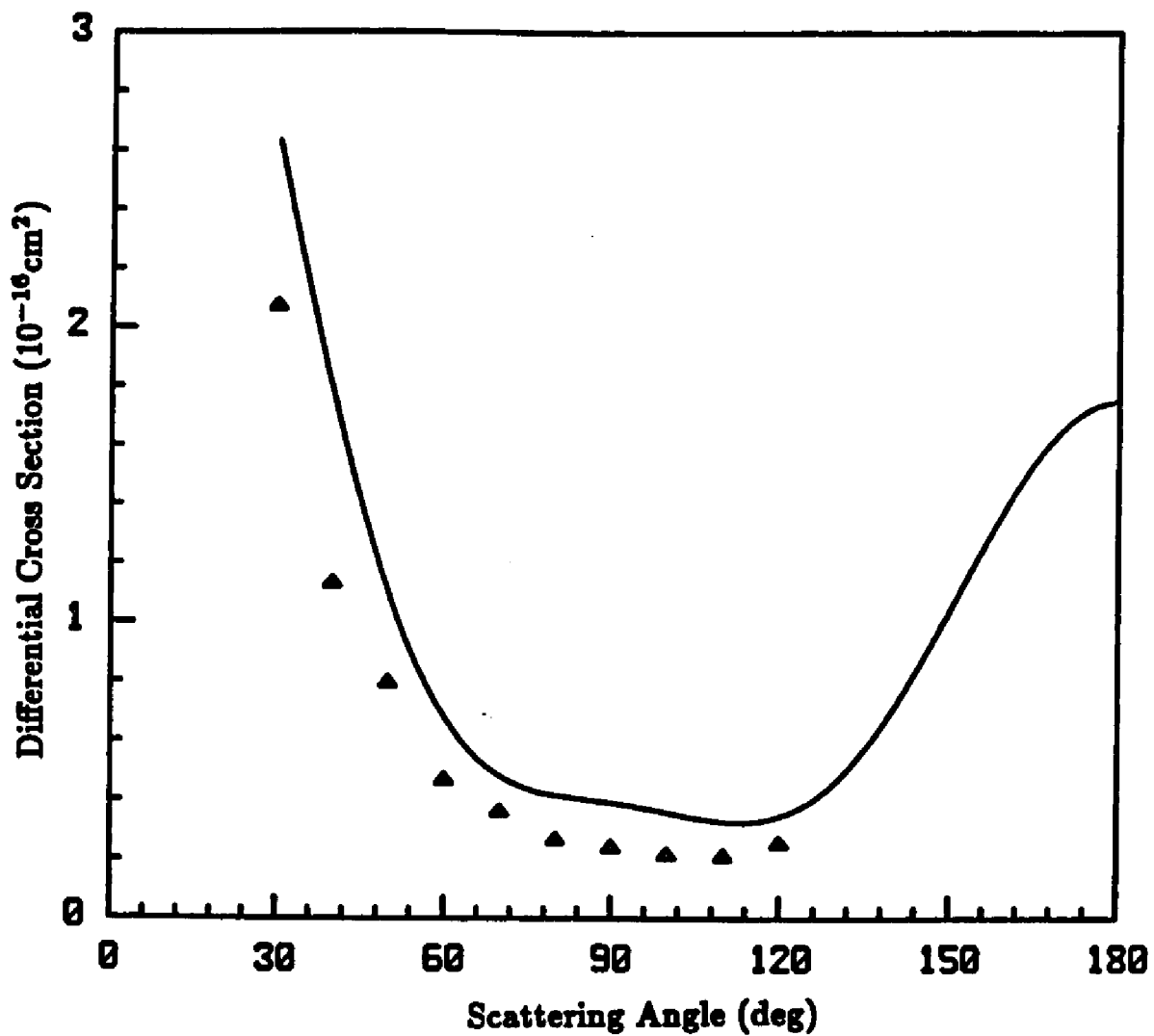


Figure 5: DCS for $e - \text{H}_2\text{O}$ scattering at 20 eV: present SE results (solid line), measured values of Ref. 8 (Δ).

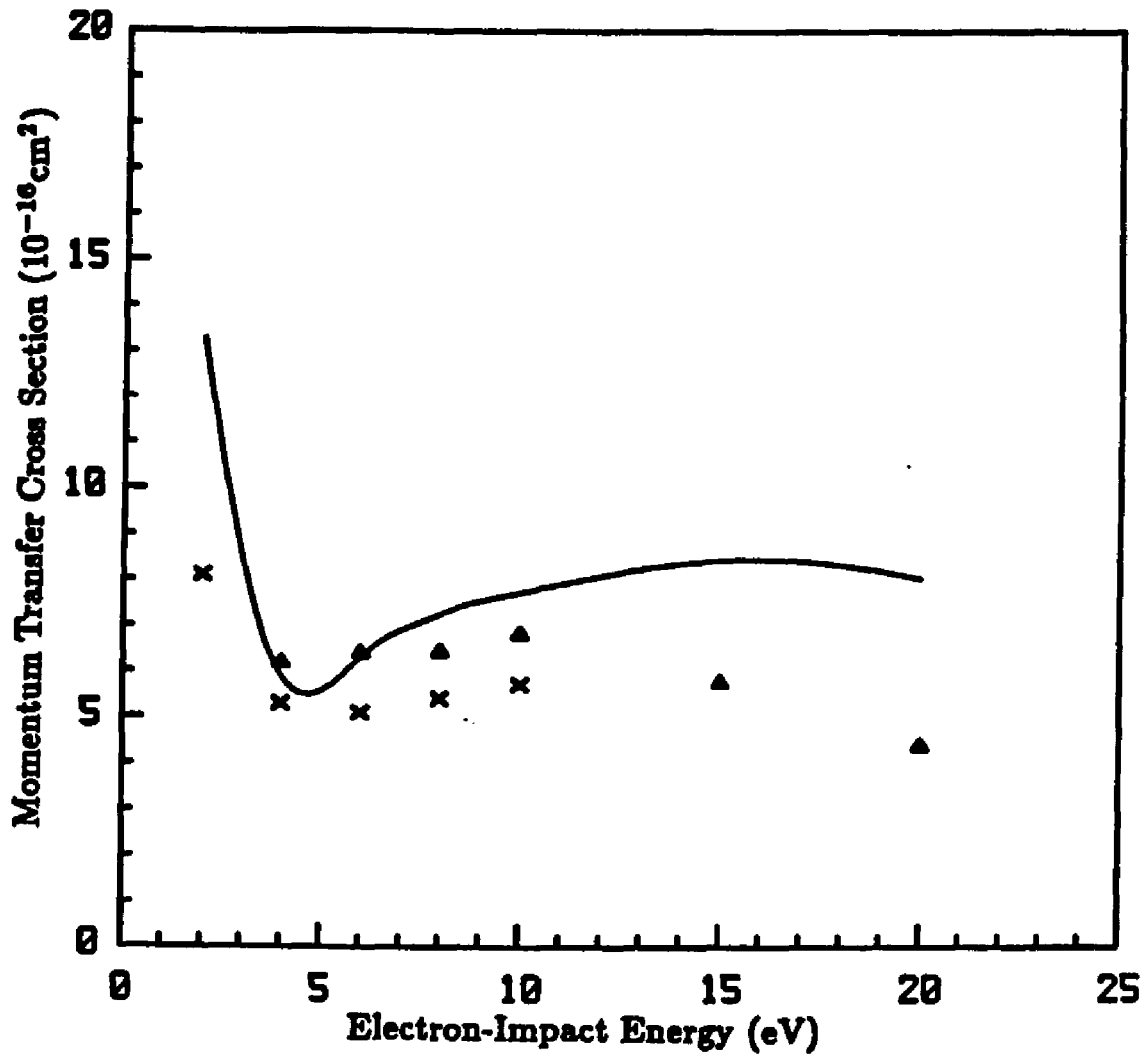


Figure 6: Elastic momentum transfer cross section for $e - \text{H}_2\text{O}$ scattering: present SE results (solid line), present SMEP results of Ref. 7 (\times), measured values of Ref. 8 (Δ).

V. Applications to Electronically Inelastic Electron-Molecule Collisions

1. Cross sections for electron impact excitation of the $a^3\Sigma_g^+$, $b^3\Sigma_u^+$, and $c^3\Pi_u$ states of H_2

As a first application of the Schwinger multichannel theory to electronically inelastic collisions, we have calculated integral and differential cross sections for electron-impact excitation of the transitions $X^1\Sigma_g^+ \rightarrow a^3\Sigma_g^+$, $b^3\Sigma_u^+$, and $c^3\Pi_u$ in H_2 for scattering energies from near threshold to 30 eV at the two-state level. Our results are seen to be in good agreement with other recent theoretical results for the $X^1\Sigma_g^+ \rightarrow b^3\Sigma_u^+$ transition of H_2 . We also find good agreement between our cross sections and the available experimental data for the $X^1\Sigma_g^+ \rightarrow a^3\Sigma_g^+$ and $b^3\Sigma_u^+$ transitions. Our method does not rely on single-center expansions to calculate the *body*-frame scattering amplitude and is designed to be applicable to molecules of arbitrary geometry.

1.1 Introduction

Accurate cross sections for the electronic excitation of molecules by low-energy (≤ 30 eV) electron impact are important for a variety of reasons. Measurements¹ in this energy region can be often difficult and time-consuming, and hence theoretical studies of these cross sections for linear and small polyatomic targets are obviously desirable. In particular, the differential cross sections give considerable insight into the physics of the electron-molecule interaction as well as provide a sensitive test of the collision theory being used. This last point is quite important since a number of theoretical approaches involving varying degrees of

approximation are available. These approaches include plane-wave theories such as the Born-Ockhur-Rudge approximations,^{2,3} the impact-parameter method,⁴ distorted-wave theories,^{5,6} and multichannel theories. Plane-wave theories are lowest-order theories containing approximations valid at high-impact energies. These theories are computationally easy to apply, but recent studies^{7,8} have shown that they lead to qualitatively and quantitatively incorrect differential cross sections at low and intermediate electron energies. The impact-parameter method⁴ is a semiclassical approach in which the projectile electron is treated classically and although this method can provide some improvement over plane-wave theories, it does not include enough of the collision physics to produce reliable differential cross sections at low energies. A distorted-wave approach is the next logical step beyond the plane-wave theories. Recently, studies using a distorted-wave approximation^{7,8} in the 20-100 eV range have shown that this method can predict differential cross sections in qualitative agreement with measured values. However, there are serious quantitative disagreements between these distorted-wave cross sections and available data in several cases.⁸ Multichannel theories of these inelastic collisions have the firmest theoretical basis, but they are considerably more difficult to apply. Two-state close-coupling calculations, *albeit* with the restrictive orthogonality constraint on the bound and continuum orbitals, have been carried out for selected transitions in H₂ by Chung and Lin⁹ and by Weatherford¹⁰ and for the a¹Π_g channel in N₂ by Holley *et al.*¹¹ Despite difficulties, in recent years efforts have been under way to extend

three different techniques, previously applied widely to electron-molecule collisions at the static-exchange level, to electronic excitation. These techniques are the linear algebraic,¹²⁻¹⁶ the R-matrix,¹⁷⁻²⁰ and the Schwinger multichannel methods.²¹⁻²⁴ The primary objectives of these efforts have been to assess the validity of the various techniques by applying them to small molecular systems and to provide benchmarks for these same systems. Here we report the results obtained from the application of the Schwinger multichannel formulation to $e - H_2$ collisions. Specifically, we have calculated integral and differential cross sections for electron impact excitations of the $a^3\Sigma_g^+$, $b^3\Sigma_u^+$, and $c^3\Pi_u$ states of H_2 for impact energies ranging from near threshold to 30 eV. In the following we discuss the relevant computational details of our calculations and compare our results with available theoretical^{6-9,16,20} and experimental²⁵⁻²⁹ data.

1.2 Procedures and Results

We have used our multichannel extension of Schwinger's variational principle to study the cross sections for excitation of the $b^3\Sigma_u^+$, $a^3\Sigma_g^+$ and $c^3\Pi_u$ states of H_2 for collision energies from near threshold to 30 eV in the two-state approximation.²

Our calculations are carried out within the framework of the fixed-nuclei and Frank-Condon approximations³⁰ with the rotational levels treated as degenerate. The physical cross sections are obtained by averaging the fixed-nuclei results over all molecular orientations. A single electronic transition matrix element is calculated with outgoing electron energy determined by the vertical transition

energy from the ground state at an internuclear distance of $1.400 a_0$ to the specific excited state (a, b or c). The values of the threshold energies determined this way are taken to be 9.98, 12.04, and 12.31 eV for the $b^3\Sigma_u^+$, $a^3\Sigma_g^+$ and $c^3\Pi_u$, respectively. For simplicity all our cross sections are reported for the complete band system; *i.e.*, summed over all final vibrational levels. Although at the lower incident energies this assumption is not quite correct, here we concentrate only on the fixed nuclei cross sections.

For the ground state we use a self-consistent field (SCF) wave function obtained with a 6s6p Cartesian Gaussian basis on the hydrogens and a 4s4p basis at the midpoint (Table I). The SCF energy for the ground state is -1.133 au. For the $b^3\Sigma_u^+(1\sigma_g 1\sigma_u)$, $a^3\Sigma_g^+(1\sigma_g 2\sigma_g)$ and $c^3\Pi_{u_x(y)}(1\sigma_g 1\pi_{u_x(y)})$ states we make the frozen-core approximation and determine the excited state orbitals ($1\sigma_u$, $2\sigma_g$, $1\pi_{u_x}$, and $1\pi_{u_y}$) by diagonalizing the V_{N-1} potential of the core in the SCF basis. The entire set of V_{N-1} eigenfunctions, *i.e.*, improved virtual orbitals (IVO) ³¹ is also available for use in expanding the (N+1)-particle wave function. A Gaussian basis set used as additional scattering functions to better describe the (N+1)-particle wave function (particularly the $^2\Delta$ symmetry) for the $c^3\Pi_u$ excitation is also shown in Table I.

In contrast to earlier close-coupling calculations we do not enforce orthogonality conditions between the scattering functions and the bound state orbitals. Such conditions are relaxed by including correlation terms in the expansion of the (N+1)-particle functions, *i.e.*, $1\sigma_g^2 1\sigma_u$ and $1\sigma_g 1\sigma_u^2$ for the $b^3\Sigma_u^+$ excitation,

$1\sigma_g^2 2\sigma_g$ and $1\sigma_g 2\sigma_g^2$ for the $a^3\Sigma_g^+$ excitation, and $1\sigma_g^2 1\pi_{u,(v)}$ and $1\sigma_g 1\pi_{u,(v)}^2$ for the $c^3\Pi_{u,(v)}$ excitation. In fact, the wave function used in recent Schwinger calculations²³ of the $b^3\Sigma_u^+$ excitation cross sections also did include these correlation terms. However, due to a computational error, the influence of the correlation terms on the cross sections was not properly incorporated in these calculations. The resulting cross sections were fortuitously similar to the earlier close-coupling results of Chung and Lin.⁹ Recent studies of the $X^1\Sigma_g^+ \rightarrow b^3\Sigma_u^+$ transition by Schneider and Collins¹⁶ show that the inclusion of these terms may contribute substantially to the cross sections.

In the body frame all calculated results include $\Sigma_g, \Sigma_u, \Pi_g,$ and Π_u symmetries of the $(N+1)$ -particle functions $\Psi_m^{(\pm)}$. For the $c^3\Pi_u$ excitation we also included Δ_g and Δ_u symmetries. Of the available scattering functions, no more than $16\sigma_g, 16\sigma_u, 10\pi_{u_z}, 10\pi_{u_y}, 6\pi_{g_z}, 6\pi_{u_z}, 6\delta_g$ and $6\delta_u$ are used to construct the $(N+1)$ -Slater determinants for the expansion of $\Psi_m^{(\pm)}$.

We first obtain the full representation of the scattering amplitude $f(\vec{k}_f, \vec{k}_i)$ in the body frame in an 8-point Gauss-Legendre quadrature for integration over θ along with 8-point quadrature for each "hemisphere" of integration over ϕ . By numerical integration we then generate the partial wave representation of the scattering amplitude in the body frame needed for the transformation into the laboratory frame.²³ For given \vec{k}_f and \vec{k}_i this requires a 128 by 128 matrix of values for $f(\vec{k}_f, \vec{k}_i)$, many of which need not actually be computed since they are related by symmetry to other matrix elements. Furthermore, for the scattering

energies considered here, we restrict the partial-wave expansion of the inelastic scattering to values of $\ell \leq 4$. Finally, after accounting for the random orientation of the target, the differential cross section is obtained in the usual manner by performing the appropriate average-over-initial and sum-over-final spin states.

a. Excitation of the $b^3\Sigma_u^+$ state of H_2

We have obtained the differential and integral cross sections for excitation of the $b^3\Sigma_u^+$ state of H_2 by 10.5 -30 eV electrons. Among the symmetries ($\Sigma_g, \Sigma_u, \Pi_g$, and Π_u) for the total wave function we included in this calculation, Π_u is unimportant for all energies, and Σ_g and Π_g are basically degenerate (they differ in less than 20 % in the entire energy spectrum). The Σ_u contribution represents almost the entire cross section at 10.5 eV, half at 15 eV and one third of the integral cross section at 30 eV. Our calculated cross section agrees quite well, symmetry-by-symmetry, with those obtained with the linear algebraic method by B. Schneider and L. Collins.¹⁶

Figure 1 shows our calculated differential excitation cross section for the $X^1\Sigma_g^+ \rightarrow b^3\Sigma_u^+$ transition at 10.5 along with the experimental data of Hall and Andrić.²⁵ Figure 2 shows the cross sections for this transition at 12 eV. At this energy we also compare our two-state results with the distorted-wave cross sections of Fliflet and McKoy.⁷ The agreement between these two-state cross sections and the experimental results at impact energies 0.5 eV and 1.5 eV above threshold is very encouraging. In Figs. 3,4,5 and 6 we compare our differential cross sections at 13, 15,20, and 30 eV, respectively, with the experimental data

of Nishimura.²⁶ In these figures we also show the distorted-wave cross sections of Fliflet and McKoy⁷ where available and the experimental data of Khakoo *et al.*²⁷ at 20 and 30 eV. The agreement between our cross sections and Nishimura's²⁶ data is good for all energies. At 13 and 15 eV impact energies, the experimental data of Nishimura²⁶ show a slight peak in the forward direction, not seen in our calculated results. The agreement above 45° for those two energies is excellent. Why these two-state cross sections agree as well as they do with the measured values at collision energies where many other target channels are open is not obvious and may be specific to the intravalence nature of this transition.

Figure 7 shows our calculated integral cross sections for the $X^1\Sigma_g^+$, $b^3\Sigma_u^+$ excitation along with the experimental data of Hall and Andrić,²⁵ Khakoo *et al.*²⁷ and Nishimura.²⁶ In this figure we also include the results of two-state calculations of Schneider and Collins,¹⁶ Baluja *et al.*,²⁰ and Chung and Lin.⁹ Our calculated cross sections together with the theoretical results of Schneider and Collins¹⁶ and Baluja *et al.*²⁰ agree well at all energies with the experimental data of Hall and Andrić,²⁵ Khakoo *et al.*,²⁷ and Nishimura.²⁶ There are, however significant differences between the two-state cross sections of Chung and Lin⁹ and the other's two-state calculations shown in Fig. 7. These differences as discussed earlier (see also References 16 and 24) are due to the orthogonality imposed on the scattering function and bound-state orbital in the calculation of Chung and Lin.⁹

b. Excitation of the $a^3\Sigma_g^+$ state of H_2

We have also studied the cross sections for excitation of the $a^3\Sigma_g^+$ state for collision energies from near threshold to 30 eV. These cross sections were obtained using only two open channels ($X^1\Sigma_g^+$ and $a^3\Sigma_g^+$) as before. We again consider only $^2\Sigma$ and $^2\Pi$ overall symmetries in the expansion of the (N+1) particle wave function. The contribution to the integral cross section from Σ symmetry is significantly more important than from Π symmetry. The Σ_g and Σ_u contributions to those cross sections are equally important near threshold, show a maximum and become virtually degenerate between 20-30 eV. The Σ_u symmetry cross section increases very sharply between 13 and 14 eV. Figures 8, 9 and 10 show our calculated differential cross sections for the $X^1\Sigma_g^+ \rightarrow a^3\Sigma_g^+$ transition at 13, 15, and 20 eV, respectively, along with the distorted wave results of Rescigno *et al.*⁶ Our calculated differential inelastic cross sections at 20 and 30 eV are compared with the experimental data of Khakoo and Trajmar²⁸ in Figs. 10 and 11, respectively. The agreement between our differential cross section and the experimental results at 20 eV is excellent. There are, however, significant differences between the calculated and measured differential inelastic cross sections at 30 eV, particularly between 30° and 80°. Our calculated integral cross sections for the $X^1\Sigma_g^+ \rightarrow a^3\Sigma_g^+$ are shown in Fig. 12. In this figure we also show the results of Chung and Lin⁹ (close-coupling), the Born-Rudge results of Ref. 9, the distorted-wave results of Rescigno *et al.*,⁶ the experimental data of Khakoo and Trajmar,²⁸ and the integral cross sections measured by Ajello.²⁹ The relative

cross section of Ajello are normalized to our calculated cross sections at 20 eV. We note that these integral cross sections are predicted to rise very sharply just above threshold, suggesting that the Franck-Condon approximation must be used carefully in the analysis of experimental data in this region.

Again, the differences between our results and the close-coupling results of Chung and Lin⁹ could arise from the absence of the correlation terms in their calculations. Reasons for the differences between our calculated differential cross sections at 30 eV and the experimental results of Khakoo and Trajmar²⁸ are unclear at present.

c. Excitation of the $c^3\Pi_u$ state of H_2

In this section we discuss the excitation cross sections for the $c^3\Pi_u$ state of H_2 obtained at the two-state level of approximation. For this calculation we considered only the $X^1\Sigma_g^+$ and $c^3\Pi_u$ states as open channels. We further carried out a three-state calculation for this transition and found no significant differences between these results and those obtained at the two-state level. For energies below 20 eV, the differences between the two- and three-state approximations do become more pronounced for particular symmetries. However, for the total excitation cross sections the largest difference between the two calculations is at most $\sim 7\%$. For our convenience here we present only the two-state cross sections for the $c^3\Pi_u$ excitation of H_2 . The contributions of each symmetry for the integral cross sections in order of importance are $^2\Pi_g, ^2\Delta_g, ^2\Pi_u, ^2\Sigma_g, ^2\Delta_u$ and $^2\Sigma_u$, where the first three symmetries account for most of the cross sections.

The energy dependence of the contribution of these three symmetries to the cross section are very similar, *i.e.*, relatively small near threshold and showing a maximum around 15 eV.

Figures 13 and 14 show our calculated differential cross section for the $c^3\Pi_u$ excitation at 20 and 30 eV, respectively, along with the experimental data of Khakoo and Trajmar.²⁸ At 20 eV we also show the distorted-wave results of Lee *et al.*⁸ Although the shapes of our calculated and the experimental cross sections are very similar, there are substantial differences in their magnitudes. The differences in the magnitudes of these two-state cross sections and the distorted-wave results⁸ are even larger. Further multichannel calculations are clearly required to determine the influence of additional open channels on these cross sections. Finally, Fig. 15 shows our integrated cross sections along with the distorted wave results of Lee *et al.*,⁸ the close-coupling results of Chung and Lin,⁹ the Born-Rudge results of Ref. 9 and experimental data of Khakoo and Trajmar.²⁸ Again, the reasons for the differences between our results and the experimental data of Khakoo and Trajmar are not clear.

1.3 Conclusions

We presented the cross sections obtained with the Schwinger multichannel theory for the $X^1\Sigma_g^+ \rightarrow a^3\Sigma_g^+$, $b^3\Sigma_u^+$ and $c^3\Pi_u$ transitions in H_2 in the two-state approximation.² These results, particularly the $X^1\Sigma_g^+ \rightarrow b^3\Sigma_u^+$ transition, assumed a special significance in view of the independent studies of these cross sections by Schneider and Collins¹⁶ and by Baluja *et al.*,²⁰ using the linear al-

gebraic and R-matrix methods, respectively, and of the experimental studies by Hall and Andrić,²⁵ Nishimura,²⁶ and Khakoo *et al.*²⁷ We also obtained very good agreement between our differential cross sections for the $a^3\Sigma_g^+$ excitation and the experimental data of Khakoo and Trajmar²⁸ at 20 eV. However, comparisons of our results with recent experimental studies of the cross sections for the $a^3\Sigma_g^+$ (30 eV) and $c^3\Pi_u$ states by Khakoo and Trajmar²⁸ revealed significant discrepancies. The reasons for those differences are presently unknown and may be resolved in the future when more elaborate calculations involving many open channels become available.

References

1. For a recent review of the experimental literature see S. Trajmar, D. F. Register, and A. Chutjian, *Phys. Rep.* **97**, 219 (1983).
2. S. Chung, C. C. Lin, and E. T. P. Lee, *Phys. Rev. A* **12**, 1340 (1975).
3. D.C. Cartwright and A. Kupperman, *Phys. Rev.* **163**, 86 (1967).
4. A. U. Hazi, *Phys. Rev. A* **23**, 2232 (1981).
5. T. N. Rescigno, C. W., McCurdy, Jr., and V. McKoy, *J. Phys. B* **7**, 2396 (1974).
6. T. N. Rescigno, C. W. McCurdy, Jr., V. McKoy, and C. F. Bender, *Phys. Rev. A* **13**, 216 (1976).
7. A. W. Fliflet and V. McKoy, *Phys. Rev. A* **21**, 1863 (1980).
8. M. T. Lee, R. R. Lucchese, and V. McKoy, *Phys. Rev. A* **26**, 3240 (1982);
M.T. Lee and V. McKoy *Phys. Rev. A* **28**, 697 (1983).
9. S. Chung and C. C. Lin, *Phys. Rev. A* **17**, 1874 (1978); T. K. Holley, S. Chung, C. C. Lin, and E. T. P. Lee, *Phys. Rev. A* **26**, 1852 (1982).
10. C. A. Weatherford, *Phys. Rev. A* **22**, 2519 (1980).
11. T. K. Holley, S. Chung, C. C. Lin, and E. T. P. Lee, *Phys. Rev. A* **24**, 2946 (1981).
12. L. A. Collins and B. I. Schneider, *Phys. Rev. A* **27**, 101 (1983)
13. B. I. Schneider and L. A. Collins, *Phys. Rev. A* **27**, 2847 (1983).
14. B. I. Schneider and L. A. Collins, *Phys. Rev. A* **28**, 166 (1983).
15. L. A. Collins and B. I. Schneider, *J. Phys. B: At. Mol. Phys.* **17**, L235

- (1984).
16. B. I. Schneider and L. A. Collins, *J. Phys. B: At. Mol. Phys.* **18**, L857 (1985).
 17. P. G. Burke, I. McKay, and I. Shimamura, *J. Phys. B: At. Mol. Phys.* **10**, 2497 (1977).
 18. P. G. Burke and C. J. Noble, *Comment At. Mol. Phys.* **12**, 301 (1983).
 19. J. Tennyson and C. J. Noble, *J. Phys. B: At. Mol. Phys.* **18**, 155 (1985).
 20. K. L. Baluja, C. J. Noble, and J. Tennyson, *J. Phys. B: At. Mol. Phys.* **18**, L851 (1985).
 21. K. Takatsuka and V. McKoy, *Phys. Rev. A* **24**, 2473 (1981).
 22. K. Takatuska and V. McKoy, *Phys. Rev. A* **30**, 1734 (1984).
 23. M. A. P. Lima, T. L. Gibson, K. Takatsuka, and V. McKoy, *Phys. Rev. A* **30**, 1741 (1984).
 24. M. A. P. Lima, T. L. Gibson, W. M. Huo, and V. McKoy, *J. Phys. B: At. Mol. Phys.* **18**, L865 (1985).
 25. R. I. Hall and L. Andrić, *J. Phys. B: At. Mol. Phys.* **17**, 3815 (1984).
 26. H. Nishimura (private communication, 1985).
 27. M. A. Khakoo, R. McAdams, and S. Trajmar, *Phys. Rev. A* (submitted for publication, 1985).
 28. M. A. Khakoo and S. Trajmar, *Phys. Rev. A* (submitted for publication, 1986).
 29. J. M. Ajello (private communication, 1986).

30. N. F. Lane, *Rev. Mod. Phys.* **52**, 29 (1980).

31. W. J. Hunt and W. A. Goddard III, *Chem. Phys. Lett.* **3**, 414 (1969).

Table I. Cartesian Gaussian Basis Set^{a,b}

Gaussian Center ^c and type	Exponents (α)
H, 6s	48.4479, 7.28346, 1.65139, 0.462447, 0.145885, 0.07
H, 6p	4.5, 1.5, 0.5, 0.25, 0.125, 0.03125
H, ^d 6d _{xy}	4.5, 1.5, 0.5, 0.25, 0.125, 0.03125
Midpoint, 4s	0.25, 0.05, 0.01, 0.002
Midpoint, 4p	0.8, 0.2, 0.0625, 0.0078125

^a Defined by $X_{lmn}^{(\alpha)} = N_{lmn} (x - A_x)^l (y - A_y)^m (z - A_z)^n e^{-\alpha|\vec{r}-\vec{A}|^2}$, where \vec{A} is the position of the Gaussian center.

^b Basis set used for the ground and excited states of H₂, in the expansion of the scattering functions, and for insertion around $V G_P^{(+)} V$.

^c At the equilibrium internuclear distance of $R_e = 1.400a_0$.

^d Additional functions used to expand the scattering functions for the $X^1\Sigma_g^+ \rightarrow c^3\Pi_u$ transition.

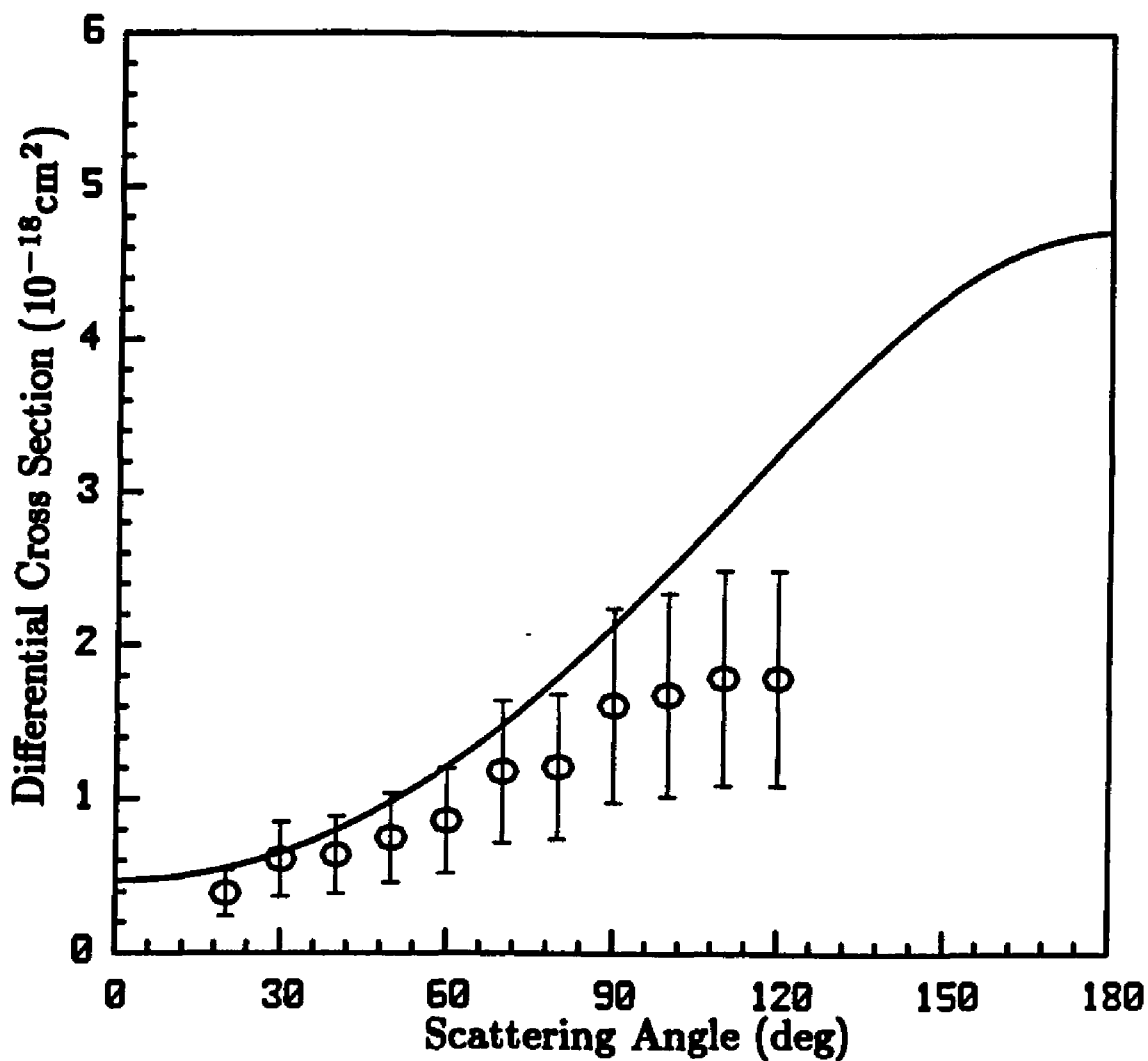


Figure 1: Differential cross sections (DCS) for excitation of the $b^3\Sigma_u^+$ state at 10.5 eV: present results (solid line), measured values of Ref. 25 (○).

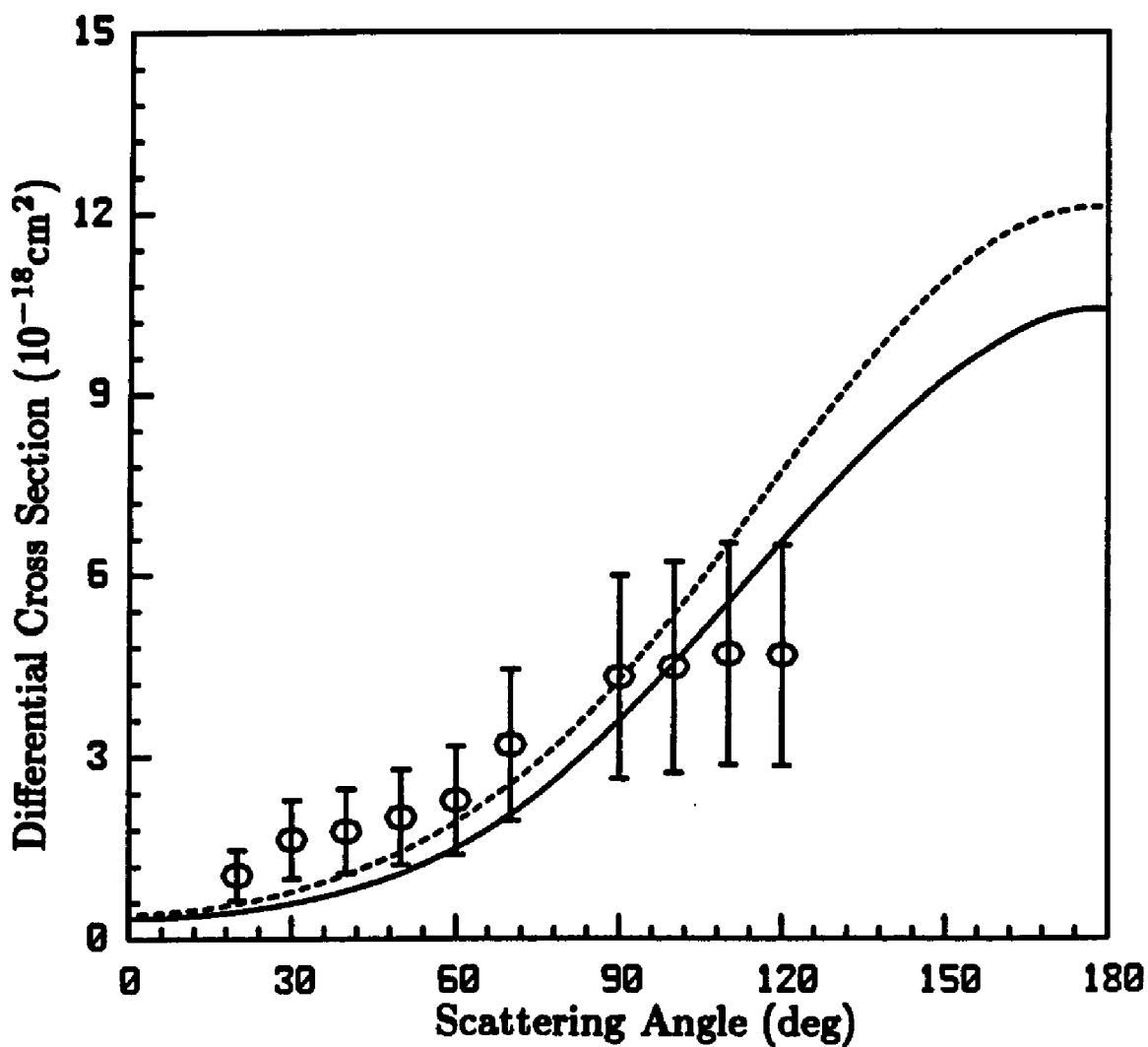


Figure 2: DCS for excitation of the $b^3\Sigma_u^+$ state at 12 eV: present results (solid line), distorted wave (DW) results of Ref. 7 (dashed line), measured values of Ref. 25 (○).

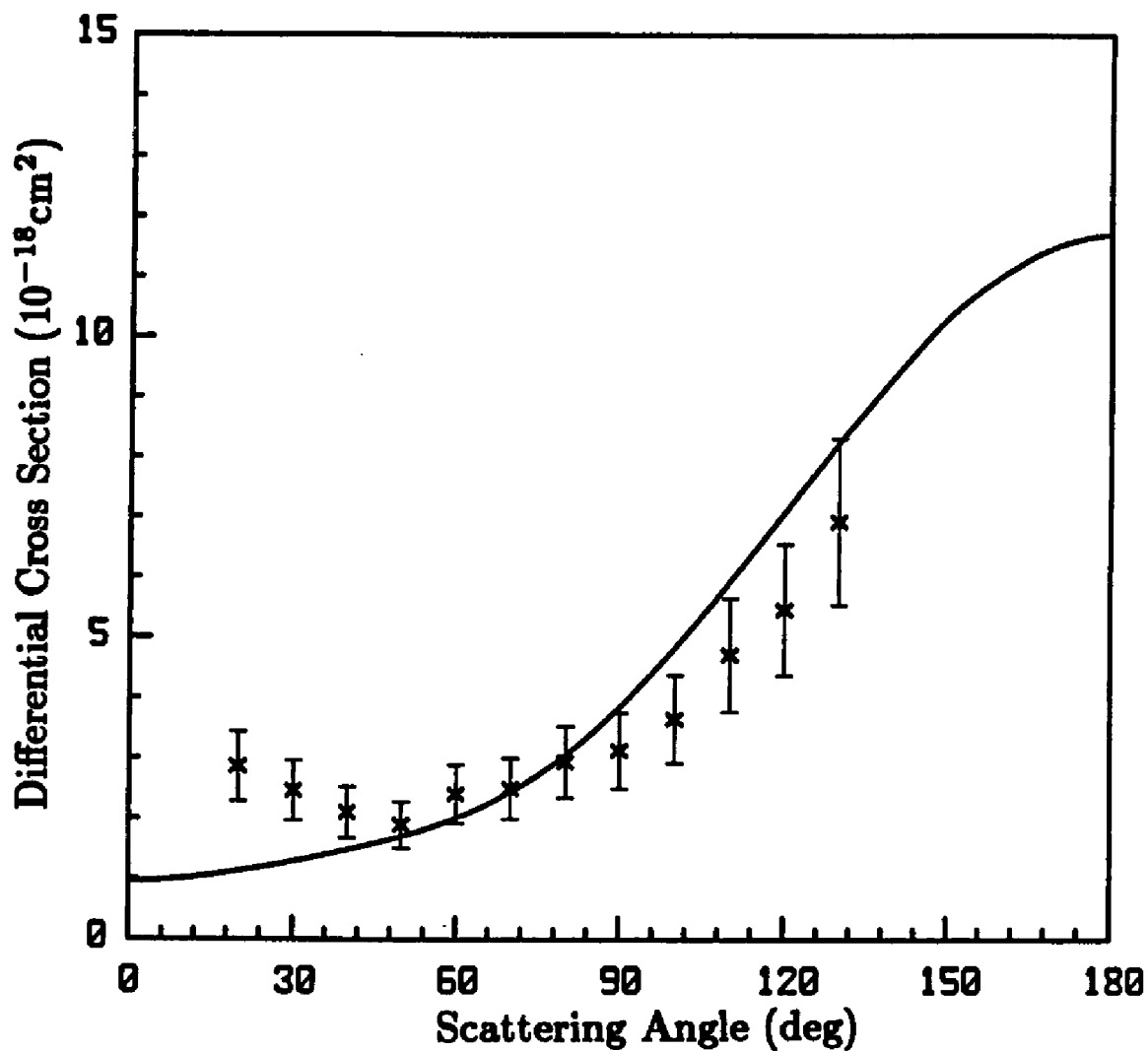


Figure 3: DCS for excitation of the $b^3\Sigma_u^+$ state at 13 eV: present results (solid line), measured values of Ref. 26 (x).

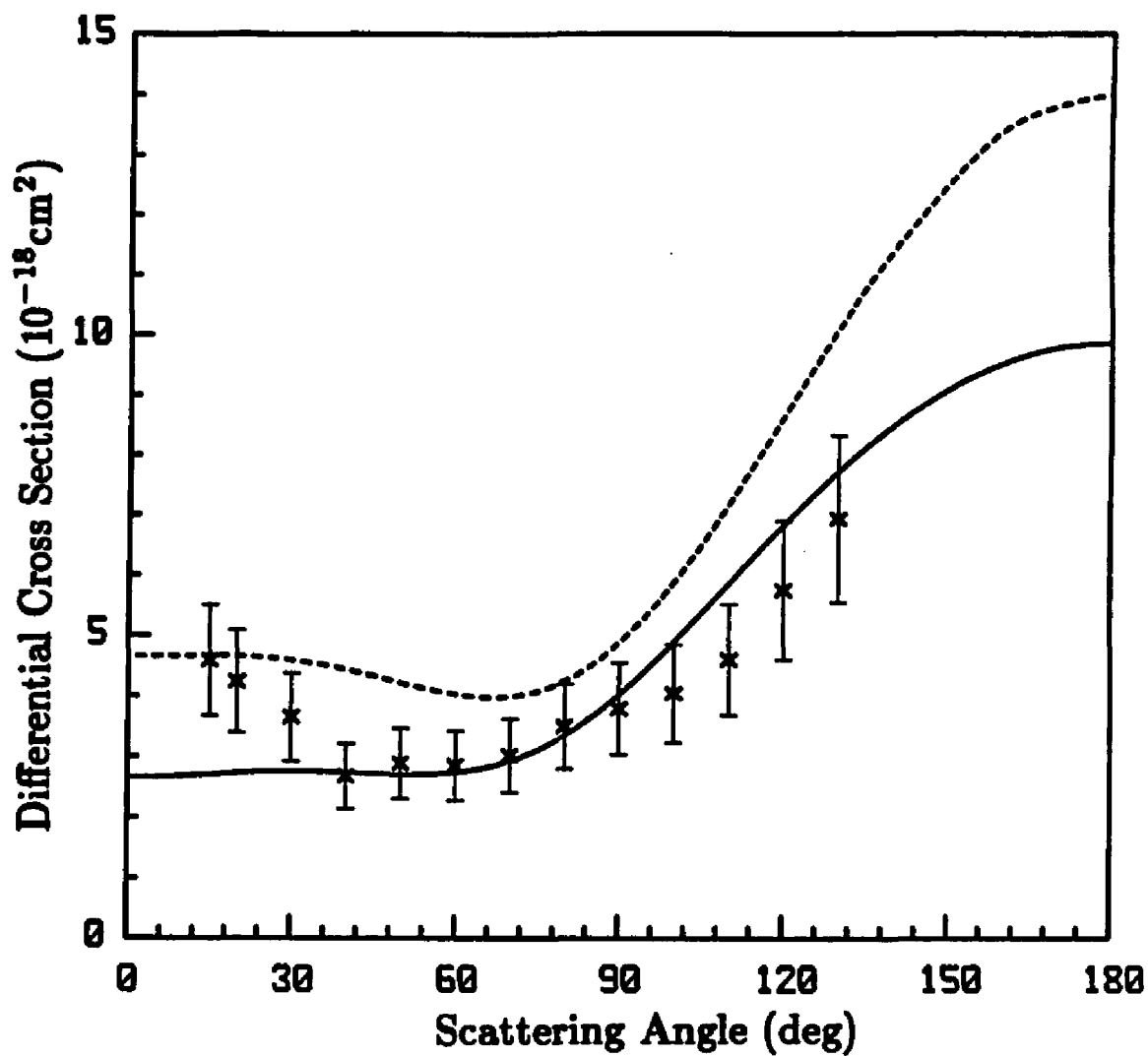


Figure 4: DCS for excitation of the $b^3\Sigma_u^+$ state at 15 eV: present results (solid line), DW results of Ref. 7 (dashed line), measured values of Ref. 26 (\times).

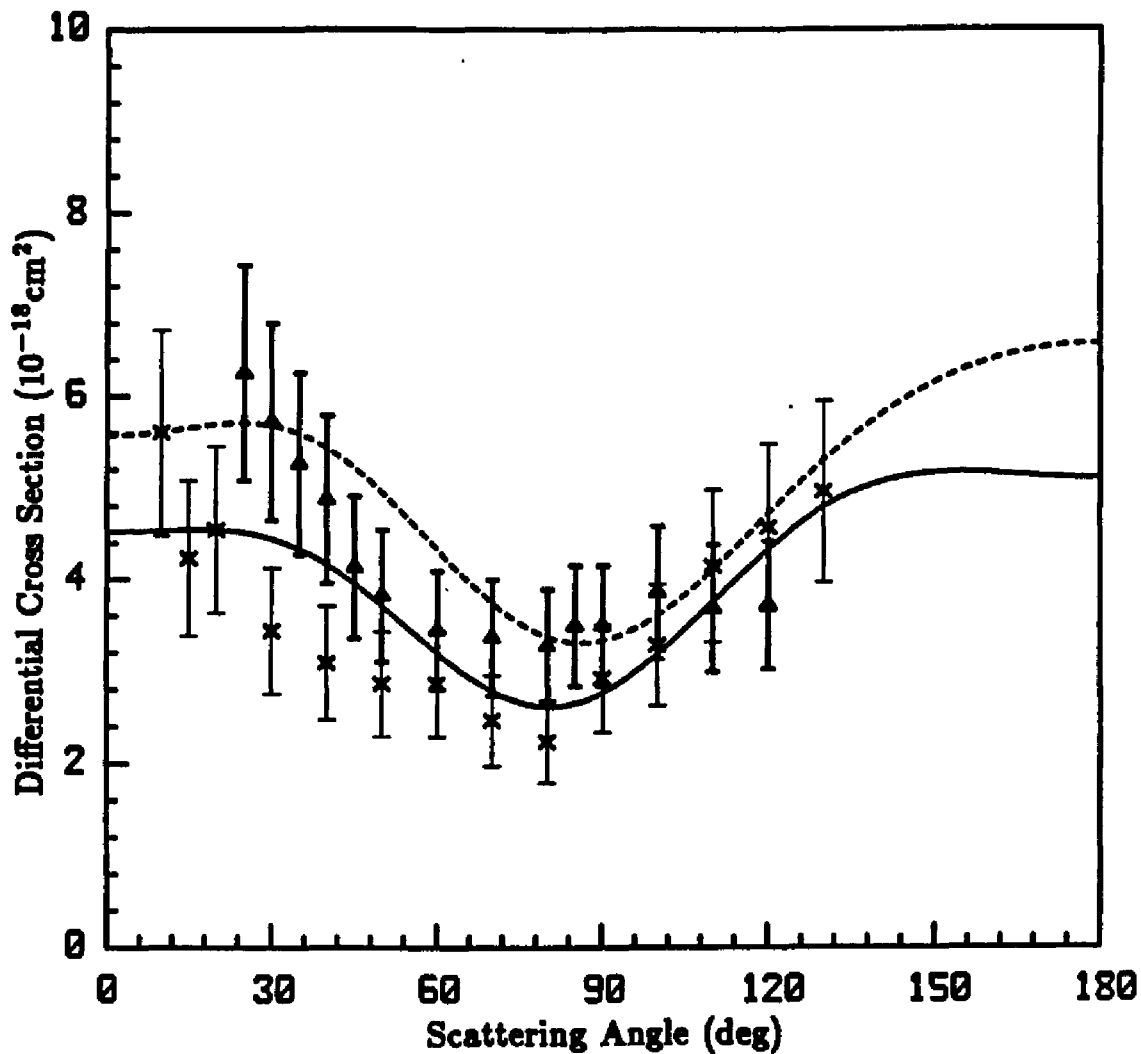


Figure 5: DCS for excitation of the $b^3\Sigma_u^+$ state at 20 eV: present results (solid line), DW results of Ref. 7 (dashed line), measured values of Ref. 26 (\times), measured values of Ref. 27 (Δ).

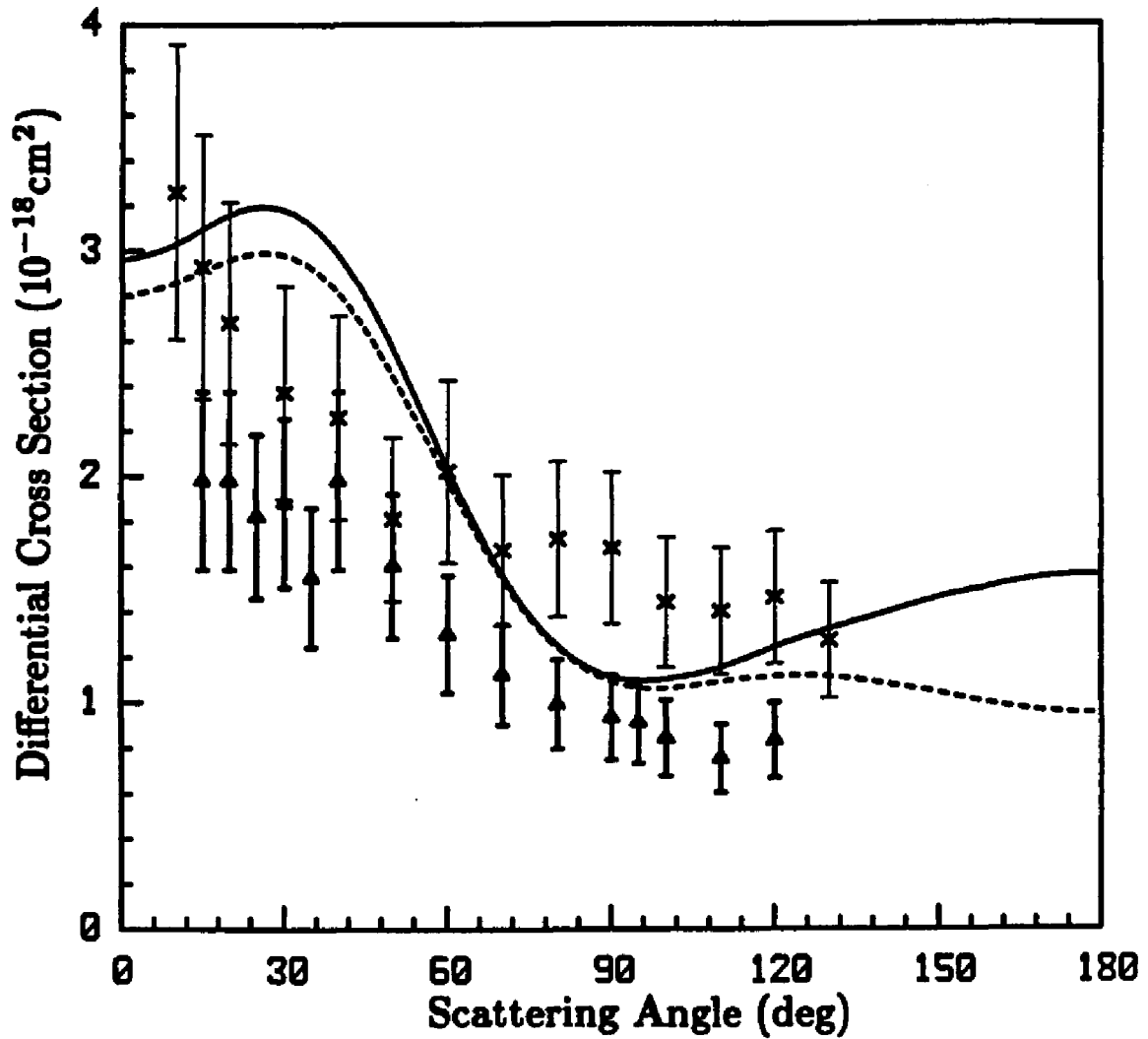


Figure 6: DCS for excitation of the $b^3\Sigma_u^+$ state at 30 eV: present results (solid line), DW results of Ref. 7 (dashed line), measured values of Ref. 26 (\times), measured values of Ref. 27 (Δ).

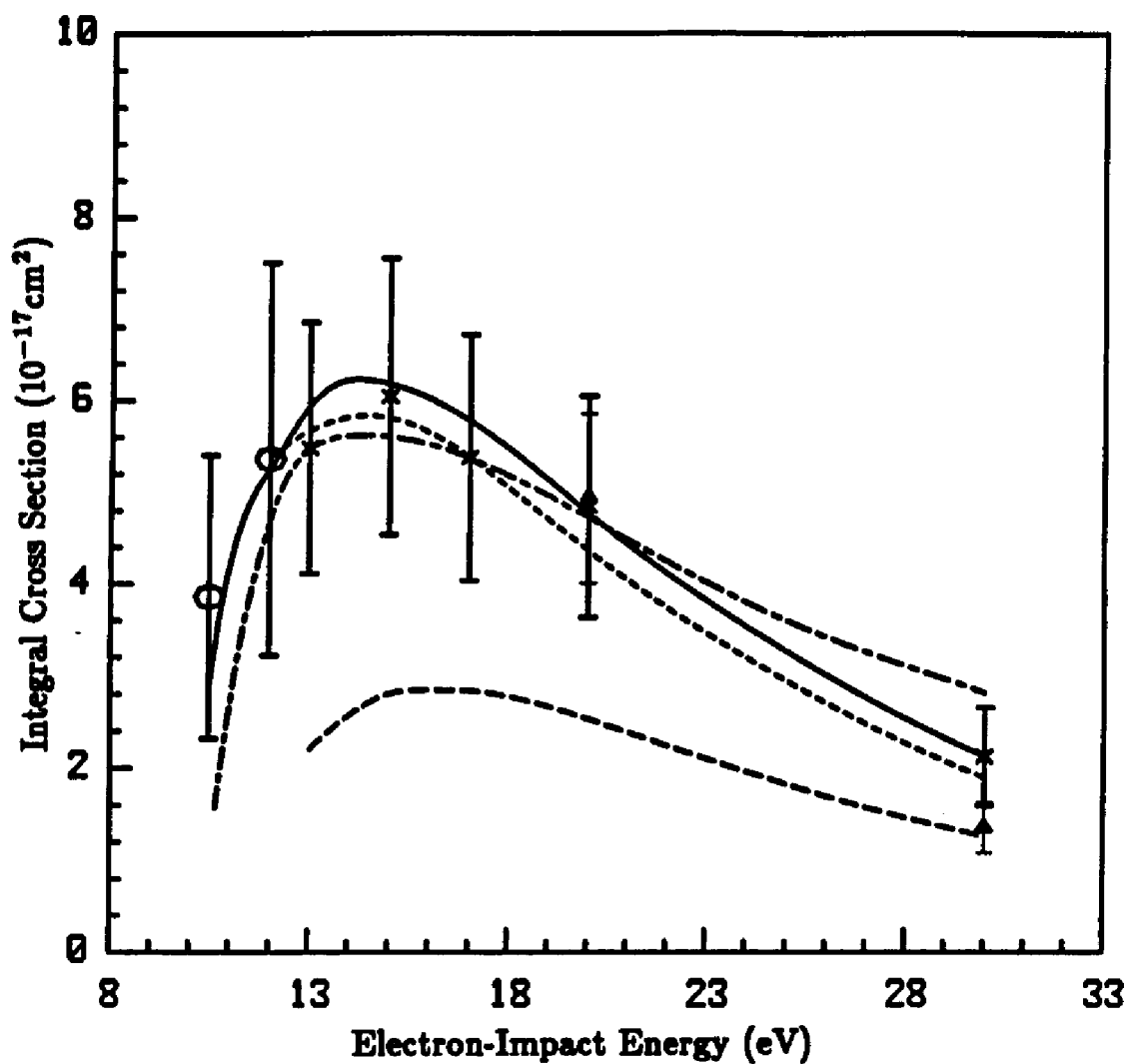


Figure 7: Integral cross section (ICS) for excitation of the $b^3\Sigma_u^+$ state: present results (solid line), linear algebraic method results of Ref. 16 (short dashed line), R-matrix results of Ref. 20 (long-short dashed line), close-coupling (CC) results of Ref. 9 (long dashed line), measured values of Ref. 25 (\circ), measured values of Ref. 26 (\times), measured values of Ref. 27 (\triangle).

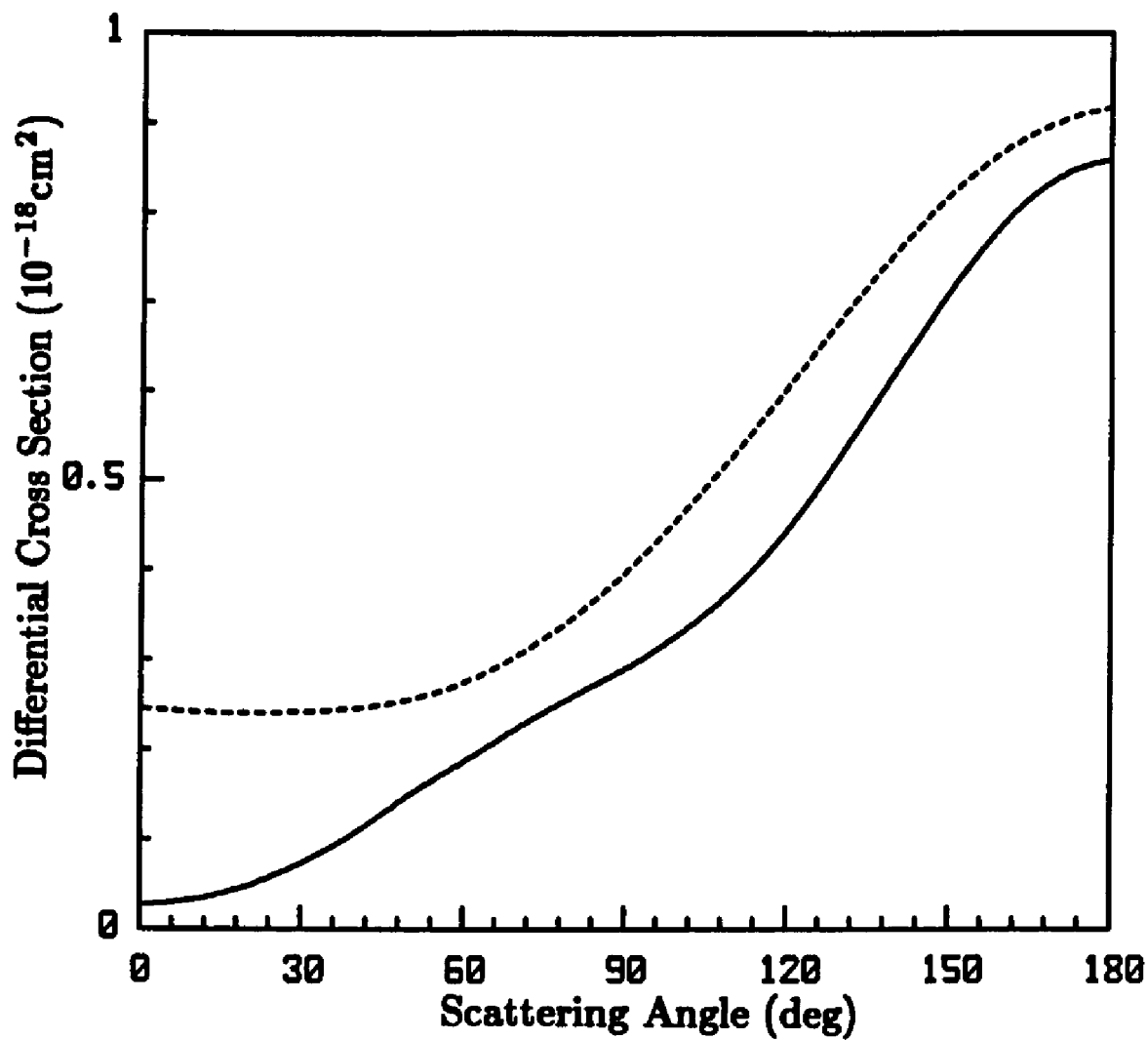


Figure 8: DCS for excitation of the $a^3\Sigma_g^+$ state at 13 eV: present results (solid line), DW results of Ref. 6 (dashed line).

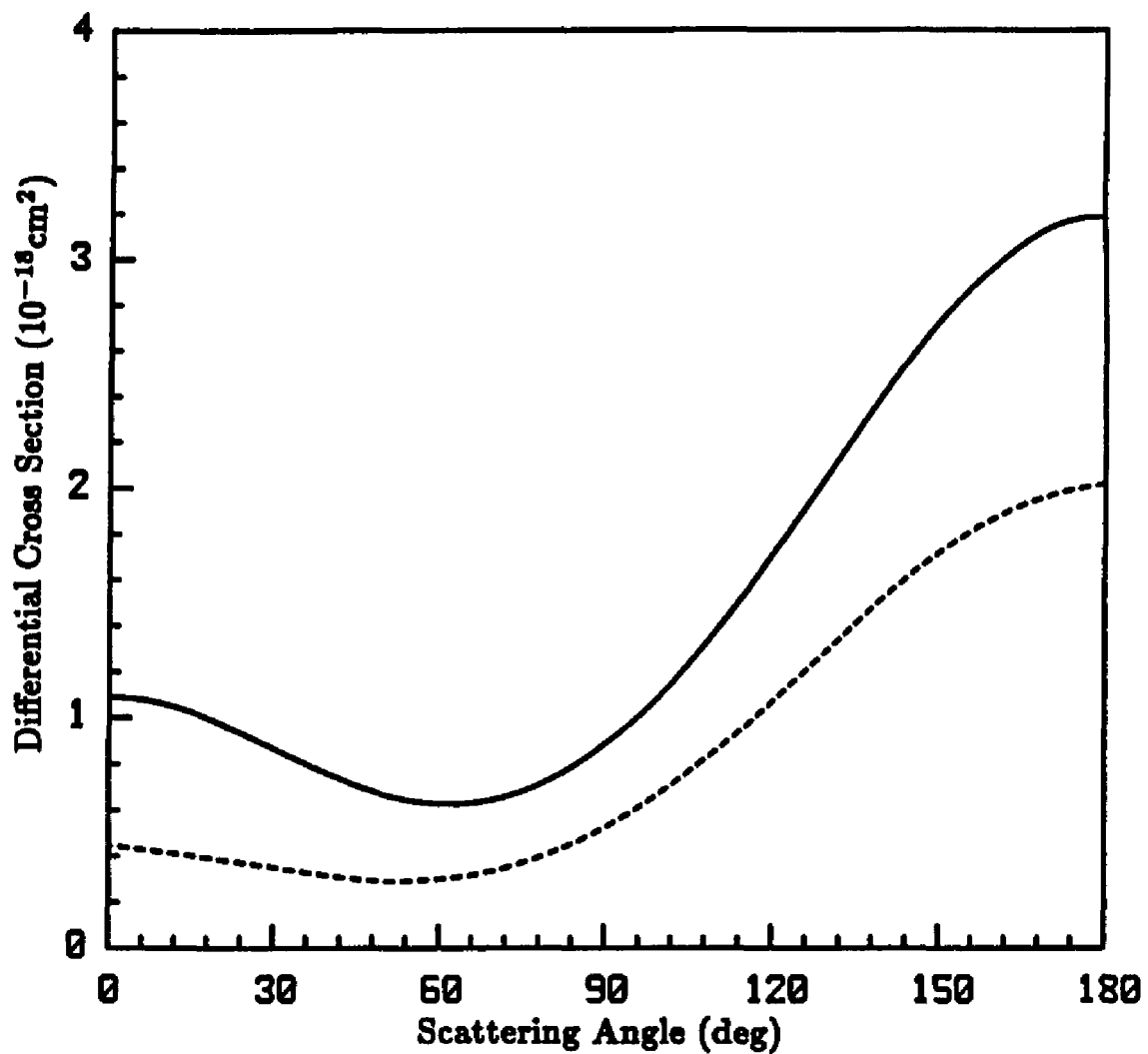


Figure 9: DCS for excitation of the $a^3\Sigma_g^+$ state at 15 eV: present results (solid line), DW results of Ref. 6 (dashed line).

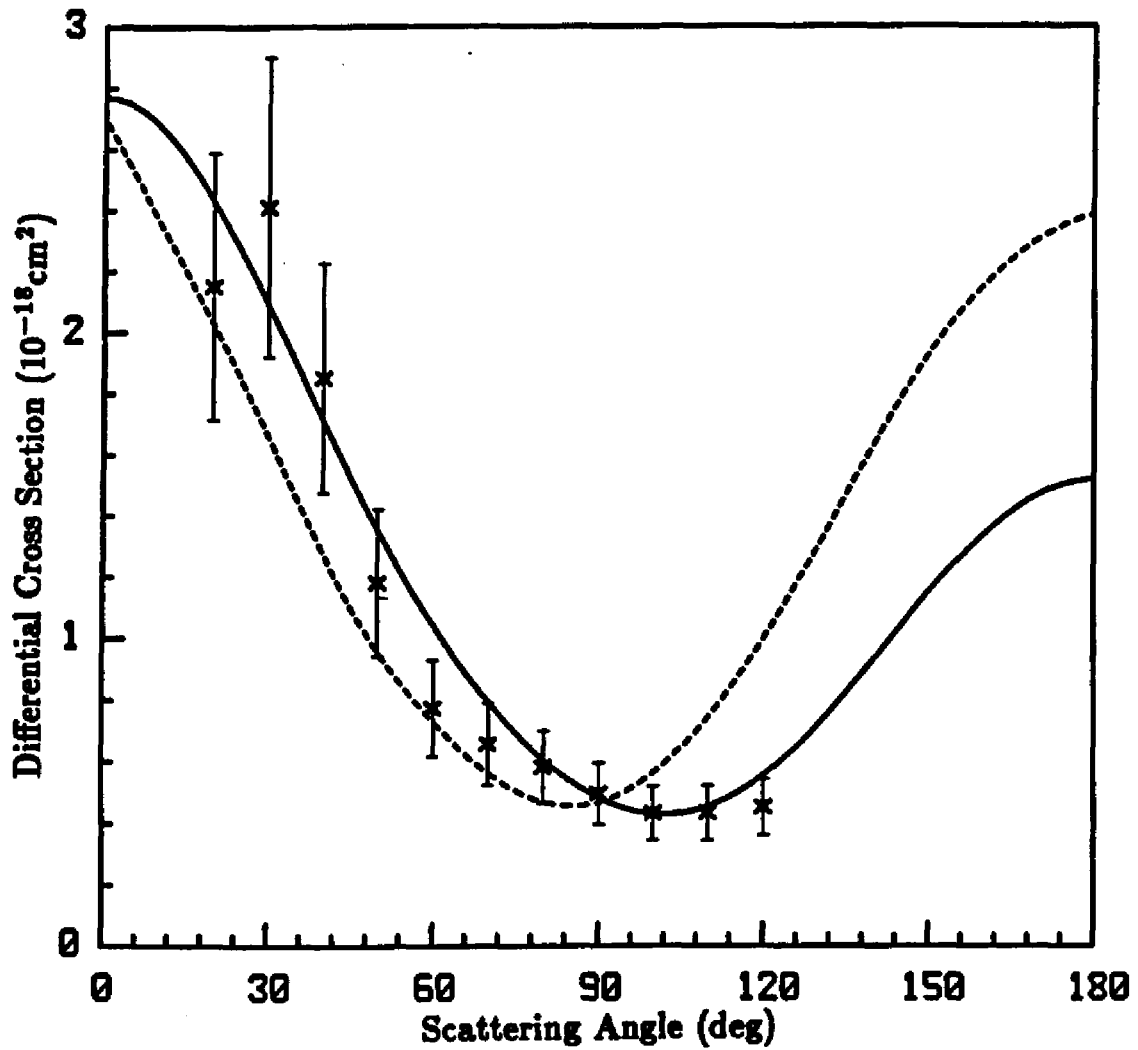


Figure 10: DCS for excitation of the $a^3\Sigma_g^+$ state at 20 eV: present results (solid line), DW results of Ref. 6 (dashed line), measured values of Ref. 28 (\times).

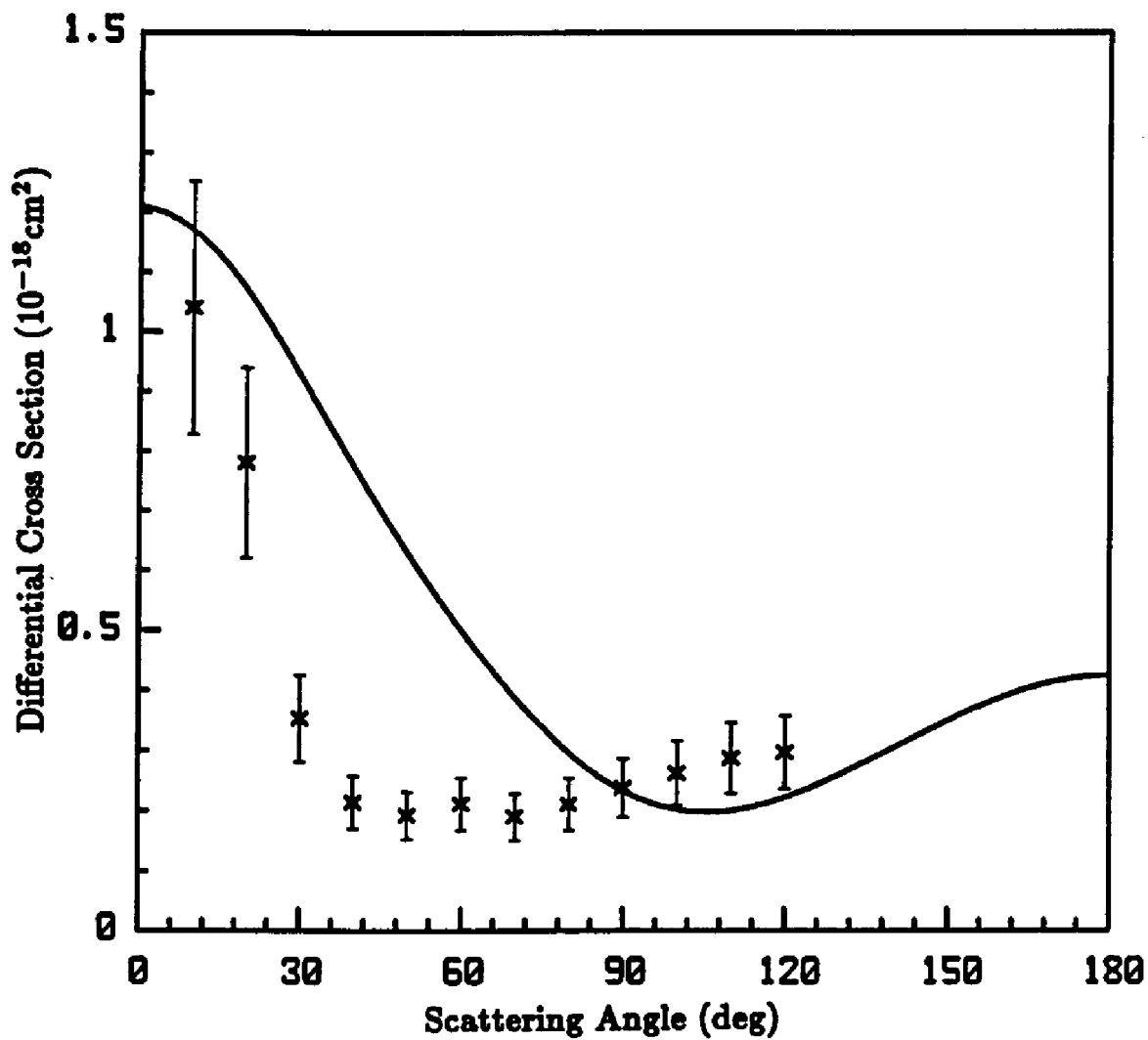


Figure 11: DCS for excitation of the $a^3\Sigma_g^+$ state at 30 eV: present results (solid line), measured values of Ref. 28 (x).

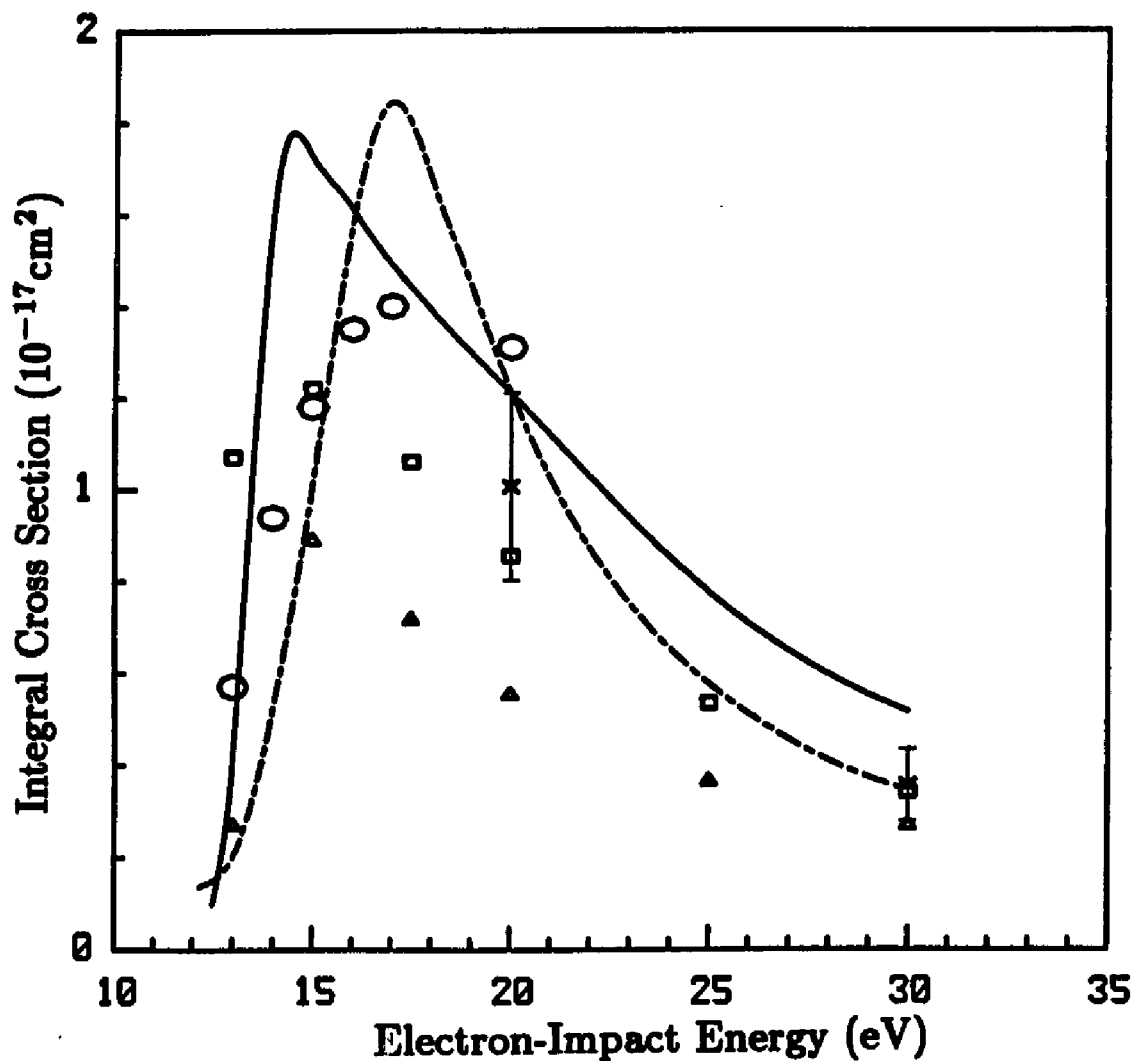


Figure 12: ICS for excitation of the $a^3\Sigma_g^+$ state: present results (solid line), DW results of Ref. 6 (○), CC results of Ref. 9 (△), Born-Rudge (BR) results of Ref. 9 (□), measured values of Ref. 28 (×), measured values of Ref. 29 (long-short dashed line).

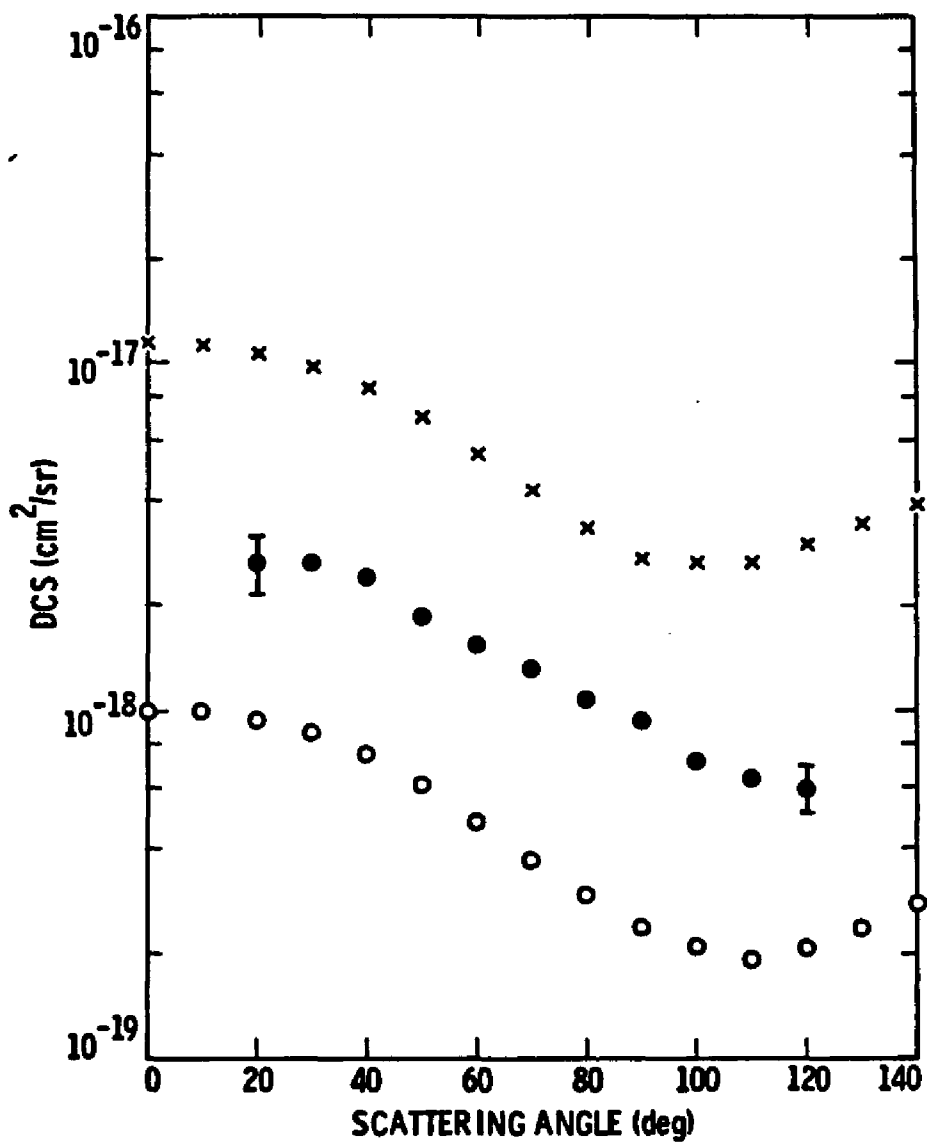


Figure 13: DCS for excitation of the $c^3\Pi_u$ state at 20 eV: present results (x), DW results of Ref. 8 (o), measured values of Ref. 28 (•).

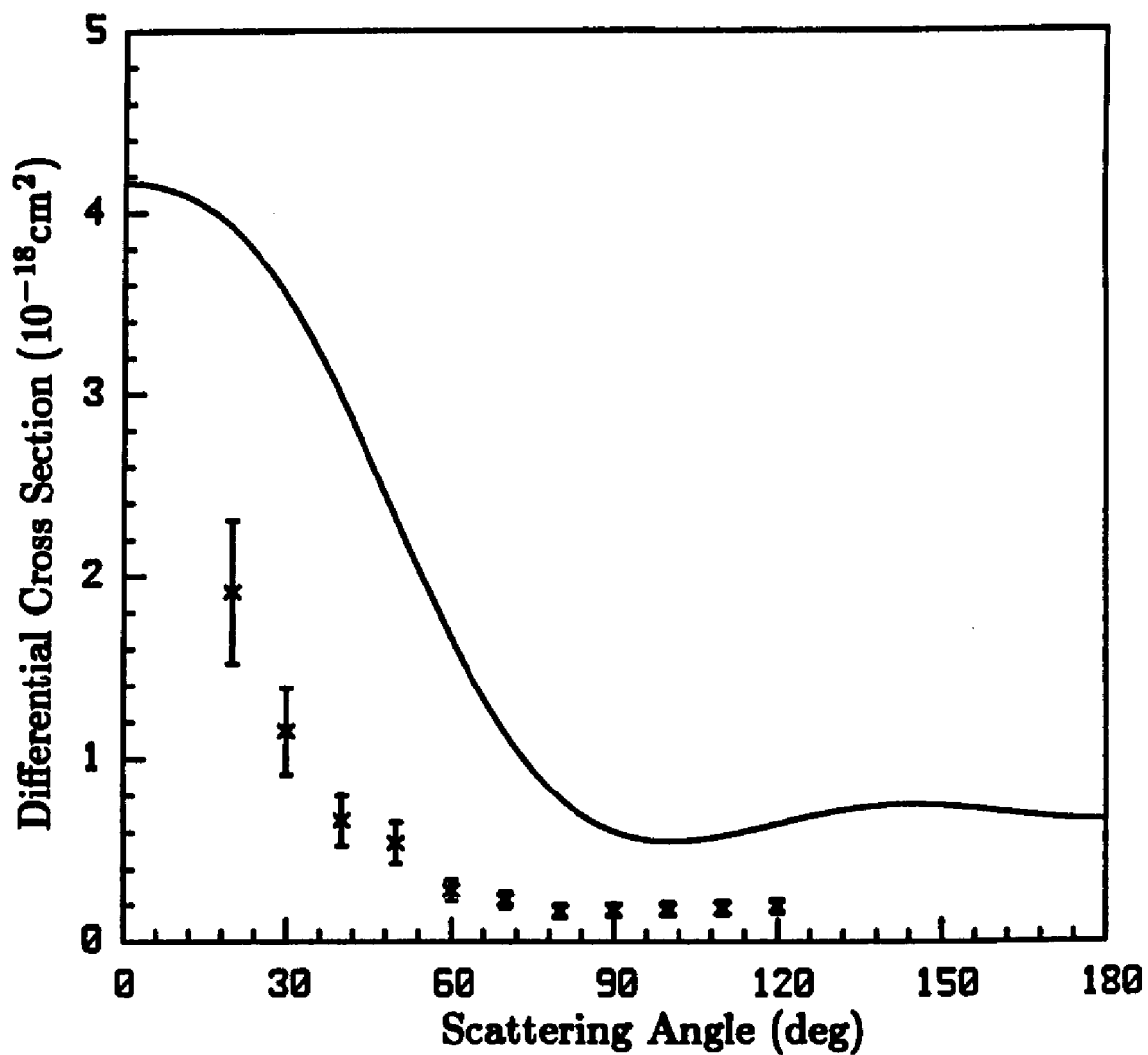


Figure 14: DCS for excitation of the $c^3\Pi_u$ state at 30 eV:
present results (solid line), measured values of Ref. 28 (x).

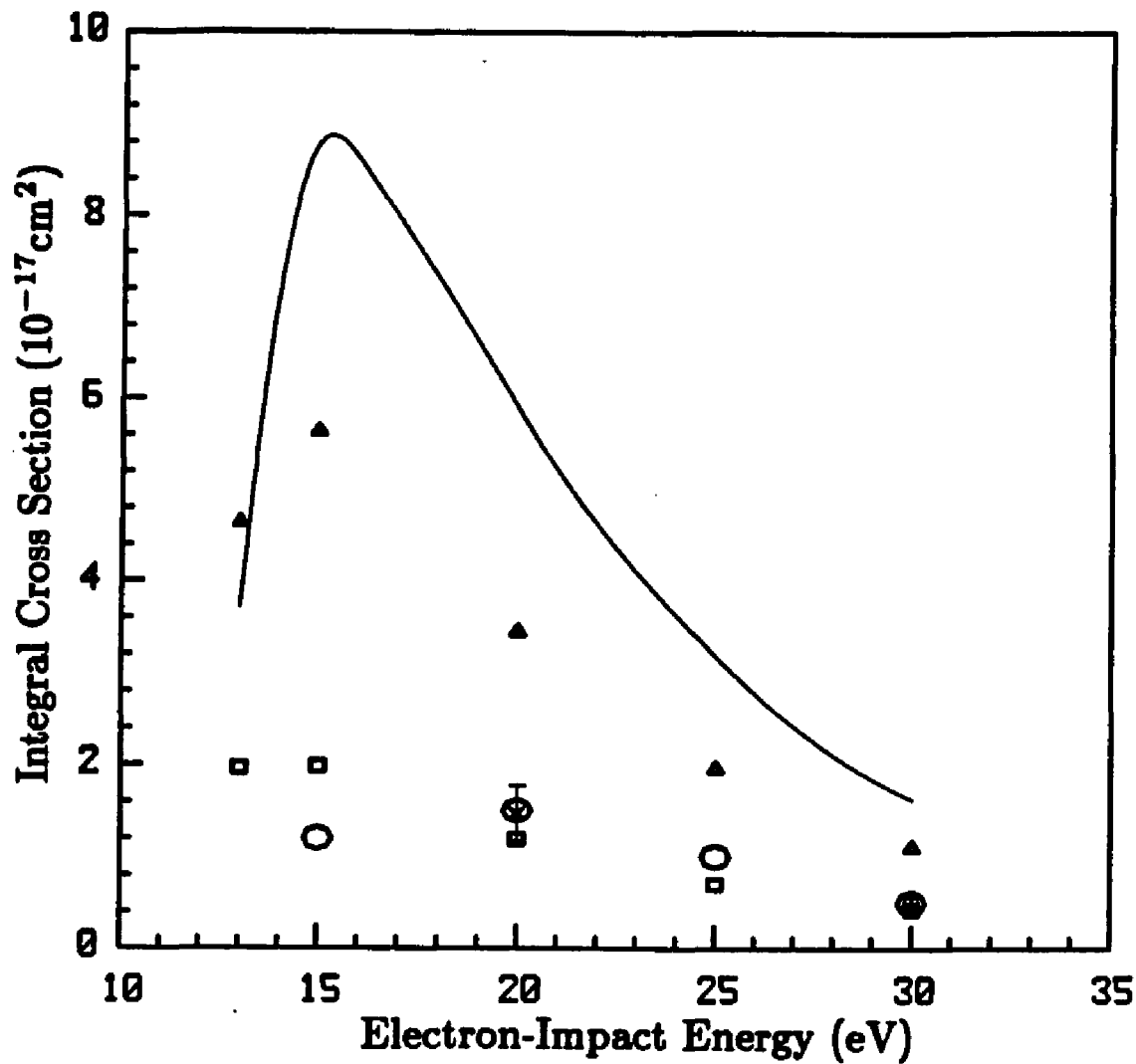


Figure 15: ICS for excitation of the $c^3\Pi_u$ state: present results (solid line), CC results of Ref. 9 (Δ), DW results of Ref. 8 (\circ), BR results of Ref. 9 (\square), measured values of Ref. 28 (\times).

2. Cross sections for electron impact excitation of the $B^1\Sigma_u^+$ state of H_2

We report the first application of the Schwinger Multichannel formulation to the electron impact excitation of a dipole-allowed electronic transition. We have obtained cross sections for electron impact excitation of the $B^1\Sigma_u^+$ state of H_2 at 15, 20 and 30 eV. Our differential cross sections are in good agreement with available experimental data at all energies. Due to the long-range nature of the direct interaction potential in this transition a Born closure method was used to represent properly the differential cross section in the forward direction.

2.1 Introduction

Accurate cross sections for the electronic excitation of molecules by low-energy (≤ 30 eV) electron impact are needed in a number of fields.¹ In particular, the differential cross section $\sigma(\theta)$ gives considerable insight into the physics of the electron-molecule collision. Measurements² in this energy region are often quite difficult and are usually restricted to the scattering angles $20^\circ \leq \theta \leq 140^\circ$. The experimental integral and momentum transfer cross sections rely on a procedure involving the extrapolation of $\sigma(\theta)$ to 0° and 180° . This extrapolation procedure can result in considerable uncertainty for the final results;^{3,4} therefore, theoretical studies of these cross sections are obviously desirable.

In the following we report electron impact excitation cross sections for the $X^1\Sigma_g^+ \rightarrow B^1\Sigma_u^+$ transition of H_2 . This is a dipole-allowed transition and hence, the long-range nature of the direct interaction potential requires that a large number of partial waves be included to represent properly $\sigma(\theta)$ in the forward

direction. However, above a certain minimum angular momentum ℓ_m , the remaining partial waves are *weakly* scattered. Thus, if a *full* treatment of the scattering is used to calculate the partial wave contribution to $\sigma(\theta)$ up to ℓ_m , the remaining terms can be obtained from a weak scattering theory such as the first Born approximation⁵ (FBA).

This scheme of using an easily applied weak scattering approximation to include contributions from high angular momenta for long-range interaction potentials has been employed in a number of investigations. Some representative examples include Crawford and Dalgarno,⁶ Collins and Norcross,⁷ and Norcross and Padiyal⁸, who utilized such methods for studies involving electron collisions with polar molecules, while electron impact excitation studies by Chung and Lin⁹ and by Fliflet and McKoy¹⁰ have used similar techniques for dipole-allowed transitions. The accuracy of cross sections obtained with this scheme depends primarily on the validity of the *full* scattering treatment used to calculate the contributions up to ℓ_m , and on the criteria for selecting the actual value of ℓ_m , since this last determines the applicability of the weak scattering approximation for the partial waves of interest.

For this study we use the Schwinger multichannel (SMC) formulation,¹¹ for our *full* scattering treatment and a modified Born-closure (BC) scheme to include contributions to $\sigma(\theta)$ from large angular momenta. In several recent applications^{3,4,12-14} of the SMC formulation to electron scattering from a variety of molecular targets, we have demonstrated the ability of our methods to produce

accurate results, especially for contributions to $\sigma(\theta)$ from the strongly scattered low angular momentum partial waves. In Sec. 2.2 we discuss the BC scheme. Our scattering cross sections are presented in Sec. 2.3 and compared with measured values and the results of other theoretical studies. We summarize our results and conclusions in Sec. 2.4.

2.2 Born Closure

In the SMC formulation the cross section includes contributions from a finite number of angular momenta since the partial wave expansion is truncated at some finite body-frame value ($\ell^{max}, |m^{max}|$) represented by ℓ_m . When the transition potential contains long-range moments, the number of partial waves required to converge $\sigma^{SMC}(\theta')$ in the forward direction can be quite large. However, above a certain value of ℓ_m , the contributions from large angular momenta can be correctly obtained by means of a weak scattering theory such as the FBA. Further, the FBA differential cross section $\sigma^{FBA}(\theta')$ can be obtained in closed form^{10,15} without resorting to a partial wave expansion. Thus, within the FBA, $\sigma^{FBA}(\theta')$ contains contributions from *all* angular momenta. Hence, our BC differential cross section $\sigma^{BC}(\theta')$ is given by

$$\sigma^{BC}(\theta') = \sigma^{FBA}(\theta') - \Delta\sigma(\theta'), \quad (1)$$

where

$$\Delta\sigma(\theta') = [\sigma^{SMC}(\theta') - \sigma_{FE}^{FBA}(\theta')]. \quad (2)$$

In Eq. (2) $\sigma_{FE}^{FBA}(\theta')$ is obtained from a finite expansion containing exactly the

same number of partial waves as $\sigma^{SMC}(\theta')$. Thus, for angular momenta below ℓ_m , contributions to $\sigma^{BC}(\theta')$ are obtained with the SMC formulation, while the FBA is used to include contributions from all of the angular momenta above ℓ_m . The criteria⁸ for the validity of Eq. (1) is that above ℓ_m the contributions to $\Delta\sigma$ are zero, and in the limit $\ell_m \rightarrow \infty$, $\sigma_{FE}^{FBA} \rightarrow \sigma^{FBA}$

2.3 Procedures and Results

To assess the effectiveness with which long-range moments of the transition potential can be treated in our BC scheme, we have calculated integral and differential cross sections for the $X^1\Sigma_g^+ \rightarrow B^1\Sigma_u^+$ transition in H_2 for electron impact energies of 15, 20, and 30 eV. This represents a reasonable test of the method since $\sigma(\theta)$ is strongly peaked in the forward direction for these energies and hence, requires a large partial wave expansion. Further, experimental^{16,17} and previous theoretical^{9,10} results are available for this transition.

Within the SMC formulation, we include only two open channels and neglect closed channels. Our calculations are performed within the framework of the fixed-nuclei and Franck-Condon approximations.¹⁸ Here, the nuclei are held fixed at their equilibrium value $R = 1.4003a_0$ and the dependence of the scattering amplitude on internuclear separation is neglected. The rotational levels are treated as degenerate and the physical cross section is averaged over all molecular orientations. Thus, the fixed-nuclei cross sections reported here are appropriate for the full-band system, i.e., "summed" over all final vibrational levels. Unless otherwise stated, atomic units are used throughout.

For the ground state we used a self-consistent field (SCF) wave function obtained with a 6s6p Cartesian Gaussian basis on the hydrogens and a 4s4p basis at the midpoint shown in Table I. For the $B^1\Sigma_u^+(1\sigma_g 1\sigma_u)$ state we make the frozen core approximation and determine the $1\sigma_u$ orbital by diagonalizing the V_{N-1} potential of the core in the SCF basis. The vertical excitation energy in this basis set is 12.73 eV. The entire set of improved virtual orbitals¹⁹ (IVO) was used to construct the (N+1)-electron wave function, including the appropriate correlation terms.¹³

For this study, we chose ℓ_m such that contributions to $\sigma^{BC}(\theta')$ for $\ell^{max} \leq 5$ and $|m^{max}| \leq 2$ were obtained in the *full* scattering method; i.e., contributions from the body frame symmetries $^2\Sigma_g, ^2\Sigma_u, ^2\Pi_u, ^2\Pi_g, ^2\Delta_g$, and $^2\Delta_u$ with $\ell \leq 5$ were calculated in the SMC formulation.

In Figs. 1,2, and 3 we present our cross sections along with the distorted wave calculations of Fliflet and McKoy¹⁰ and the experimental data of Srivastava and Jensen¹⁶ for electron impact energies of 15, 20 and 30 eV, respectively. At 20 and 30 eV we also show the experimental data of Khakoo and Trajmar.¹⁷ For these two energies we calculated the Born closure cross sections only for low angles. Above 40° at 20 eV and 50° at 30 eV the cross sections presented, respectively, in Fig. 2 and 3 are the pure SMC results. The Born closure is introduced in these calculations only to give the expected behavior of the differential cross section in the forward direction. We find good agreement between our results and the experimental data at all energies. In Table II we present our integral cross sec-

tion (ICS) along with the distorted wave calculation of Fliflet and McKoy¹⁰ and the experimental results of Srivastava and Jensen¹⁶ and Khakoo and Trajmar.¹⁷ Care must be used in assessing the quality of these results in a comparison with measured integral cross sections. In our calculations about 27 % of the ICS at 20 eV comes from the differential cross sections between 0° and 20 ° and about 38 % of the ICS comes from the interval 0° - 30°. For 30 eV the situation is even more dramatic because 59 % of the ICS comes from the angular interval 0° - 20° and 72 % from 0° - 30°. The angular range from 0° to 30° is the most difficult region for experimental measurements and, therefore, such data usually show very large uncertainties. Furthermore, in this angular region the differential cross section is usually extrapolated from the higher angular region where the interference between incident and scattered beams is less severe. On the theoretical side there exist also some difficulties because the low-angle scattering corresponds to the angular region in which the Born closure has its largest contribution.

2.4 Conclusions

In this section we have reported the first application of the Schwinger multichannel formulation to the electron-impact excitation of a dipole-allowed electronic transition. We have obtained integral and differential cross sections for the $X^1\Sigma_g^+ \rightarrow B^1\Sigma_u^+$ transition of H_2 at 15,20 and 30 eV. Due to the long-range nature of the direct interaction potential in this transition a Born closure method was used to properly represent the differential cross sections in the forward di-

reaction. We found very good agreement between our calculated differential cross sections and available experimental data at all energies. We have also seen that the agreement between our calculated integral cross sections and the measured data at higher energies is poor. These discrepancies probably arise from uncertainties in the measured differential cross sections below 30° and from limitations of the two-state calculation.

References

1. S. C. Brown, *Electron-Molecule Scattering* (Wiley, New York, 1979).
2. For a recent review of the experimental literature, see S. Trajmar, D. F. Register, and A. Chutjian, *Phys. Rep.* **97**, 219 (1983).
3. M. A. P. Lima, T. L. Gibson, W. M. Huo, and V. McKoy, *Phys. Rev. A* **32**, 2696 (1985).
4. L. M. Brescansin, M. A. P. Lima, T. L. Gibson, V. Mckoy, and W. M. Huo, *J. Chem. Phys.* (submitted for publication, 1986).
5. J. R. Taylor, *Scattering Theory* (Wiley, New York, 1972); B. L. Moisewitsch and S. J. Smith, *Rev. Mod. Phys.* **40**, 238 (1968); K. J. Miller and M. Krauss, *J. Chem. Phys.* **47**, 3754 (1967).
6. O. H. Crawford and A. Dalgarno, *J. Phys. B.* **4**, 494 (1971).
7. L. A. Collins and D. W. Norcross, *Phys. Rev. A* **18**, 467 (1978).
8. D. W. Norcross and N. T. Padial, *Phys. Rev. A* **25**, 226 (1982).
9. S. Chung and C. C. Lin, *Phys. Rev. A* **17**, 1874 (1978).
10. A. W. Fliflet and V. McKoy, *Phys. Rev. A* **21**, 1863 (1980),
11. K. Takatsuka and V. McKoy, *Phys. Rev. A* **24**, 2473 (1981); **30**, 1734 (1984).
12. T. L. Gibson, M. A. P. Lima, K. Takatsuka and V. McKoy, *Phys. Rev. A* **30**, 3005 (1984).
13. M. A. P. Lima, T. L. Gibson, K. Takatsuka and V. McKoy, *Phys. Rev. A* **30**, 1741 (1984); M.A. P. Lima, T. L. Gibson, W. M. Huo and V. McKoy,

- J. Phys. B* **18**, L865 (1985).
14. W. M. Huo, T. L. Gibson, M. A. P. Lima and V. McKoy, *Phys. Rev. A* (submitted for publication, 1986).
 15. D. K. Watson and V. McKoy, *Phys. Rev. A* **20**, 1474 (1979); D. K. Watson, R. R. Lucchese, V. McKoy, and T. N. Rescigno, *Phys. Rev. A* **21**, 738 (1980).
 16. S. K. Srivastava and S. Jensen, *J. Phys. B* **10**, 3341 (1971). In our figures we used the renormalized results of Reference 2.
 17. M. A. Khakoo and S. Trajmar (private communication, 1985).
 18. N. F. Lane, *Rev. Mod. Phys.* **52**, 29 (1980).
 19. W. A. Goddard III and W. J. Hunt, *Chem. Phys. Lett.* **24**, 464 (1974).

Table I. Cartesian Gaussian Basis Set^{a,b}

Gaussian Center ^c and type	Exponents (α)
H, 6s	48.4479, 7.28346, 1.65139, 0.462447, 0.145885, 0.07
H, 6p	4.5, 1.5, 0.5, 0.25, 0.125, 0.03125
H, ^d 6d _{xy}	4.5, 1.5, 0.5, 0.25, 0.125, 0.03125
Midpoint, 4s	0.25, 0.05, 0.01, 0.002
Midpoint, 4p	0.8, 0.2, 0.0625, 0.0078125

^a Defined by $X_{lmn}^{(\alpha)} = N_{lmn}(x - A_x)^l (y - A_y)^m (z - A_z)^n e^{-\alpha|\vec{r}-\vec{A}|^2}$, where \vec{A} is the position of the Gaussian center.

^b Basis set used for the ground and excited states of H₂, in the expansion of the scattering functions, and for insertion around $V G_P^{(+)} V$.

^c At the equilibrium internuclear distance of $R_e = 1.400a_0$.

^d Additional functions used to expand the ²Δ scattering functions.

Table II. Integral Cross Sections for excitation of the $B^1\Sigma_u^+$ state ($\times 10^{-18}\text{cm}^2$)

Impact energy (eV)	present results	FM ^a	SJ ^b	KT ^c
15	14.1	10.5	14± 4	
20	26.6	30.9	19± 6	21± 4
30	40.0	44.6	20± 6	24± 5

^a Distorted wave results of Ref. 10.

^b Experimental results of Ref. 16.

^c Experimental results of Ref. 17.

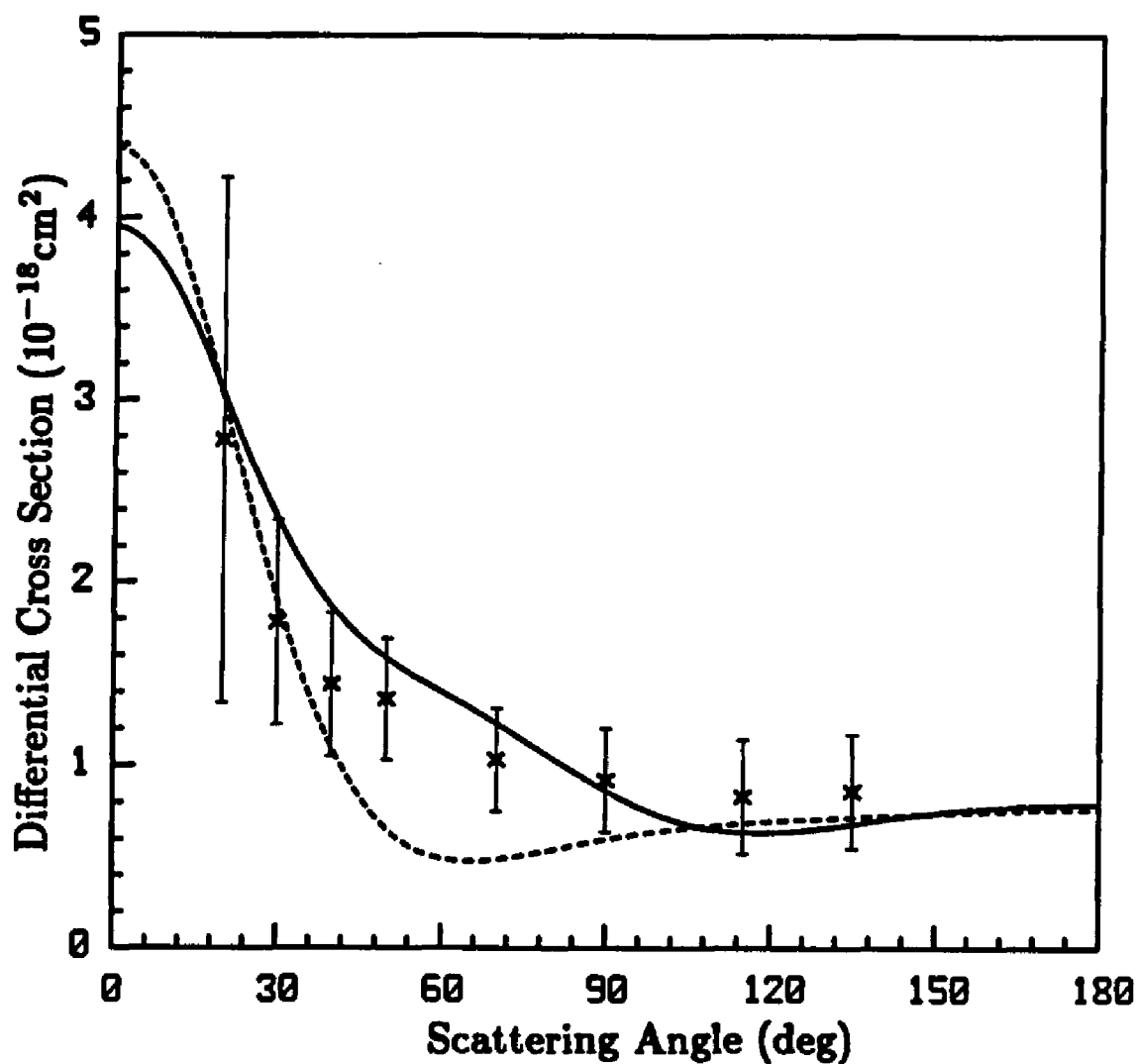


Figure 1: Differential cross sections (DCS) for excitation of the $B^1\Sigma_u^+$ state at 15 eV: present results (solid line), distorted wave (DW) results of Ref. 10 (dashed line), measured values of Ref. 16 (x).

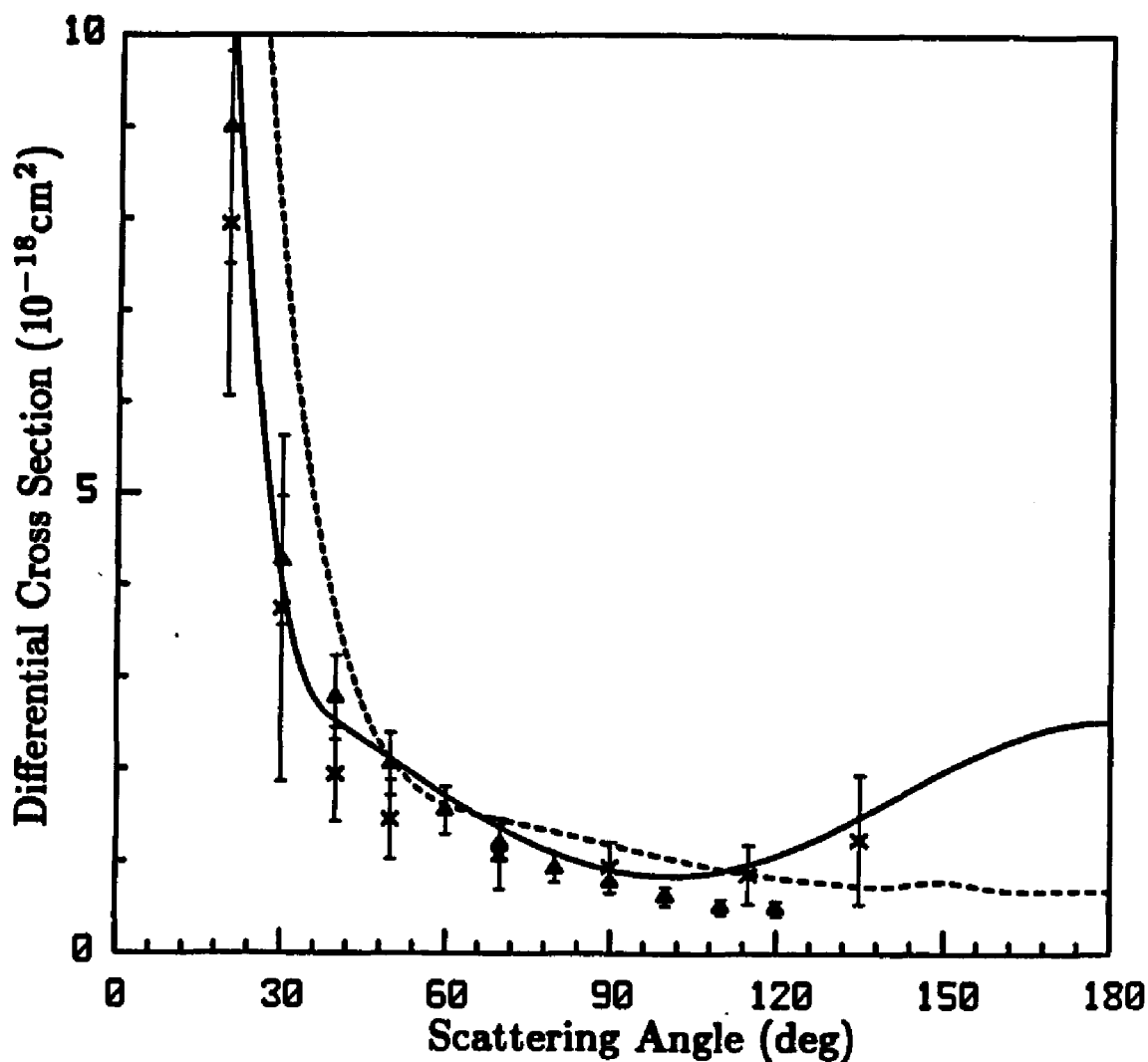


Figure 2: DCS for excitation of the $B^1\Sigma_u^+$ state at 20 eV: present results (solid line), DW results of Ref. 10 (dashed line), measured values of Ref. 16 (\times), measured values of Ref. 17 (Δ).

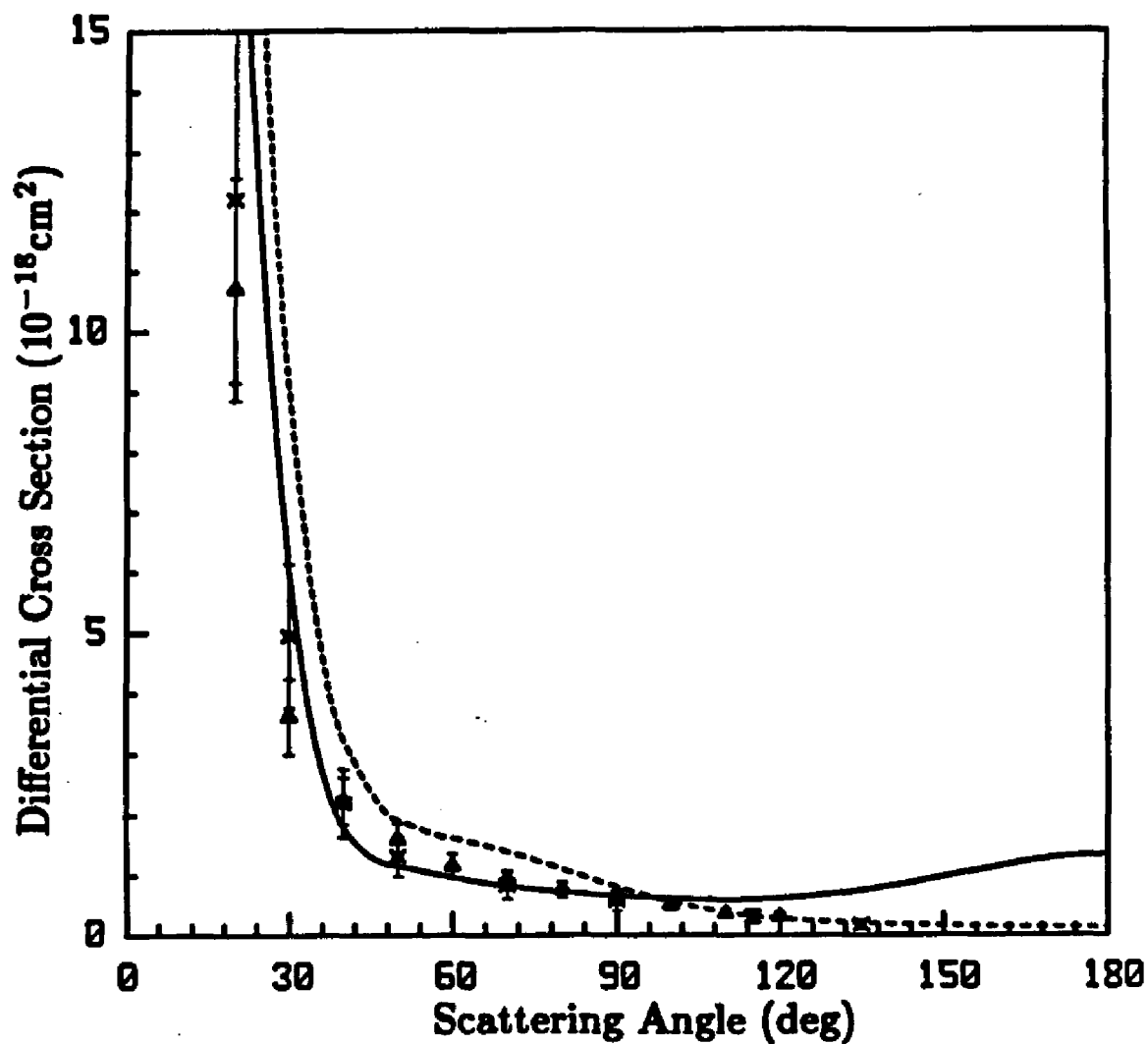


Figure 3: DCS for excitation of the $B^1\Sigma_u^+$ state at 30 eV: present results (solid line), DW results of Ref. 10 (dashed line), measured values of Ref. 16 (\times), measured values of Ref. 17 (Δ).